EVALUATING SPACE WEATHER EFFECTS OF
COMMUNICATION BLACKOUTS, GNSS-BASED
NAVIGATION AND SURVEILLANCE FAILURE,
AND COSMIC RADIATION ON AIR TRAFFIC
MANAGEMENT

DABIN XUE

PhD

The Hong Kong Polytechnic University

2023

This page is intentionally left blank.

The Hong Kong Polytechnic University

Department of Land Surveying and Geo-Informatics

Evaluating space weather effects of communication blackouts, GNSS-based navigation and surveillance failure, and cosmic radiation on air traffic management

Dabin Xue

A thesis submitted in partial fulfillment of the requirement for the degree of Doctor of Philosophy

May 2023

This page is intentionally left blank.

CERTIFICATE OF ORIGINALITY

I hereby declare that this thesis is my own work and that, to the best of my knowledge and belief, it reproduces no material previously published or written, nor material that has been accepted for the award of any other degree or diploma, except where due acknowledgment has been made in the text.

Signature: _____

Name of student: _____ Dabin Xue _____

This page is intentionally left blank.

ABSTRACT

The booming civil aviation is challenging the limited airspace resources, generating safety and efficiency problems in Air Traffic Management (ATM). In response, the International Civil Aviation Organization (ICAO) proposed the Communication, Navigation, and Surveillance/Air Traffic Management (CNS/ATM), which employs digital technologies, including the Global Navigation Satellite System (GNSS) and various automation to support a seamless global air traffic management system.

However, space weather, such as solar flares and coronal mass ejection, can hinder routine aviation operations from communication blackouts and GNSS-based navigation and surveillance failure. In addition, the elevated cosmic radiation induced by space weather can also cause hazardous aviation radiation exposure, which poses a threat to the health of aircrew and passengers. Hence, these effects of space weather necessitate flight plan adjustments. Although space weather events have been heavily emphasized, few studies on the implications of space weather on aviation operations have been conducted. Consequently, this thesis aims to quantify these effects from the standpoint of air traffic management by utilizing some historical space weather events and indispensable assumptions.

Space weather can cause HF communication blackouts, disrupting transpolar flight operations. Therefore, airlines may choose to cancel flights or reroute to low-latitude airspace to maintain satellite communications. To evaluate the economic impact of the HF communication blackouts, we developed a scenario based on the assumption that a space weather event as intense as the Halloween solar storm of 2003 would have occurred in 2019. The results indicate that the potential daily economic losses associated with polar aircraft rerouting and cancellations might vary from €0.21 million to €2.20 million.

Additionally, space weather can impact GNSS performance, resulting in GNSS satellite navigation failure. To explore the effects of satellite navigation failure and the associated economic costs, we chose the Halloween storm of 2003 as a starting point. Results indicate that 2,705 flights in the Continental United States (CONUS)

would be affected during the course of space weather events. Failures in the Continuous Descent Approach (CDA) and Area Navigation (RNAV) can result in an increase of up to €2.43 million in expenses. Besides, we investigate the effects of an ionosphere storm on Hong Kong flights in 2030 by simulating a period of satellite navigation failure (9-16 LT) on a geomagnetic storm day. Our modeling results indicate that if the duration of satellite navigation cannot be forecast, the costs associated with arrival flights will reach €2 million. If the ionospheric impact can be accurately forecasted, the cost could be decreased to €1 million. In addition, the time costs related to passengers due to flight delays might reach €3 million.

GNSS serves as the basis for Automatic Dependent Surveillance-Broadcast (ADS-B). Consequently, ADS-B will be ineffective during GNSS positioning failure. To investigate the effects of ADS-B failure, we simulated the failure duration from 9 LT to 16 LT on 5 September 2018. The total increased flight time for arrival flights in Hong Kong is 1,864 minutes and increased fuel consumption is 65.24 tons, resulting in an additional €0.33 million economic cost including time cost and fuel cost.

Massive cosmic radiation can significantly affect the health of flight crew and passengers. Consequently, during a solar radiation storm, aviation radiation exposure will increase dramatically. In this case, airlines can choose to cancel flights, reroute flights, or lower flight altitudes. To analyze the economic costs of flight cancellations due to the elevated cosmic radiation, we assumed that a space weather event as intense as the Halloween solar storm of 2003 would have occurred in 2019. Results show that flight cancellation costs can be from €2.77 million to €48.97 million, depending on the cosmic radiation dose limits for a given flight plan.

In addition, a multi-objective optimization model has been proposed to minimize aviation radiation exposure and fuel consumption by assigning flight altitudes and speeds while maintaining normal aircraft performance. The study is based on a Tokyo-to-London international flight in 2018 under the assumption that a space weather event comparable to the solar radiation storm that occurred on 20 January 2005. Results show that the proposed method can efficiently reduce fuel

consumption while adhering to cosmic radiation restriction regulations. Our research provides insight for future decisions on air transportation in hazardous space weather conditions.

Our study indicates that powerful space weather events may briefly disrupt normal aviation operations and cause substantial economic losses if future aviation equipment and technology are fragile to its effects.

This page is intentionally left blank.

LIST OF PUBLICATIONS

1. Xue, D., Yang, J., Liu, Z., & Yu, S. (2023). Examining the economic costs of the 2003 Halloween storm effects on the North Hemisphere aviation using flight data in 2019. *Space Weather*, 21(3), e2022SW003381.

2. Xue, D., Yang, J., & Liu, Z. (2022). Potential Impact of GNSS Positioning Errors on the Satellite-Navigation-Based Air Traffic Management. *Space Weather*, 20(7), e2022SW003144.

3. Xue, D., Yang, J., Liu, Z., & Wang, B. (2022). An optimized solution to long-distance flight routes under extreme cosmic radiation. *Space Weather*, e2022SW003264.

4. Xue, D., Hsu, L. T., Wu, C. L., Lee, C. H., & Ng, K. K. (2021). Cooperative surveillance systems and digital-technology enabler for a real-time standard terminal arrival schedule displacement. *Advanced Engineering Informatics*, 50, 101402.

5. Xue, D., Liu, Z., Wang, B., & Yang, J. (2021). Impacts of COVID-19 on aircraft usage and fuel consumption: A case study on four Chinese international airports. *Journal of Air Transport Management*, 95, 102106.

This page is intentionally left blank.

ACKNOWLEDGMENTS

This page is intentionally left blank.

TABLE OF CONTENTS

This page is intentionally left blank.

LIST OF ABBREVIATIONS

AAR	Airport acceptance rate
ACFJ	The consortium of Australia, Canada, France, and Japan
ADS-B	Automatic Dependent Surveillance-Broadcast
ALP	Aircraft Landing Problem
ANSPs	Air Navigation Service Providers
ASM	Airspace Management
ATCOs	Air Traffic Control Officers
ATFM	Air Traffic Flow Management
ATM	Air Traffic Management
ATS	Air Traffic Services
AVIDOS	Aviation Dosimetry
BADA	The base of Aircraft Data
CARI	Civil Aviation Research Institute
CDA	Continuous Descent Approach
CME	Coronal Mass Ejection
CNS/ATM	Communication, Navigation, Surveillance for Air Traffic Management
CONUS	Continental United States
CPDLC	Controller-Pilot Data Link Communications
CR	Cosmic Radiation
CTA	Controlled Time of Arrival
CTD	Controlled Time of Departure
DME	Distance Measuring Equipment
ECEF	Earth-Centered Earth-Fixed
ENU	East North Up
EU	Council of the European Union
EVA	Extra Vehicular Activity

FAA	Federal Aviation Administration
FC	Fuel Consumption
FLT	Forecast Lead Time
FTE	Flight Technical Error
GBAS	Ground-Based Augmentation System
GCR	Galactic Cosmic Radiation
GDP	Ground Delay Programs
GIC	Geomagnetically Induced Current
GIM	Global Ionosphere Maps
GLE	Ground Level Enhancement
GNSS	Global Navigation Satellite Systems
GOES	Geostationary Operational Environmental Satellites
GPS	Global Positioning System
GS	Ground Speed
HF	High Frequency
HF COM	HF Communication
HKIA	Hong Kong International Airport
ICAO	International Civil Aviation Organization
ICME	Interplanetary Coronal Mass Ejections
ICRP	International Commission on Radiological Protection
IGS	International GNSS Service
ILS	Instrument Landing System
IMF	Interplanetary Magnetic Field
ISES	International Space Environment Services
JAEA	Japan Atomic Energy Agency
LHR	London Heathrow Airport
LLA	Longitude, latitude, and Altitude
LPV	Localizer Performance with Vertical Guidance
LT	Local Time

MILP	Mixed-Integer Linear Programming
MLS	Microwave Landing System
MOD	Moderate
MTOW	Maximum Take-Off Weight
NAIRAS	Nowcast of Aerospace Ionizing Radiation System
NASA	National Aeronautics and Space Administration
NCEP	National Centers for Environmental Prediction
NDB	Non-Directional Beacon
NICT	National Institute of Information and Communications Technology
NIPR	National Institute of Polar Research
NOAA	National Oceanic and Atmospheric Administration
NRT	Tokyo Narita Airport
NSE	Navigation System Error
OTA	Original Time of Arrival
OTD	Original Time of Departure
PBN	Performance-Based navigation
PCA	Polar Cap Absorption
PDE	Path Definition Error
PECASUS	Pan-European Consortium for Aviation Space weather User Services
PSR	Primary Surveillance Radar
RAIM	Receiver Autonomous Integrity Monitoring
RCP	Required Communication Performance
RNAV	Area Navigation
RNP	Required navigation performance
RSP	Required Surveillance Performance
SATCOM	Satellite Communications
SBAS	Satellite-Based Augmentation System
SEC	Space Environment Center

SEP	Solar Energetic Particles
SEV	Severe
SPE	Solar Proton Events
SPP	Single Point Positioning
SPS	Standard Position Service
SSR	Secondary Surveillance Radar
SWXC	Space Weather Center
TEC	Total Electron Content
TECU	TEC Units
TMA	Terminal Maneuvering Area
TOA	Time of Applicability
TSE	Total System Error
UAV	Unmanned Aerial Vehicles
UHF	Ultra-High Frequency
VHF	Very High Frequency
VOR	Very High-Frequency Omnidirectional Range
WAAS	Wide Area Augmentation System
WASAVIES	Warning System for AVIation Exposure to Solar energetic particle

LIST OF FIGURES

This page is intentionally left blank.

LIST OF TABLES

This page is intentionally left blank.

Chapter 1

Introduction

Space weather can damage space-based and ground-based systems, consequently affecting human activity. The main topic of this thesis is to investigate the consequences of space weather on air traffic management and associated economic costs. The space weather effects in our study include communication blackouts, satellite navigation failure, satellite-based surveillance failure, and elevated cosmic radiation. This chapter provides an overview of this thesis, including the research background, objectives and methods, and the thesis organization.

1.1   Research Background

1.1.1   Space Weather

Space weather is associated with solar activity, including on its surface and in the solar wind and the interplanetary magnetic field (Poppe and Jorden, 2006; Telloni et al., 2020). Numerous physical phenomena, such as geomagnetic storms and substorms, ionospheric disturbances, and scintillation, are related to space weather (Alberti et al., 2017). The abrupt release of electromagnetic energy stored in the magnetic fields is connected to solar flares. Emitted radiation comprises a substantial percentage of the electromagnetic spectrum, from radio waves to X-rays (Hudson, 2011; Svestka, 2012). Coronal Mass Ejections (CME) are huge releases of billions of tons of charged particles and magnetic field from the sun's surface (Manchester IV et al., 2004; Webb and Howard, 2012), which can cause magnetosphere compression and geomagnetic storms (Brown, 1978; Hundhausen, 1999). Solar Energetic Particles (SEP) are protons and heavy ions accelerated by CME or solar flares (Marqué et al., 2006; Ryan et al., 2000; Shea and Smart, 2012).

The interaction between CME and the Earth's magnetic field can lead to major geomagnetic storms (Gonzalez et al., 1999). Three primary forms of space weather are radio blackouts, solar radiation storms, and geomagnetic storms (Eastwood et al., 2017). Due to the intricacy and interconnection of the underlying physical

processes, all three of these phenomena are capable of occurring inside a single space weather event with varied temporal, spatial, and intensity imprints. The consequences of space weather events on space-based and ground-based systems are depicted in Figure 1.1. Therefore, it is crucial to monitor space weather conditions because they can impair the performance and reliability of satellites, navigation systems, and radio communications. The duration of the impacts of space weather events might range from a few seconds to many days (Schwenn, 2006). The influence of solar radiation storms, geomagnetic storms, and ionospheric storms are accounted for in space weather predictions for international air navigation (Morozova et al., 2020). These predictions allow operators to be cognizant of potential dangers and devise alternate strategies if oncoming conditions are of a scale and/or nature that might interrupt routine operations.

Sun	Earth	Effect	System Impact
Solar flare	Solar Radio Noise	Wireless Interference	GPS; Mobile Connectivity
	X-Ray Flare	Radio Absorption	High Frequency Comms
	Minutes		
CME	Magnetic Storm	Geomagnetically Induced Current	Power Grid; Pipe Lines
		Ionosphere Storm	High Frequency Comms; GNSS
	Days	Ionosphere Scintillation	Satcom; GNSS
		Spacecraft Charging	Satellite Operation
		Spacecraft Drag	Satellite Operation
SEP	Radiation Storm	Single Event Effects	Satellite Operation; Avionics
	Minutes/hours	Polar Radiation Absorption	High Frequency Comms
		Radiation Dose	Aircrew; Passenger
		Solar Array Discharge	Satellite Ops Power

Figure 1.1. Space weather impact tree.

Kp and Dst are two geomagnetic indices (Nagai, 1988) that are widely used for space weather research. The Kp index depicts the worldwide geomagnetic activity based on 3-hour observations from magnetometers on Earth's surface (Thomsen, 2004). Each station is calibrated based on its latitude and reports a particular Kp index based on the geomagnetic activity detected at the magnetometer's location. Dst (Disturbance Storm Time) index is produced from a network of four near-equatorial geomagnetic observatories that monitor the ground magnetic disturbance in the low latitude region (Sugiura, 1963).

1.1.2 Air Traffic Management

Air traffic management (ATM) can be broadly divided into three levels: (1) the strategic level by runway expansion or shorter separation standards; (2) the pre-tactical level by splitting traffic flows and sectors; and (3) the tactical level by sequencing and re-sequencing aircraft during flight operations (Gwiggner and Nagaoka, 2014). Figure 1.2 shows that ATM includes Air Traffic Services (ATS), Airspace Management (ASM), and Air Traffic Flow Management (ATFM). Traditional ATM methods include group delay programs (Glover and Ball, 2013; Liu et al., 2019), airport surface management (Bolat, 2001; Corlu et al., 2020; Ng et al., 2018), flight rerouting (Ding et al., 2018; McCrea et al., 2008), flight scheduling (Birolini et al., 2021; Eufrásio et al., 2021), and flight sequencing (Eun et al., 2010; Xu et al., 2022).
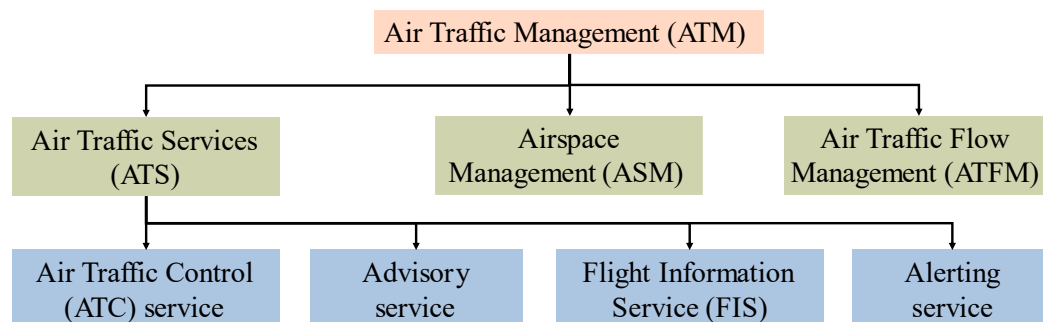
Figure 1.2. ATM architecture diagram (ICAO, 2007). ATS aims to ensure safe and orderly traffic flow and provides the necessary information to aircrew. ASM aims to manage scarce airspace to satisfy flight demands from civil users and military users. ATFM aims to regulate flight flows to avoid air traffic congestion.

However, the growing flight demand exceeds the limited airspace capacity, causing severe flight congestion and costly delays (Bubalo and Gaggero, 2021; Starita et al., 2020). Therefore, to satisfy the predicted growth in air traffic demand, the current ATM system will need to be upgraded. In response, the International Civil Aviation Organization (ICAO) has proposed CNS/ATM based on satellite navigation, digital communications, performance-based navigation (PBN), and Automatic Dependent Surveillance-Broadcast (ADS-B) to increase airspace capacity and flight efficiency (Osunwusi, 2020; Vismari and Junior, 2011). Figure 1.3 illustrates the components of CNS/ATM. Based on the advanced CNS/ATM system, aviation safety, and security capabilities can be modernized, consequently increasing airport capacity and reducing flight delays. Furthermore, the possibility of aircraft collision can be decreased due to safety alerts and warnings.

Figure 1.3. Components of CNS/ATM. Specifically, Controller-Pilot Data Link Communications (CPDLC) will replace voice communication as the main communication technology. Satellite navigation will play an important part in guiding aircraft. Along with radar systems, ADS-B will be used to monitor flight situations.

Communication

Voice communication is important in routine and emergency air-to-ground

communications based on Very High Frequency (VHF) radio (Haynes, 2015). Although numerous pilots have described the calming impact of hearing ATCOs' voices, VHF can only transfer information at the speed of human talking, and it cannot handle several broadcasts on the same frequency simultaneously (Tuysuz et al., 2013). In contrast, Controller-pilot data link communications (CPDLC) can greatly minimize the bandwidth and time requirements (Gurtov et al., 2018). Therefore, air-ground communication services will increasingly rely on data communications, reserving voice for real-time and crucial communication. Aircraft can respond to ATCOs using either a predefined message format or free text (Glaser-Opitz and Glaser-Opitz, 2015). Messages from a controller typically adhere to a defined structure, and most messages demand a response. The benefits of CPDLC include a reduction in voice channel congestion, fewer miscommunications, and a reduced workload of pilots and ATCOs (Bajaja and Majumdar, 2021).

Navigation

Performance-based navigation (PBN) is the regulatory framework for implementing Area Navigation (RNAV), which requires a particular level of accuracy, integrity, continuity, and functionality (Fellner and Konieczka, 2019; Pamplona et al., 2021). PBN relies on enabling technologies such as on-board integrated navigation systems and GNSS receivers. The aircraft determines its current latitude, longitude, and position relative to the desired flight route. As long as the aircraft can determine the real-time positions, they may fly anywhere within the GNSS system's service area (Eldredge et al., 2010; Walter, 2017). In contrast, non-directional beacons (NDB), Distance Measuring Equipment (DME), and VHF omnidirectional range (VOR) are examples of traditional terrestrial navigation aids that can only direct aircraft along specified routes (Skrypnik, 2019).

Surveillance

In addition to radar systems, the Automated Dependent Surveillance-Broadcast (ADS-B), as an emerging surveillance technology, employs GNSS to calculate longitude, latitude, altitude, and speed (Eskilsson et al., 2020). The onboard ADS-

B Out system then broadcasts this information together with the aircraft's identification twice every second. This update interval is shorter than the radar with an update interval of 4-15 seconds ([Ali et al., 2017b](#)). Therefore, ATCOs will increase confidence in aircraft's real-time positions, reducing the separation between aircraft without compromising flight safety, which can optimize airspace capacity and improve flight safety ([Kunzi, 2013](#)).

ATM benefits of CNS

The primary benefits of CNS for ATM include higher airspace capacity particularly in crowded airspace, more schedule flexibility, improved flight path efficiency, less disruption due to flight delays and diversions, and enhanced efficiency from a lowered separation minimum ([Kistan et al., 2017](#)). Currently, aircraft may fly closer together without compromising safety. Specifically, the separation standards in oceanic airspace have decreased from 180 nautical miles to 50 nautical miles and subsequently to 30 nm ([Builta, 2016](#); [Qing et al., 2022](#)), with the potential that ADS-B would permit a shorter separation standard of less than 15 nautical miles ([Marais, 2016](#)).

1.1.3 Space Weather Effects on Aviation

Space Weather Effects on Communication

Space weather can have significant effects on communication systems, particularly those that rely on radio waves and satellite technology. The ionosphere, a region of Earth's upper atmosphere, plays a crucial role in reflecting radio signals back to the surface ([Atiq, 2018](#); [Nielsen et al., 2007](#); [Walsh et al., 2015](#)). Space weather can affect the ionosphere by causing ionization irregularities, electron density fluctuations, and scintillation ([Rodrigues and Moraes, 2019](#); [Xiong et al., 2016](#)). These disturbances can lead to signal fading, signal absorption, and increased errors in data transmission for high-frequency (HF) and very high-frequency (VHF) radio communication systems ([Goodman, 2005](#); [Hapgood et al., 2021](#); [Maxama and Markus, 2018](#); [Tao et al., 2020](#)).

Geostationary satellites provide a wide range of communication services, including television broadcasting, internet access, and long-distance telephony ([Su et al., 2019](#); [Whalen, 2010](#)). Space weather events, such as solar radiation

storms and geomagnetic storms, can damage satellite electronics and disrupt satellite communication links (Bothmer et al., 2007; Knipp et al., 2016; Moldwin, 2022). Operators may need to take protective measures to safeguard satellite systems during such events. Moreover, geomagnetic storms, driven by solar activity, can induce electric currents in power lines and pipelines on Earth's surface (Marshall et al., 2010; Pirjola, 2005). These induced currents can damage transformers and other electrical equipment, leading to power outages (Panteli et al., 2016; Schrijver et al., 2015). Additionally, ground-based communication systems, such as undersea cables, may experience increased noise and signal degradation during geomagnetic storms (Bothmer et al., 2007; Pirjola et al., 2005).

Space weather can also affect communication between aircraft and air traffic control (Eastwood et al., 2017). Radio waves used for communication can experience interference or signal fading due to ionospheric disturbances, potentially impacting the safety and efficiency of aviation operations (Dave et al., 2022; Elmarady and Rahouma, 2021; Goodman, 2005; Li et al., 2006). Besides, during geomagnetic storms, auroras become more prominent and extend to lower latitudes. These beautiful natural phenomena can disrupt radio signals by ionizing the atmosphere, causing absorption and signal fading in the affected regions (Knipp et al., 2016; Smith et al., 2008).

To mitigate the effects of space weather on communication systems, operators and agencies often monitor space weather conditions closely. They may implement measures such as rerouting flights, temporarily shutting down sensitive equipment, or using alternate communication frequencies or backup systems during periods of heightened space weather activity. Additionally, advancements in technology and research help improve our understanding of space weather and its potential impacts, allowing for better preparedness and response.

Space Weather Effects on satellite navigation GNSS

Space weather can have significant effects on GNSS, such as the Global Positioning System (GPS), Galileo, GLONASS, and BeiDou. These systems rely on signals from satellites in orbit to provide accurate positioning, navigation, and timing information (Hapgood, 2017; Sreeja, 2016a). The ionosphere, a region of

the Earth's upper atmosphere, can be affected by space weather events such as solar flares, solar radiation storms, and geomagnetic storms (Cander, 2019; Moen et al., 2013; Yiğit et al., 2016). These disturbances can lead to rapid changes in the ionospheric electron density, causing fluctuations in the speed of radio signals passing through it (Coster and Komjathy, 2008; Moen et al., 2013; Singh et al., 2010). This results in errors in the calculation of signal travel time, which in turn leads to positioning errors (Vankadara et al., 2022; Vesnin, 2022; Warnant et al., 2007). Differential GNSS techniques and real-time ionospheric modeling can help mitigate these effects (Memarzadeh, 2009; Wang et al., 2022; Yasyukevich et al., 2020).

Scintillation is a rapid and random fluctuation in the amplitude and phase of GNSS signals as they pass through the ionosphere (Aquino et al., 2009; Kintner et al., 2009; Pi et al., 2017; Vilà-Valls et al., 2020). It is most common in equatorial and high-latitude regions during geomagnetic storms (Andalsvik and Jacobsen, 2014; Jiao and Morton, 2015). Scintillation can degrade the signal quality, making it challenging to accurately track and decode the signals from satellites (Luo et al., 2020; Pi et al., 2017; Romano et al., 2013). Specialized receivers with scintillation monitoring capabilities can help mitigate the impact (Aquino et al., 2009; Nguyen et al., 2019; Zhao et al., 2022).

The ionosphere can introduce signal delays and dispersion in GNSS signals, particularly at (Camps et al., 2016; Guo et al., 2014; Zhao and Lei, 2023). This can result in errors in distance measurements, affecting position accuracy. Dual-frequency GNSS receivers are less susceptible to these effects because they can calculate and correct for ionospheric delays by comparing signals at different frequencies (Glenn Lightsey et al., 2014; Luo et al., 2023; Nie et al., 2020; Sun et al., 2021a).

Space weather events, particularly solar radiation storms, can affect the onboard electronics of GNSS satellites (Eastwood et al., 2017; Horne et al., 2013; Roy and Paul, 2013). High-energy particles can cause single-event upsets, latch-ups, or other anomalies in satellite systems. When this occurs, satellite signals may become less reliable, or certain satellites may go temporarily offline (Hapgood,

2017; Roy and Paul, 2013; Sreeja, 2016a). In addition, GNSS receivers on Earth can also be affected by space weather events (Fajardo et al., 2019; Hapgood, 2017; Ishii, 2017). Interference from solar radio bursts, for example, can disrupt the receiver's ability to track and decode satellite signals accurately. Modern GNSS receivers often include features to mitigate interference and improve signal tracking during adverse conditions. The cumulative effect of ionospheric disturbances, scintillation, and other space weather-related issues can lead to navigation errors in GNSS applications. These errors can impact industries such as aviation, maritime navigation, agriculture, surveying, and emergency services (Meehan, 2010; Pankratius et al., 2014; Rockville, 2019; Viereck et al., 2014).

To mitigate the effects of space weather on GNSS, various strategies and technologies are employed. These include the development of more robust and resilient GNSS receivers, the use of dual-frequency receivers, real-time monitoring of ionospheric conditions, and the development of advanced ionospheric models for real-time corrections. Additionally, users of GNSS data are encouraged to remain aware of space weather forecasts and potential impacts on their operations so that appropriate measures can be taken when necessary.

Space Weather Effects on cosmic radiation

Space weather can have significant effects on cosmic radiation in our solar system. Cosmic radiation primarily consists of high-energy particles, primarily protons and atomic nuclei, originating from various sources, including the sun, Galaxy, and distant galaxies (Erlykin and Wolfendale, 2006; Schlickeiser, 2013). Solar flares and coronal mass ejections are explosive events on the Sun that release a burst of high-energy particles into space, including protons and heavier ions (Durante and Kronenberg, 2005; Simonsen et al., 2020). These SEPs can significantly enhance the flux of cosmic rays in the inner solar system. When SEPs interact with Earth's magnetic field, they can lead to geomagnetic storms (Kress et al., 2010) and potentially disrupt satellite operations, aviation communication, and power grids (Bothmer et al., 2007; Eastwood et al., 2017; Redmon et al., 2018). The Sun's activity, including its 11-year solar cycle, affects the strength of the solar magnetic field and the solar wind (Ataç and Özgüç, 2006; Schatten, 2003). Therefore, during the solar activity maximum, the cosmic radiation intensity

9

increases significantly. Generally, the cosmic radiation rates are higher in the higher altitudes and latitudes due to the less protection from atmosphere and magnetosphere (Bottollier-Depois et al., 2003; Matthiä et al., 2014).

When it comes to aviation, especially at high altitudes, such as during long-haul flights, there are potential effects of cosmic radiation on both passengers and crew members. As aircraft climb to higher altitudes, they enter the Earth's stratosphere and, eventually, the mesosphere, where they are exposed to cosmic radiation. At cruising altitudes, the Earth's atmosphere provides less shielding from cosmic radiation compared to being at sea level (Almeida Filho et al., 2023; Matthiä et al., 2015).

The dose of cosmic radiation that passengers and crew members are exposed to during a flight depends on several factors, including flight altitude, route, and duration (Bottollier-Depois et al., 2003; Lee et al., 2015). Generally, the longer the flight and the higher the altitude, the greater the radiation dose.

The health risks associated with exposure to cosmic radiation are a topic of concern, especially for frequent flyers, flight crews, and airline personnel. Prolonged exposure to high levels of cosmic radiation can increase the risk of cancer over a person's lifetime (Barcellos-Hoff et al., 2015). The risk is relatively low for occasional air travelers but is of greater concern for those who spend significant time in the air.

Aviation authorities, such as the Federal Aviation Administration (FAA) in the United States and the International Commission on Radiological Protection (ICRP), have established guidelines and regulations to limit the exposure of flight crews to cosmic radiation (Friedberg et al., 2000; Lochard et al., 2016). Airlines are required to monitor and record the radiation doses of their crews and provide protection measures when necessary (Bartlett, 2004). Pregnant passengers and crew members are typically more susceptible to the effects of cosmic radiation (Barish, 2014). Airlines often have policies in place to provide alternative work assignments for pregnant crew members or offer recommendations to pregnant travelers. Airlines can take measures to reduce the exposure of passengers and crew to cosmic radiation. This may include altering flight routes to avoid regions

of increased cosmic radiation (e.g., polar routes), flying at lower altitudes when possible, and limiting the time spent at higher altitudes during long-haul flights (Di Trolio et al., 2015; Shouop et al., 2020; Xue et al., 2022c). Some aircraft are designed with features that provide additional shielding against cosmic radiation. For example, certain materials and structures can help reduce radiation exposure inside the aircraft (Gaisser et al., 2016).

In summary, while cosmic radiation is a concern in aviation, the associated health risks are generally considered low for most passengers and crew members. However, those who frequently fly at high altitudes may be exposed to higher levels of radiation and should take precautions, such as following guidelines and regulations set by aviation authorities and airlines.

1.1.4 Space Weather Service for Aviation

Although the Sun is far away from the Earth (about 150 million km), space weather can affect a vast array of technologies and activities in space and on Earth (Tóth et al., 2012), such as critical national infrastructure such as power grids (Watari, 2015), the oil and gas industry (Viljanen et al., 2006), communications (Kelly et al., 2014), ground transportation (Eroshenko et al., 2010), satellite infrastructure (Loto'aniu et al., 2015), and GNSS (Sreeja, 2016b). Solar storms exist in three varieties and can have detectable effects on Earth's atmosphere and magnetosphere: a solar flare can produce a Radio Blackout, a disturbed solar wind can cause a Geomagnetic Storm, and rapid solar particles can cause a Radiation Storm. Therefore, the effects of space weather on aviation include degraded radio/satellite communication, excessive radiation doses for aircrew and passengers, and signal reception disturbances from navigation satellites. The effects of space weather on aviation are summarized as follows from the perspective of Solar Flare Radio Blackouts, Solar Radiation Storms, and Geomagnetic Storms.

Solar Flare Radio Blackouts: ionospheric disruptions produced by solar X-ray emissions, which can deteriorate HF radio communication at medium and low latitudes (Reddybattula et al., 2020).

Solar Radiation Storms: increased levels of radiation due to an increase in the

volume of energetic particles. Solar radiation storms typically impair satellite tracking and power systems and pose radiation risks to humans in flight at high altitudes or latitudes (Shea and Smart, 2012). In addition, solar radiation storms may cause HF radio blackouts at high latitudes and GNSS positioning errors (Yasyukevich et al., 2018).

Geomagnetic Storms: perturbations in the Earth's geomagnetic field induced by solar wind gusts (Rathore et al., 2011). Geomagnetic storms typically have negative impacts on high-frequency radio communications, satellite navigation, and low-frequency radio navigation systems (Gulati et al., 2019). In addition to disrupting electrical power networks, geomagnetic storms can affect ATC facilities and other national air space components. Geomagnetic storms diminish the Earth's magnetic field capacity to deflect incoming charged particles (Bamford et al., 2014).

To reduce the detrimental effects on aviation, space weather service is implemented by the joint operation of three global space weather centers, i.e. the Pan-European Consortium for Aviation Space weather User Services (PECASUS), NOAA Space Weather Center (SWXC), and the consortium of Australia, Canada, France, and Japan (ACFJ) (Hapgood, 2022), which have been operational since November 2019 for providing information on space weather phenomena to the aviation industry. The ICAO space weather service is operated jointly by three global space weather centers, with each center delivering the service every two weeks (Aleshin et al., 2021). One center is constantly on duty, while the other two centers serve as backups. In addition, the Sino-Russian space weather monitoring center has begun to provide services for global aviation operators since 16 November 2021 (Li, 2021). Detailed information is illustrated in Figure 1.4. Specifically, PECASUS consists of ten ICAO members including Finland, Belgium, the United Kingdom, Austria, Germany, Italy, the Netherlands, Poland, Cyprus, and South Africa. PECASUS initiated the ICAO space weather service, which was afterwards followed by the NOAA Space Weather Prediction Center and the consortium of Australia, Canada, France, and Japan (ACFJ).
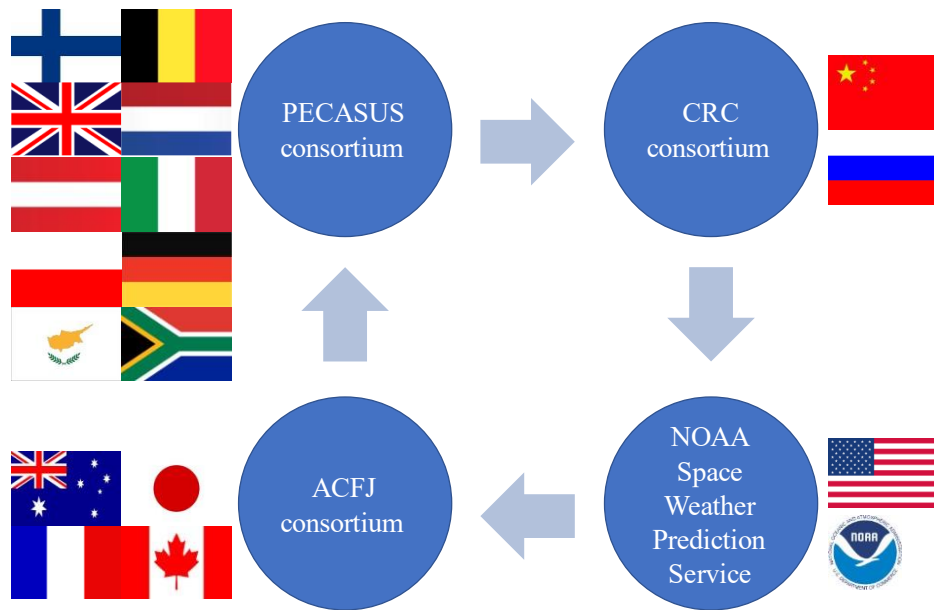
Figure 1.4. The four ICAO Global Space Weather Centers (PECASUS, CRC, SWXC, and ACFJ).

The National Oceanic and Atmospheric Administration (NOAA) Space Weather Scales were developed as a means of sharing the present and future space weather conditions with the general public. NOAA space weather scales describe the effects of space weather from geomagnetic storms, solar radiation storms, and radio blackouts (https://www.swpc.noaa.gov/noaa-scales-explanation).

The space weather advisory service focuses on three significant space weather effect areas, which are related to aviation, i.e. HF Communications (HF COM), GNSS-based navigation and surveillance, and radiation effects on avionics and human health (RAD). A fourth effect area (Satellite Communication) has been identified, but advisories for SATCOM will not be published until more work is conducted to create and confirm operationally applicable advisory limits for this impact area. Additional information is available in the Space Weather Hazard companion pamphlet. There are two intensity criteria at which advisories are issued: Moderate (MOD) and Severe (SEV). The related thresholds are listed in Table 1.1. The ICAO Manual on Space Weather Information in Support of International Air Navigation defines alerting criteria (ICAO Doc 10100) (ICAO, 2018b).

Table 1.1. Effects of space weather and corresponding thresholds.

Effect	Parameter	MOD	SEV
RAD	Effective dose	30 μSv/h	80 μSv/h
GNSS			
Amplitude Scintillation	S_4	0.5	0.8
Phase Scintillation	σ_φ	0.4 rad	0.7 rad
Total Electron Content	TECU	125	175
HF COM			
Auroral Absorption	Kp	8	9
Polar Cap Absorption	Riometer abs.	2 dB	5 dB
Shortwave Fadeout	Solar X-rays	10^{-4}W/m^2 (X1)	10^{-3}W/m^2 (X10)
Post Storm Depression	MUF	30%	50%

1.2   Objectives and Methods

Routine aviation operations can be impeded by space weather effects such as HF communication blackouts, GNSS-based navigation and surveillance failures, and elevated cosmic radiation, which necessitates flight plan adjustments. Although space weather effects have been heavily emphasized, the literature on the economic effects on aviation is limited. That is due to a lack of flight data and/or relatively weak space weather events in the past solar cycles. Therefore, this thesis aims to explore the space weather effects on air traffic management and its cost implication from the perspectives of communication blackout, satellite navigation failure, GNSS-based surveillance failure, and elevated aviation radiation exposure. We have suggested corresponding measures for solving the problems from the standpoint of air traffic management. The induced economic costs are quantified by considering flight delays, flight cancellations, flight rerouting, fuel consumption, etc.

The probability that severe space weather events will occur is low, but statistically, they will occur in the future. It is not a matter of if but when, and the issue cannot be overlooked. Therefore, we simulated some scenarios using historical space weather events and actual flight data. Specifically, the detailed methods are

presented in Figure 1.5.

(1)   Communication blackouts: Solar energetic protons can penetrate the Earth at the magnetic poles and create additional ionization, rendering High Frequency (HF) radio communication impossible for several days, which may affect the normal operation of polar flights. In response to HF communication blackouts, airlines can cancel polar flights and reroute flights to avoid HF communication failure. Therefore, we simulate a scenario based on the Halloween storm in 2003 and polar flights in 2019 to quantify the economic costs (Xue et al., 2023).

(2)   Satellite navigation failure: Space weather can cause ionosphere storms and consequently degrade the GNSS performance. As a result, aircraft cannot rely on satellite navigation and instead have to use ground navigation aids. To investigate the effects of satellite navigation failure on flight operation, we simulate two scenarios. First, the effects on the Continental United States (CONUS) flights are quantified in the background of the Halloween storm in 2003 (Xue et al., 2023). Then, we evaluate the future effects on Hong Kong flights in 2030 by presuming a certain satellite navigation failure period caused by ionosphere storms (Xue et al., 2022a).

(3)   GNSS-based surveillance failure: Due to the degraded GNSS performance, ADS-B will also be out of work. As a result, Air Traffic Control Officers (ATCOs) can only utilize surveillance radars to manage aircraft into and out of crowded airspace (Xue et al., 2021a). Currently, radars are more common at major airports due to their reliable performance. Therefore, we explore the potential benefits of ADS-B and then make a comparison with radar control to show the effect of ADS-B failure on air traffic management.

(4)   Elevated cosmic radiation: During radiation storms, aircraft need to take some actions to avoid excessive aviation exposure. We discuss the effects of elevated cosmic radiation on flight operation from two study scenarios. First, we calculate the cosmic radiation dose of flights in the Northern Hemisphere in the background of the Halloween storm in 2003 and

evaluate the economic costs of flight cancellations and lowering flight altitudes (Xue et al., 2023). Second, a multi-objective model is proposed to minimize fuel consumption and cosmic radiation by optimizing flight altitudes and flight speeds (Xue et al., 2022b).

Operation effects	Scenarios	Objects	ATM measures
HF communication blackouts	Halloween storm in 2003	Polar flights in 2019	Flight cancellation Flight rerouting
Satellite navigation failure	Halloween storm in 2003	CONUS flights in 2019	Ground navigation Step-down approach
	Simulated storm in 2030	Hong Kong flights in 2030	Flight cancellation Flight delay
GNSS-based surveillance failure	Simulated ADS-B failure	Hong Kong flights in 2018	Radar control
Excessive cosmic radiation	Halloween storm in 2003	Northern Hemisphere flights in 2019	Flight cancellation Lower flight altitude
	Radiation storm in 2005	Tokyo-London flight	MILP-based model Lower flight altitude

Figure 1.5. The effects of space weather on air traffic management from communication blackout, satellite navigation failure, ADS-B failure, and massive radiation dose.

The reason why the Halloween storm in 2003 is selected as the study background is that this space weather event includes a series of solar flare eruptions, Interplanetary Coronal Mass Ejections (ICME), and a two-dip super geomagnetic storm (Gopalswamy et al., 2005). According to (NOAA, 2004), the impacts on aviation are summarized from the perspectives of communication, navigation, and cosmic radiation. Figure 1.6 shows the Dst index from 28 October 2003 to 31 October 2003.
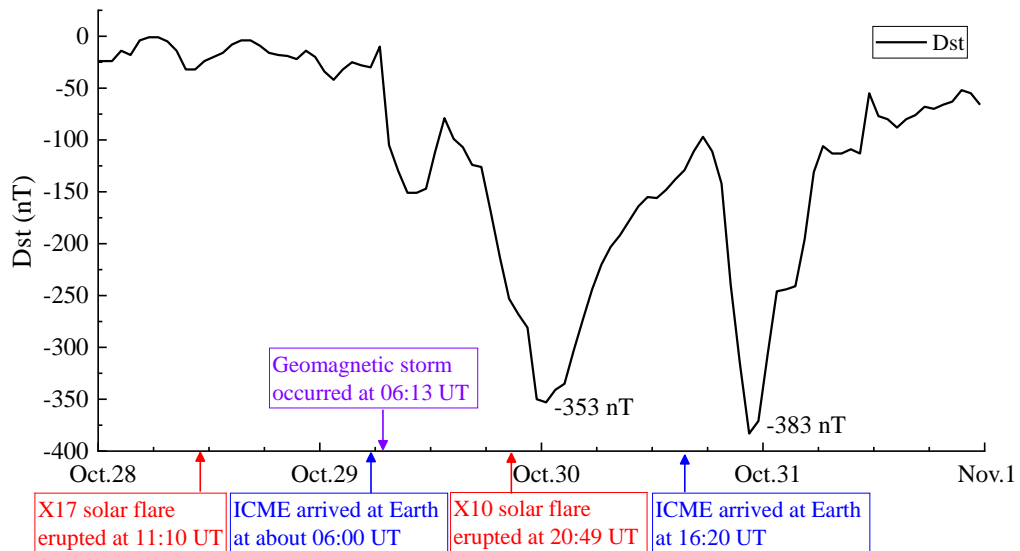
Figure 1.6. Dst index during the Halloween storm on 28-31 October 2003 (Sparks et al., 2022).

1.3   Thesis Organization

This thesis has seven chapters. The remaining parts of this thesis are structured as follows:

Chapter 2 introduces the air-ground communication methods, which mainly rely on Very High Frequency (VHF). However, polar flights can only use HF when flying over the polar region. When solar energetic particles reach the atmosphere over the polar areas, there will be an increase in ionosphere ionization at altitudes of 50-100 km. Consequently, HF radio signals will be absorbed, resulting in HF communication blackouts in the polar regions. In order to quantify the corresponding economic costs of HF communication blackouts caused by space weather, a scenario was simulated by assuming an extremely strong space weather event like the 2003 Halloween solar storm would have occurred in 2019. In response to HF communication blackouts, airlines may choose to cancel polar flights or design a new flight route (always longer flight distance). As a result, the induced daily economic costs could be from €0.21 million (flight rerouting) to €2.20 million (flight cancellation). This study has been published in *Space Weather* with the title: Examining the economic costs of the 2003 Halloween

storm effects on the North Hemisphere aviation using flight data in 2019 ([Xue et al., 2023](#)).

Chapter 3 analyzes the effects of satellite navigation failure caused by space weather on flight operations. Space weather can result in a considerable increase in total electron contents and irregularities in the ionosphere, significantly degrading GNSS positioning accuracy. Consequently, GNSS cannot navigate aircraft, especially during the final approach and landing phases. Aircraft will not operate the Continuous Descent Approach (CDA) or Area Navigation (RNAV). In addition, the separation standards between any two aircraft will be enlarged for flight safety concerns, increasing landing time intervals. To explore the impact of satellite navigation failure on flight operation and estimate the induced economic costs, we have finished two case studies. Firstly, we simulated a scenario by assuming an extremely strong space weather event like the 2003 Halloween solar storm would have occurred in 2019. We concluded that 2,705 flights in the Continental United States (CONUS) would be affected by ionosphere disturbance. The economic cost was estimated to be €2.43 million due to CDA failure and RNAV failure. This study has been published in *Space Weather* with the title: Examining the economic costs of the 2003 Halloween storm effects on the North Hemisphere aviation using flight data in 2019 ([Xue et al., 2023](#)). Secondly, we simulated a scenario by assuming a space weather event would occur in 2030. The projected Hong Kong flight data in 2030 were used to evaluate the potential effects of satellite navigation failure on flight operations. The simulation assumed satellite navigation failure from 9 to 16 Local Time. Results suggest that if the duration of satellite navigation failure cannot be forecast, the economic cost from flight delays, flight cancellations, and flight diversions would be more than 2 million Euros. In contrast, if satellite navigation failure duration can be forecast, the economic cost related to airlines can be reduced to €1 million. Another conclusion is that increased forecast lead time would reduce the cost. Furthermore, inaccurate forecasts can also cause additional costs. Therefore, it is crucially important to improve the forecast accuracy and extend the forecast lead time of satellite navigation failure to reduce impacts and economic costs on the aviation industry during space weather events. This study has been published in *Space*

Weather with the title: Potential Impact of GNSS Positioning Errors on Satellite-Navigation-Based Air Traffic Management (Xue et al., 2022a).

Chapter 4 studies the effects of ADS-B failure on flight operation. Currently, radar systems are widely used in major airports, especially in the terminal control areas. ATCOs manage air traffic based on the blips on the radar screen. ADS-B is a digital technology with many advantages based on the GNSS solution (e.g. longitude, latitude, and altitude). However, space weather events can hinder the normal operation of GNSS, and consequently cause the failure of ADS-B-based surveillance. In response, the radar system will be the only surveillance technology. Without the digital advantages of ADS-B, aircraft separation standards will be enlarged, and simultaneously airspace capacity will decrease sharply. As we cannot get the flight data during ADS-B failure caused by space weather, we have to adopt another research method to explore the effects of ADS-B failure on flight operation. The details are as follows. Firstly, we proposed a novel heuristic search method for aircraft landing scheduling based on ADS-B digital technology considering the time separation standards regulated by ICAO. Then improvement in flight operation based on ADS-B can be obtained. After that, a scenario was simulated by assuming ADS-B failure duration from 9 LT to 16 LT in Hong Kong. Using the flight data of Hong Kong International Airport on 5 September 2018, we calculated the economic costs caused by ADS-B failure to be €0.33 million. Moreover, the increased workload of ATCOs and pilots cannot be ignored, although we did not quantify or evaluate it. This study has been published in *Advanced Engineering Informatics* with the title: Cooperative surveillance systems and digital-technology enabler for a real-time standard terminal arrival schedule displacement (Xue et al., 2021a).

Chapter 5 investigates the effects of solar radiation storms (elevated cosmic radiation) on flight operation and potential economic costs for flight cancellations and rerouting. During solar radiation storms, Solar Energetic Particles (SEP) increase dramatically, and consequently, there will be a significant increase in cosmic radiation levels. For the concern of the biological health of aircrew and passengers, canceling flights, lowering flight altitudes, or changing flight routes to lower-latitude areas can be adopted. However, these three methods sometimes

may be not effective due to increased economic cost and/or environmental pollution. To estimate the effects of elevated cosmic radiation during solar radiation storms on flight operation and incurred economic costs, two case studies were conducted. Firstly, assuming an extremely strong space weather event like the 2003 Halloween solar storm would have occurred in 2019, the aviation radiation exposures of the Northern hemisphere flights were calculated. If the cosmic radiation dose limit for a given plan is set to be 100 μSv (or 1,000 μSv), the economic cost of flight cancellations can be €48.97 million (or €2.77 million). Then the cosmic radiation dose limit for one flight trip in Europe during severe space weather events is estimated to be 400 μSv, which can be a guideline for policy recommendations. Furthermore, a multi-objective optimization method is presented to minimize aviation radiation exposure and fuel consumption by assigning flight altitudes and speeds while maintaining normal flight operation. Our research gives insight into future air transportation decisions during solar radiation storms. The results of this chapter have been published in *Space Weather* with the title: An optimized solution to long-distance flight routes under extreme cosmic radiation (Xue et al., 2022b) and Examining the economic costs of the 2003 Halloween storm effects on the North Hemisphere aviation using flight data in 2019 (Xue et al., 2023).

Chapter 6 discusses the possibility of space weather events and the economic costs of other disasters, followed by the operational implication of GNSS integrity monitoring procedures.

Chapter 7 gives a complete summary of findings based on the studies in this thesis, as well as plans for future research.

Chapter 2

Communication Blackouts Effects on Air Traffic Management

Air traffic management relies on communications to send messages between the air and the ground promptly, which plays a significant role in ensuring flight safety. However, space weather can generate ionospheric disturbances that result in HF communication blackouts. This issue can significantly impact flight operations, particularly polar flights. This chapter studies the effects of HF communication blackouts on air traffic management and assesses the incurred economic cost.

2.1   Introduction

High-Frequency (HF, 3-30 MHz) radio waves can be reflected to Earth by the ionosphere, which is utilized for intercontinental communication. HF signals can be prevented from reaching the intended receivers by several factors, such as solar flares, ionospheric storms, geomagnetic storms, system failures, and frequency selection.

Satellite Communication (SATCOM) systems mainly use Very High Frequency (VHF, 30 to 300 MHz) and the lower portion of Ultra High Frequency (UHF, 300 MHz to 3 GHz), which can be impacted by even mild ionospheric scintillation. If ionospheric scintillation is more severe, the L-band (1-2 GHz) for civilian satellite communication systems will be affected, which is more prevalent when the signal goes through the equatorial ionosphere or the polar ionosphere. Solar radio bursts are capable of disrupting VHF, UHF, and L-band satellite communications. During the equinox, when geostationary satellites are near the Sun's direction at specific times of the day, this phenomenon is more apparent.

Aircraft generally use VHF to communicate with ground stations. To be specific, the Aircraft Communications Addressing and Reporting System (ACARS, 131.550 MHz) based on geostationary satellites is used to communicate between pilots and airlines (Smith et al., 2018), while the Controller Pilot Data Link

Communication (CPDLC, 118.000-136.975 MHz) is used to achieve the communications between pilots and Air Traffic Control Officers (ATCOs) (Lin et al., 2012). Polar flights departing from the origin airports communicate with ATC through VHF. Before the flights enter the polar region, pilots will switch to Arctic radio, which is responsible for delivering communications between aircrew and ground stations. Initial communications using Arctic Radio are often conducted on VHF, but pilots will soon migrate to HF. Although SATCOM can be a backup for communications, it will be unavailable poleward of 82 degrees latitude (Sauer and Wilkinson, 2008).

The ionosphere is utilized by several communication devices to reflect radio communication across long distances. During space weather events, radio signals will be absorbed, whilst others are reflected, resulting in fluctuating signals and unanticipated propagation pathways. If the consequences become particularly severe, total communication blackouts may be caused. Polar Cap Absorption (PCA) is a sort of disruption caused by SPEs, which may last for several days. When solar energetic particles enter the ionosphere over the pole regions, the increased ionization produced at these low ionospheric altitudes (50-100 km) would absorb HF radio signals, rendering HF communications in the polar regions impossible. The ICAO requires that aircraft maintain continuous and effective communications throughout their entire flight routes (ICAO, 2008). Consequently, flights need to reroute, resulting in additional flight time and fuel consumption. Delta Airline requires that all aircraft utilize HF radio as the primary mode of communication when flying in the area where the latitudes are higher than the latitude of waypoint ORVIT (79.00°N, 168.97°W). Figure 2.1 shows the detailed information (Delta, 2010).
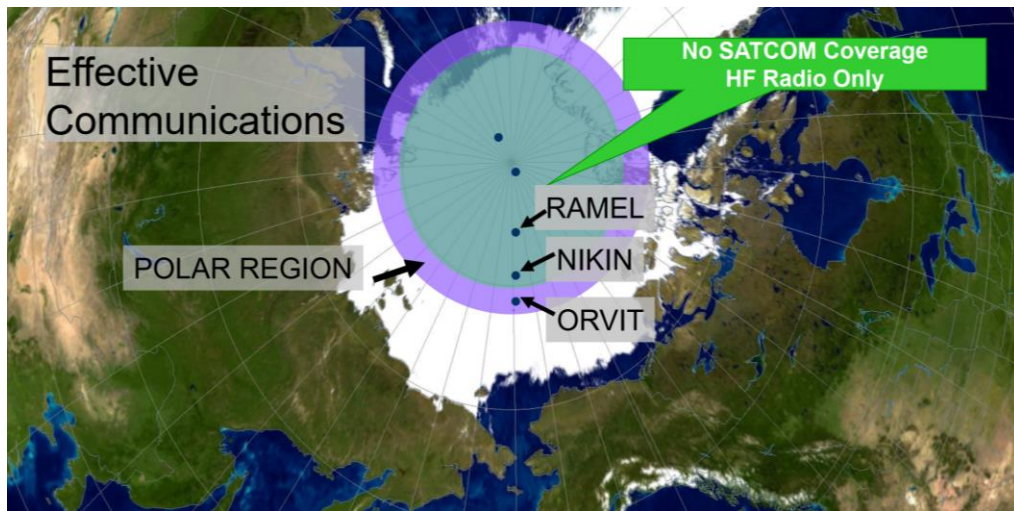
Figure 2.1. Polar region and waypoints (Delta, 2010).

2.2   Communication Blackouts

Multiple forms of space weather can influence HF radio transmission. In the normal course of space weather events, the initial effects are from the solar flares. The Sun's x-rays reach the ionosphere to a depth of around 80 kilometers above the Earth's surface, ionizing the atmosphere and raising the D layer of the ionosphere. As a result, the improved D-layer functions as both a reflector and an absorber of radio waves at different frequencies. Radio blackout caused by solar flares happens on Earth's dayside and is strongest when the sun is directly above. In addition, the Radiation Storm, which is associated with a solar proton event, may interfere with HF radio transmission. At the poles, the magnetic field of the Earth leads protons to smash with the upper atmosphere. The fast-moving protons have the same impact as the x-ray photons, enhancing the D-Layer and inhibiting HF radio communications at high latitudes. Electrons that precipitate during auroral displays can enhance other ionospheric layers and similarly disturb and impede radio transmission. This is more prevalent on the night side of Earth's polar regions, where the aurora is the brightest and most frequent (Cameron et al., 2022; Neal et al., 2013). PCA can disrupt HF communications in the polar regions, and therefore aircraft in the polar regions cannot communicate with HF radio. On the sunlit side of the Earth, solar flares can disable HF communications for a few hours, while solar radiation storms can affect HF radios for several days (Rutledge

and Desbios, 2018), depending on the size and location of the eruptions on the Sun. Consequently, polar flights are required to reroute to latitudes below 82° to keep the line of sight with the satellites (National Research Council, 2008). Figure 2.2 depicts a schematic of HF communication failure caused by space weather. Variations in the density and structure of the ionosphere can completely impede the HF radio transmissions, which are used by commercial flights.
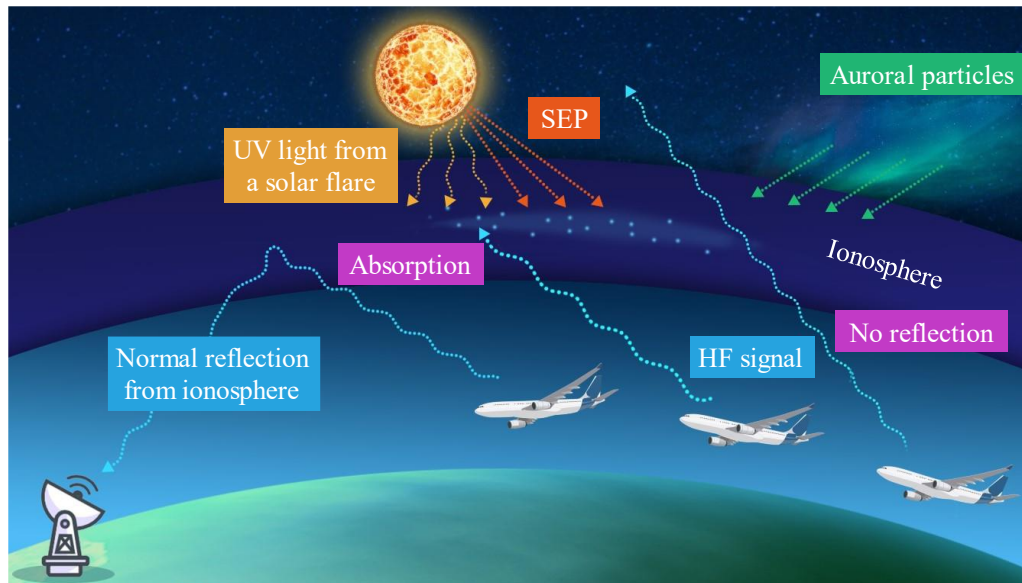
Figure 2.2. HF communication blackout caused by solar flares and SEP.

According to the ICAO Manual on Space Weather Information in Support of International Air Navigation (ICAO Doc 10100) (ICAO, 2018b), the space weather advisories about HF communication degradation are provided as follows.

Inflight or enroute

 HF MOD (moderate): Examine the conditions on all local frequencies and select the optimal one.

 HF SEV (severe): List the optimal HF frequencies. Ensure SATCOM is available. No aircraft should be dispatched to locations where HF is the primary mode of communication.

Dispatch or before departure

 HF MOD: Examine the conditions on all local frequencies and select the optimal one. If necessary, use datalink or SATCOM voice.

 HF SEV: No aircraft should be dispatched to locations where HF is the

primary mode of communication. Consider adding 30 minutes of extra fuel.

2.3   Economic Cost Caused by HF Communication Blackouts

From 19 October 2003 to 5 November 2003, communication disruption occurred every day, posing a threat to regular flight operations (Horne et al., 2005; Pulkkinen et al., 2005). Following an X1.1 (R3 [Strong]) solar flare during 16:29-17:04 UT on 19 October 2003 (see Figure 2.3), HF service was impaired for more than two hours, causing three polar trips (New York-Hong Kong) rerouting to more favorable datalink and Satellite Communication (SATCOM) routes, which resulted in the additional consumption of 26,600 pounds of fuel and the confiscation of over 16,500 pounds of cargo (NOAA, 2004). In addition, additional staff was required to handle air traffic due to poor communications on October 30 (NOAA, 2004).
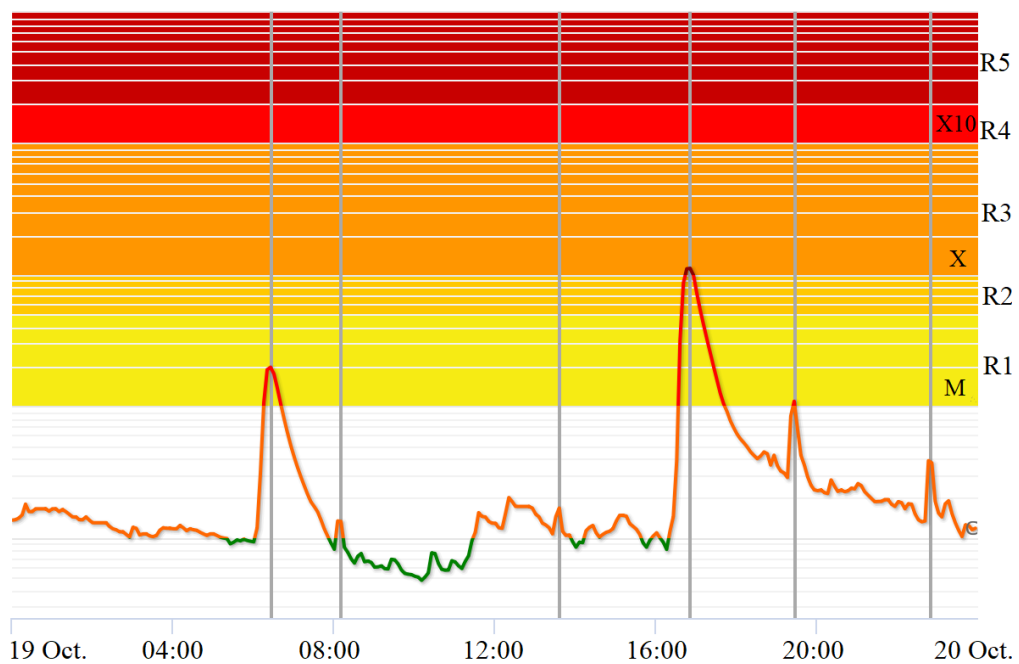
Figure 2.3. GOES X-ray satellite 1-minute solar X-ray average in the 1-8 Angstrom passband.

(https://www.spaceweatherlive.com/en/archive/2003/10/19/xray.html)

In response to the communication blackout, airborne flights would reroute to the destination airport or land at an alternative airport, but those flights on the ground would probably not be allowed to take off as scheduled (Cannon et al., 2013). Although airlines can reroute flights with the assistance of Air Navigation Service Providers (ANSPs) to avoid the PCA region, it has several drawbacks from the viewpoint of air traffic management. First, rerouting always causes increased fuel consumption, aircraft emissions, and additional wear and tear on aircraft, which can disturb normal aircrew schedules and contradict the green aviation concept. Second, the temporary or unauthorized flight routes will infringe on the sovereignty of the airspace. Third, communication blackouts are always accompanied by increased cosmic radiation exposure, which can pose a threat to the health of aircrew and passengers. Due to the aforementioned three reasons, airlines would like to cancel polar flights justifiably, notwithstanding the associated cancellation costs (Yamashiki et al., 2020).

We assume that a space weather event as strong as the Halloween storm will cause the cancellations of polar flights for one entire day due to communication blackouts. To quantify the costs associated with cancellations, the historical flight data on 7 April 2019 is adopted in this simulation, which includes a total of 48 polar flights, 38 flights of 400 seats, 3 flights of 250 seats, and 7 flights of 180 seats. Figure 2.4 depicts the polar flight routes via the Arctic. Please note that we do not consider polar flights via the Antarctic because no airline has scheduled such a route. Space weather is classified as extraordinary circumstances, so airlines are not required to compensate passengers. According to Table 2.1, the projected daily cost of polar flight cancellations is about €2.20 million per day ((120,830-68,390)×38+(82,730-42,740)×3+(24,900-13,090)×7). If all polar aircraft were to be rerouted, the total increased fuel cost would be €0.21 million (26,600×0.4536÷3×48×1.139) based on the additional fuel consumption caused by flight rerouting (rerouting three polar flights causes an additional fuel consumption of 26,600 pounds) (NOAA, 2004) and the price of €1139 per ton of fuel (IATA, 2022).
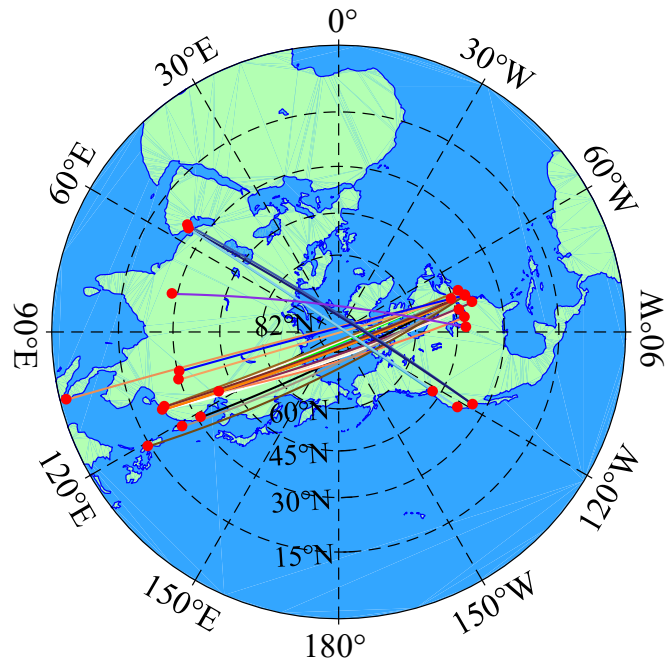
Figure 2.4. Polar flight routes. The red dots denote airports. Arctic polar routes are now common to airlines connecting Asia to North America.

Table 2.1. EUROCONTROL recommended flight cancellation costs (EUROCONTROL, 2020).

Cancellation cost (€)	Narrow-body aircraft			Wide-body aircraft	
Seats	50	120	180	250	400
Value (€)	6,540	16,040	24,900	82,730	120,830
within passenger care and compensation (€)	3,280	8,020	13,090	42,740	68,390

2.4   Summary

Aircraft communications mainly rely on the VHF, but HF communication is the only means of communication when flights fly over the poles. Space weather can cause HF communication blackouts, affecting normal flight operations in the polar region. In response, airlines may choose to cancel flights or reroute to low-latitude airspace to achieve the SATCOM. To estimate the economic cost of HF communication blackouts, we simulated a scenario by assuming an extremely strong space weather event like the 2003 Halloween solar storm would have

occurred in 2019. The results show that possible daily economic costs could range from €0.21 million to €2.20 million caused by polar flight rerouting and cancellations.

Chapter 3

Satellite Navigation Failure Effects on Air Traffic Management

Navigation is the base of the aircraft's safe and efficient flying. Generally, navigation methods include ground navigation and satellite navigation. Space weather can degrade GNSS and lead to satellite navigation failure, and consequently affect flight operation. This chapter describes the causes of satellite navigation failure in detail and quantifies the incurred economic costs based on simulated scenarios.

3.1   Introduction

Traditional ground-based navigational aids, such as VOR, DME, and NDB, are widely used in the terminal control area of some major airports. In the concept of CNS/ATM, satellite-based navigation via the GNSS will replace the traditional ground navigation system as the primary source for aircraft navigation (Blanch et al., 2012), as GNSS can provide more accurate lateral and vertical guidance during enroute, terminal, and approach phases. Satellite-navigation-based aircraft can even land on runways in poor meteorological conditions (Lee et al., 2016), and fly along any desired flight paths instead of the traditional less efficient routes between two ground-based radio navigation points (Enge et al., 2015). Therefore, runway and airspace capacity can be improved due to the highly accurate and reliable real-time, three-dimensional aircraft position.

GNSS is anticipated to offer aviation users extended satellite-based navigation. In particular, the Wide Area Augmentation System (WAAS) started to work in 2003 through the deployment of the GNSS Approach with Vertical Guidance (APV), providing aircraft with vertical guidance during the final approach phase even in poor visibility conditions. The GPS service in WAAS is augmented based on time correction, satellite orbit correction, and ionospheric correction. As a result, the WAAS system can satisfy rigorous aviation standards for accuracy, availability,

and reliability. The schematic diagram of satellite-based air traffic management is shown in Figure 3.1.
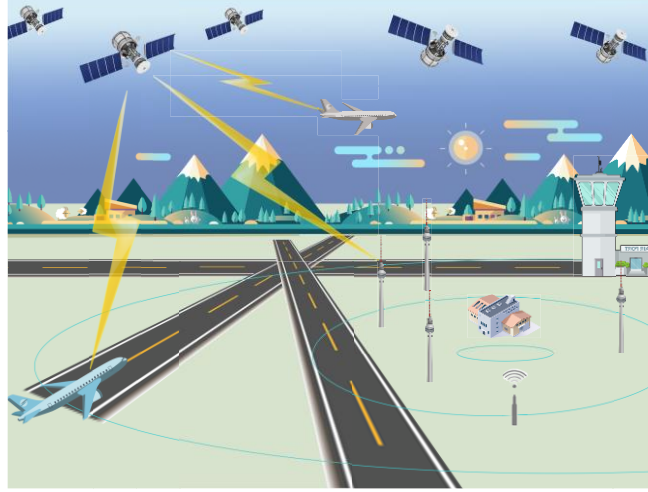
Figure 3.1. Schematic diagram of satellite-navigation-based air traffic management.

The operation of GNSS is based on the trilateration mathematical principle. The accuracy of GNSS positioning depends on many factors, such as satellite clock error (Guo and Geng, 2018), satellite orbit error (Zhang et al., 2019), ionospheric delay (Yu and Liu, 2021b), tropospheric delay (Chen and Liu, 2015), receiver noise (Kim et al., 2019), and multipath effect (Sun et al., 2019). The main observation in GNSS positioning is the pseudorange measurements $\tilde{\rho}$ from the receiver (r) to the satellite (s) (Langley et al., 2017):

$$\tilde{\rho} = \rho + c(\Delta t_r - \Delta t^s) + \Delta\rho_I + \Delta\rho_T + \varepsilon \tag{3.1}$$

where ρ is the geometric distance between the satellite and the receiver; c is the speed of light in vacuum; Δt_r is the offset of the receiver clock to GNSS time at signal reception time; Δt^s is the offset of the satellite clock to GNSS time at signal emission time; $\Delta\rho_I$ is the ionospheric delay correction; $\Delta\rho_T$ is the tropospheric delay correction; ε is the measurement error of the observation. Among these errors, the ionospheric delay is the most important factor ranging from a few meters to tens of meters or even hundreds of meters (Hoque and Jakowski, 2012; Yang et al., 2020). When GNSS signals propagate in the ionosphere, the

propagation speed is different from that in the vacuum. In addition, spatial gradients in the refractive index cause a propagation curve. Both effects can lead to increased vulnerability and degraded accuracy in satellite-based positioning and navigation. The ionospheric delay error is proportional to the ionospheric total electron content (TEC) along the propagation path and inversely proportional to the square of the radio frequency f, which can be expressed as follows:

$$\Delta\rho_I = -\kappa\frac{TEC}{f^2} \qquad (3.2)$$

where $\kappa \approx 40.3\ m^3 s^{-2}$, f is the radio frequency (in Hz), and TEC is the total number of electrons integrated between two points along a tube with a one-meter square cross section, measured in TEC units (1 TECU=10^{16} electron/m^2) ([Hoque and Jakowski, 2012](#)).

3.2   Satellite Navigation Failure

The increased TCE and irregularities in the ionosphere caused by space weather can lead to ionospheric scintillation ([Kintner et al., 2007](#)). Severe scintillation circumstances can make it difficult to determine a position and prohibit a GNSS receiver from grabbing onto the signal ([Seo et al., 2009](#)). Less severe scintillation circumstances may cause positioning results to be less accurate and confident ([Xu et al., 2015](#)). Figure 3.2 illustrates the impacts of ionospheric scintillation of GNSS ([Peng and Scales, 2021](#)).
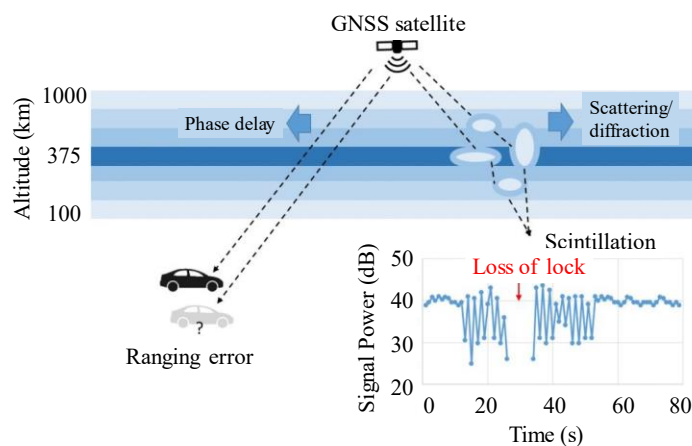
Figure 3.2. An illustration of ionospheric impacts on GNSS ([Peng and Scales, 2021](#)).

Airspace management is dependent on the increased use of GNSS for airplane navigation to minimize aircraft separation, position aircraft on approach, and land in all weather conditions. Nevertheless, ionospheric disturbances caused by solar and geomagnetic activity impact the accuracy of satellite signals. Currently, GNSS can provide aircraft with a positioning accuracy of 5-20 meters in calm geomagnetic conditions, which is insufficient for aircraft landing (Sharma and Hablani, 2014). This is because GNSS satellite signals are affected by several errors including satellite clock error (Guo and Geng, 2018), satellite orbit error (Zhang et al., 2019), tropospheric delay error (Ziv et al., 2021), receiver noise (Kim et al., 2019), multipath (Sun et al., 2019), and ionospheric error (Yu and Liu, 2021a, b). Specifically, the positioning error caused by the ionosphere is one of the most important factors and it is heavily affected by geomagnetic storms, one kind of the most intense space weather events. The electric field, neutral wind, and its composition in the ionosphere can be strongly disturbed during geomagnetic storms. The low-latitude ionosphere is especially vulnerable due to the equatorial plasma fountain effect (Tsurutani et al., 2004), which lifts the plasma to higher altitudes by an eastward electric field and generates enhanced ionization regions on the sides of the magnetic equator as the particles slide down along magnetic field lines. Figure 3.3 shows the schematic of the effects of ionospheric storm on aviation operations.
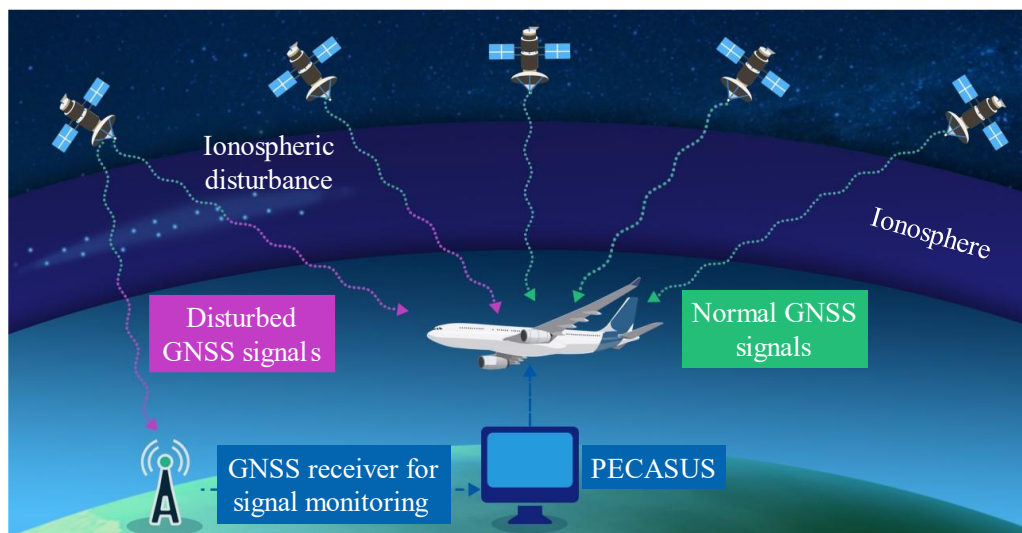
Figure 3.3. Schematic of the effects of the ionospheric storm on aviation operation.

Geomagnetic storms with minimum Dst <-250 nT are usually denoted as super storms (Astafyeva et al., 2014). Several super storms occurred in the past such as those on 13 March 1989, 15 July 2000, and 29 October 2003 with the minima Dst=-589, -300, and -383 nT, respectively. The ionospheric storms in October 2003 caused vertical navigation guidance unavailable for aircraft precisely approaching for a long time throughout most of the United States, leading to considerable societal and economic consequences. The non-availability of vertical service in WAAS on 29 October 2003 is shown in Figure 3.4 (National Research Council, 2008).
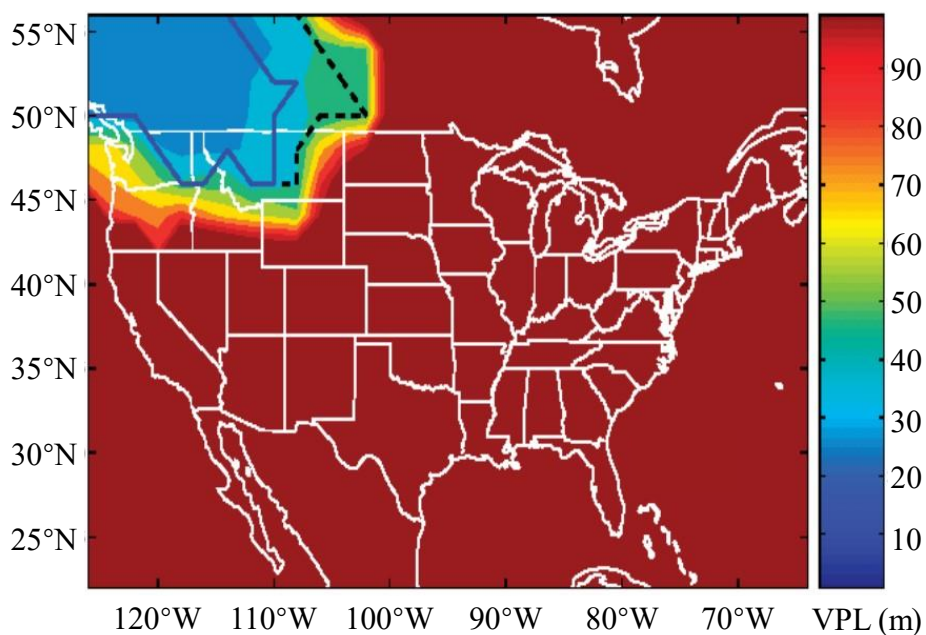
Figure 3.4. WAAS vertical service non-availability at the height of the storm on 29 October 2003 (National Research Council, 2008).

The ionospheric correction for single-frequency GNSS receivers usually uses a thin shell model, which considers the three-dimensional ionosphere to condense on a two-dimensional thin shell (Huang and Yuan, 2013). The accuracy of positioning using the thin shell model is generally acceptable. However, during periods of considerable ionospheric disturbance, the thin shell model may be insufficient to describe the more complex three-dimensional fluctuations, resulting in decreased positioning accuracy and possible loss of integrity. GNSS positioning performance can be severely degraded during strong space weather

33

periods, as illustrated in Table 3.1. Coster and Yizengaw (2021) summarized the effects of geomagnetic storms in three categories: (1) large gradients in ionospheric electron density can cause significant range errors and bend (Hoque and Jakowski, 2011); (2) small-scale irregularities in the ionosphere can cause GNSS signal fluctuations (or scintillation) or even loss of lock; and (3) solar radio bursts can also cause notable effects on GNSS signals by raising the background noise level (Cerruti et al., 2008). Therefore, to reduce the degradation effects of space weather on the ionosphere, the ionospheric TEC forecast is vitally important (Cesaroni et al., 2020; Tsagouri et al., 2018).

Table 3.1. Cases of large GNSS positioning errors caused by space weather events.

Time	Geographical location	Condition	Minimum Dst	Positioning errors	Source
7-8 Sept. 2017	78.2°N, 16.0°E	Intense geomagnetic condition	-122 nT	Increase from 2 meters to 6 meters at Longyearbyen, Norway	(Linty et al., 2018)
Sept. 2002 to Apr. 2003	13.7°N, 100.8°E	S_4 (~0.6)	-181 nT	Exceed 10 meters at KMLT, Thailand	(Phoom chusak et al., 2013)
Jan. to Dec. 2001	19.6°N, 99.5°E	S_4 (>0.7)	-387 nT	Reach 14 meters in longitude and 22 m in latitude at Chiang Rai, Thailand	(Dubey et al., 2006)
Apr. 2004	3.0°S, 40.2°E	Severe ionospheric scintillation	-117 nT	Reach 4 meters in vertical components at Malindi, Kenya	(Moren o et al., 2011)

Note: The S_4 index is derived from the detrended signal intensities of GNSS signals.

Because the ground navigation systems such as the Instrument Landing System (ILS) are widely utilized worldwide to provide accurate lateral and vertical

approach guidance ([Kim and Choi, 2016](#)), flights have never officially suffered a landing failure despite low GNSS positioning performance in space weather circumstances. However, ATM is transitioning from ground-based navigation to satellite-based navigation to meet the expected growth of flight demands. Satellite-based navigation will become more common in the future. If a severe geomagnetic storm occurs, GNSS positioning errors will increase due to the increased ionospheric impacts, particularly in the low-altitude regions. As a result, aircraft cannot perform a safe approach or land solely based on satellite navigation, causing flight delays, flight diversions, and flight cancellations ([Pejovic et al., 2009](#)). According to ICAO Manual on Space Weather Information in Support of International Air Navigation (ICAO Doc 10100) ([ICAO, 2018b](#)), the space weather advisories about GNSS degradation are provided as follows.

Inflight or enroute

GNSS MOD: Pilots need to verify additional navigation methods such as DME, NDB, and VOR; check RNAV/RNP-capability and requirements; check if conventional approach procedures at destination and alternate may be employed and prepare appropriately.

GNSS SEV: Pilots need to verify additional navigation methods such as DME, NDB, and VOR; check if conventional approach procedures at the destination and alternate may be employed and prepared appropriately. Ensure the accessibility of the intended route/RNAV/RNP. Consider making a diversion and landing at an available airport.

Dispatch or before departure

GNSS MOD: Pilots need to verify additional navigation methods such as DME, NDB, and VOR. Ensure the accessibility of the intended route/RNAV/RNP. Check whether standard approach procedures can be employed at the destination and alternate, then prepare the second alternate. Consider adding 30 minutes of extra fuel for unanticipated circumstances.

GNSS SEV: Pilots need to verify additional navigation methods such as DME, NDB, and VOR. Check whether standard approach

procedures can be employed at the destination and alternate, then prepare the second alternate. Check the availability of airspace and routes (RNAV/RNP). Consider including a 1-hour fuel reserve for unanticipated circumstances. Consider flight cancellations.

3.3   Economic Cost Caused by Satellite Navigation Failure

Under normal circumstances after sunset, the recombination of free electrons and positive ions reduces the background ionization. However, during space weather events, plasma density structures displaying substantial TEC gradients remained for many hours into the night after the sunsets. Ionospheric irregularity occurring on the morning of 31 October 2003 had TEC levels that were more than 60 TECU. This intense plasma formation arose over northern Florida and was subsequently designated the Florida Event. Figure 3.5 illustrates the temporal and spatial distribution of TEC at 00 UCT on 31 October 2003.
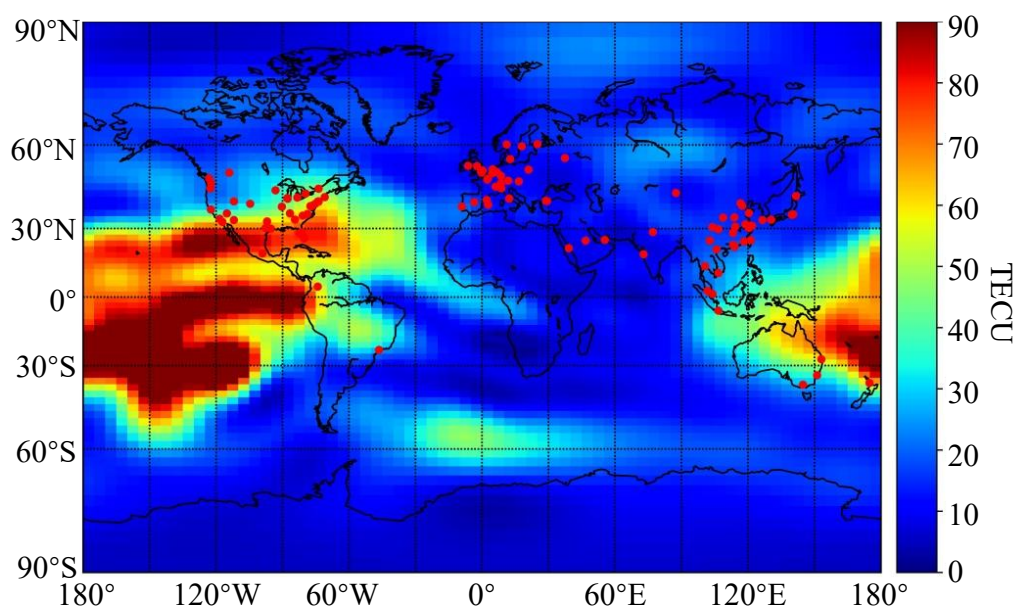
Figure 3.5. TEC map at 00:00 UTC on 31 October 2003. Data source: Global Ionosphere Maps (GIM).

According to (Doherty et al., 2004), the WAAS was affected severely by the Halloween storm in 2003, prohibiting aircraft from utilizing WAAS for precise approaches in Continental United States (CONUS). The greatest effect of the

ionospheric storm on WAAS was the loss of Localizer Performance with Vertical Guidance (LPV) service. LPV service was stopped for ~15 hours from 17:00 UTC on 29 October 2003 to 8:00 UTC on 30 October 2003. The second LPV service disruption lasted ~11.3 hours from 19:00 UTC on 30 October 2003 to 6:20 UTC on 31 October 2003. (FAA/William J. Hughes Technical Center, 2004)

In this thesis, we focus on the top 50 busiest airports in the CONUS and select corresponding Continuously Operating Reference Stations (CORS) to quantify the GNSS positioning errors. Figure 3.6 shows that positioning errors of nine GNSS stations are correlated with the Dst index. It is required that GPS Standard Position Service (SPS) positioning errors for aviation operations should not exceed 17 m horizontally and 37 m vertically (ICAO, 2018a). As a result, we can calculate the duration of satellite navigation failure (Table 3.2). Due to onboard data restrictions, we characterize satellite navigation failure only in terms of accuracy rather than integrity, continuity, or availability. The affected airports are denoted 'Y' in Figure 3.7 based on the Single Point Positioning (SPP) method results.
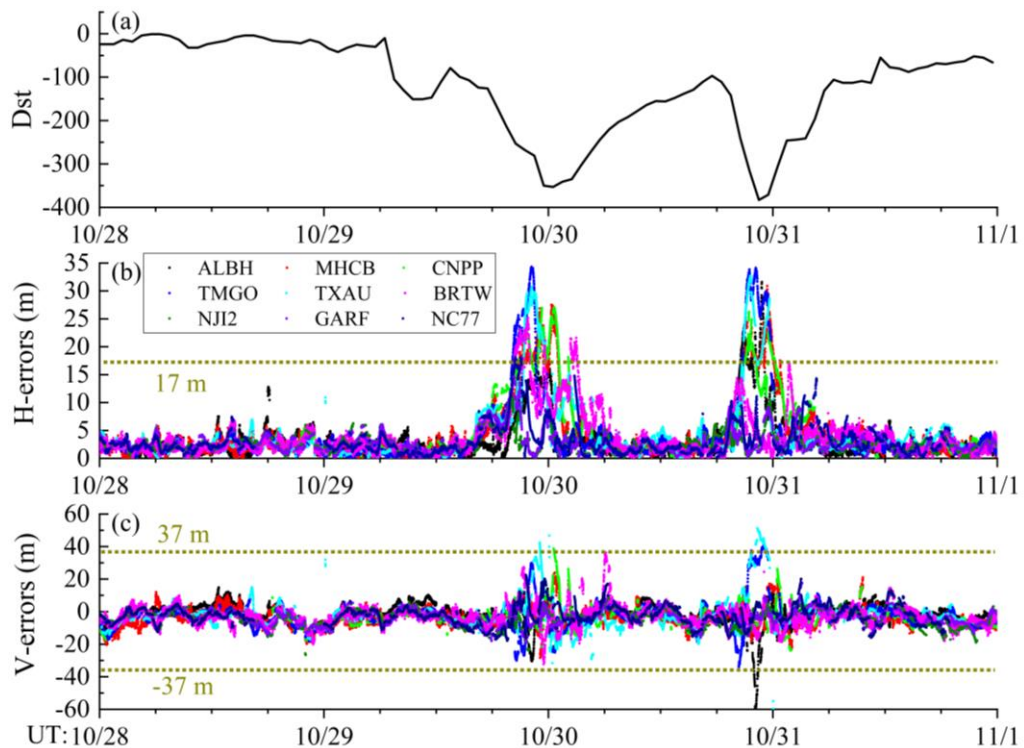
Figure 3.6. (a) The time-series Dst, (b) GNSS positioning horizontal errors, and (c) GNSS positioning vertical errors of nine CORS.

37

Table 3.2. Satellite navigation failure duration (in the form of DDHHMM) of each GNSS station.

ICAO code	City	CORS Code	Lat °N	Lon °W	Satellite navigation failure duration
KPDX	Portland	ALBH	48.39	123.49	292237-300007 (90 min) 302032-302307 (155 min)
KSEA	Seattle	ALBH	48.39	123.49	292237-300007 (90 minutes) 302032-302307 (155 minutes)
KSFO	San Francisco	OHLN	38.01	122.27	292056-300104 (248 minutes) 302048-310005 (197 minutes)
KOAK	Oakland	OHLN	38.01	122.27	292056-300104 (248 minutes) 302048-310005 (197 minutes)
KSJC	San Jose	MHCB	37.34	121.64	292054-300104 (250 minutes) 302050-310008 (198 minutes)
KSMF	Sacramento	SUTB	39.21	121.82	292059-300058 (239 minutes) 302040-302359 (199 minutes)
KLAX	Los Angeles	TORP	33.80	118.33	292045-300112 (267 minutes) 302054-310025 (211 minutes)
KSNA	Santa Ana	CNPP	33.86	117.61	292043-300109 (266 minutes) 302052-310015 (203 minutes)
KSAN	San Diego	BILL	33.58	117.06	292045-300040 (235 minutes) 302053-310015 (202 minutes)
KLAS	Las Vegas	BKAP	35.29	116.08	292046-300049 (243 minutes) 302052-310043 (231 minutes)
KPHX	Phoenix	AZGB	33.40	110.77	292020-300044 (264 minutes) 302051-310107 (256 minutes)
KSLC	Salt Lake City	TMGO	40.13	105.23	292008-292241 (153 minutes) 302045-302348 (183 minutes)
KDEN	Denver	TMGO	40.13	105.23	292008-292241 (153 minutes) 302045-302348 (183 minutes)
KSAT	San Antonio	TXAN	29.49	98.58	292124-292349 (145 minutes) 302051-302345 (174 minutes)
KAUS	Austin	TXAU	30.31	97.76	292120-292344 (144 minutes) 302054-302340 (166 minutes)
KDEW	Dallas	TXAU	30.31	97.76	292120-292344 (144 minutes) 302054-302340 (166 minutes)
KIAH	Houston	TXAU	30.31	97.76	292120-292344 (144 minutes) 302054-302340 (166 minutes)
KHOU	Houston	TXAU	30.31	97.76	292120-292344 (144 minutes) 302054-302340 (166 minutes)
KMSY	New Orleans	TXAU	30.31	97.76	292120-292344 (144 minutes) 302054-302340 (166 minutes)
KTPA	Tampa	BKVL	28.47	82.45	292021-292200 (99 minutes) 300219-300304 (45 minutes)
KRSW	Fort Myers	NAPL	26.15	81.78	292024-292208 (104 minutes) 300207-300332 (85 minutes) 300600-300612 (12 minutes)

					302119-302131 (12 minutes)
KJAX	Jacksonville	PLTK	29.66	81.69	292019-292155 (96 minutes) 292337-292346 (9 minutes) 300159-300303 (64 minutes) 310155-310204 (9 minutes)
KMCO	Orlando	BRTW	27.95	81.78	292020-292201 (101 minutes) 292330-292341 (11 minutes) 300221-300307 (46 minutes)
KMIA	Miami	MTNT	25.87	80.91	292024-292207 (103 minutes)
KFLL	Miami	MTNT	25.87	80.91	292024-292207 (103 minutes)
KPBI	Palm Beach	OKCB	27.27	80.86	292021-292159 (98 minutes) 300224-300301 (37 minutes)
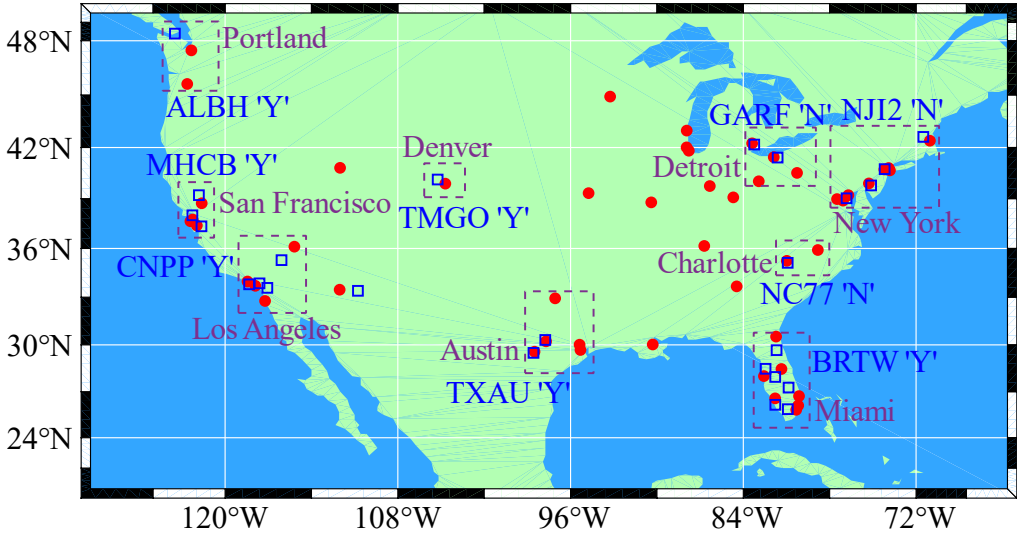
Figure 3.7. Locations of the top 50 busiest airports (red circles) and International GNSS Service (IGS) stations (blue squares) in the CONUS. The areas affected by satellite navigation failure are labelled with 'Y'. Otherwise, labelled with 'N'.

The traditional ground-based navigational aids, such as VOR, DME, and NDB, will be employed as a backup in the absence of GNSS-based navigation. The flight distance and time will rise since ground navigational routes are typically curved due to the outage of Area Navigation (RNAV). Taking the Jackson Hole airport as an example, the flight route based on ground navigation is 14 miles and 3 minutes longer than the satellite navigation router (Enge et al., 2015). According to the Base of Aircraft Data (BADA) (Nuic, 2010), it would take an average of 105 kg of fuel for each aircraft during a three-minute approaching flight. Besides, satellite

navigation failure will hinder the Continuous Descent Approach (CDA), which will increase fuel consumption by 147 kg during the descent phase for each flight at the Hartsfield-Jackson Atlanta International Airport (Cao et al., 2014). Figure 3.8(a) illustrates the comparison between RNAV and conventional flight routes. Aircraft can fly directly from one waypoint to another waypoint based on satellite navigation. However, aircraft have to fly along the ground navigation aids without satellite navigation. Figure 3.8(b) shows that aircraft can achieve CDA from cruise altitude to the runway in a smooth glide trajectory using low power based on satellite navigation, reducing fuel consumption and noise pollution. During satellite navigation failure, step down approach will minimize the volume of protected airspace around the airport.
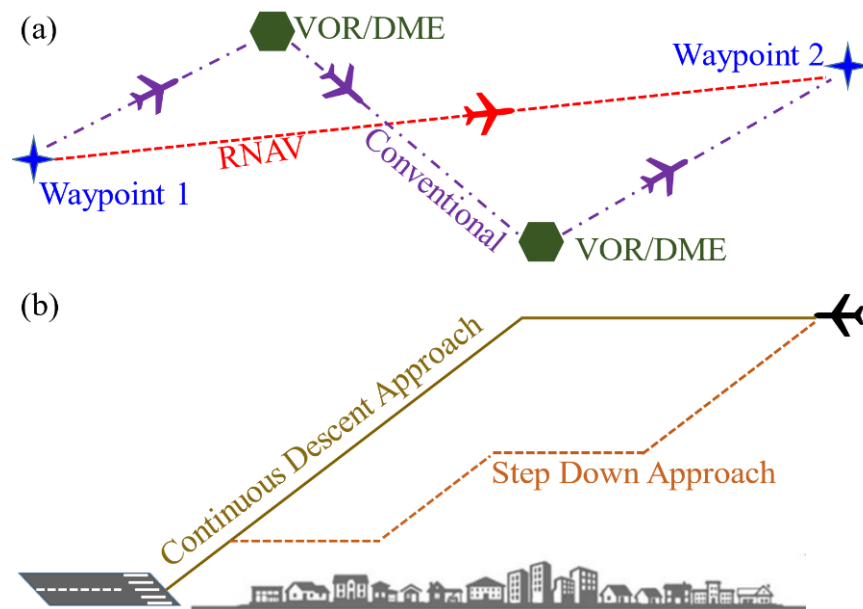
Figure 3.8. The schematic of RNAV and CDA.

The induced economic costs are assessed from the perspectives of several stakeholders, including airlines, passengers, and the environment. The fuel cost is the top expenditure of airlines (Wen et al., 2022), with fuel price C_F=€1139/ton (IATA, 2022). Passengers need to spend more time in flight. For a typical B757 configuration with an occupancy of 80%, the unit time cost for all onboard passengers C_T is equal to €93/min (Xue et al., 2022a). Additionally, environmental impacts such as the greenhouse effect of CO_2 are significant. The social cost of

CO₂ is C_{CO_2}=€417/ton ([Ricke et al., 2018](#)). On average, aircraft burning 1 kg of fuel will emit 3.15 kg of CO₂ during flight ([Xue et al., 2021b](#)). Therefore, the average total induced cost for one aircraft is $\Delta C = C_F \cdot \Delta F + C_T \cdot \Delta T + C_{CO_2} \cdot \Delta CO_2$=€897, with fuel cost (€287), time cost (€279), and environmental cost (€331). There was a total of 17,922 flights arriving at these top 50 busiest airport on 7 April 2019 (UT). Based on satellite navigation failure durations in Table 3.2, we can conclude that 2,705 flights would be affected during the whole space weather events, leading to an economic cost of €2.43 million.

3.4 Satellite navigation failure effects on future aviation

CNS/ATM, which is replacing traditional ATM, depends on precise GNSS navigation service, especially during the final approach and landing stages. But if there is severe space weather, there may be a substantial increase in TEC and irregularities in the ionosphere, which can increase GNSS positioning errors. As a consequence, satellite navigation mode will be replaced by ground navigation mode, lowering the airport acceptance rate and causing an imbalance problem between flight demands and airport capacity. To solve this problem, some ATM methods are necessary, such as flight rescheduling and flight cancellations. As one of the busiest airports in the world, Hong Kong International Airport (HKIA) is located in the equatorial ionosphere anomaly region and is prone to space weather effects. In this study, we used the predicted flight data from the HKIA during a simulated geomagnetic storm to create a hypothesis scenario. Calculations show that if there is not an ionospheric delay forecast, the costs of flight delays, flight cancellations, and flight rerouting could be more than €2 million. If the lead time of ionospheric delay forecast can be increased, these related economic costs will decrease significantly. Besides, an inaccurate ionospheric delay forecast can also cause significant costs.

3.4.1 Scenario assumptions and air traffic management methodology

As shown in Figure 3.9(a), a two-dip intense geomagnetic storm occurred during 8-11 September 2017, with the minima Dst = -122 nT at Hong Kong 10:00 local time (LT) on 8 September and -109 nT at 01:00 LT on 9 September. Figure 3.9(b) shows that there was a sharp increase in the ionospheric TEC towards ~12:00 LT.

The two vertical lines denote T_s=09:00 LT and T_e=16:00 LT on 8 September 2017. The ionospheric delay error τ (in the unit of meters) is proportional to the TEC and can be calculated using Eq. (3.2). The ionospheric delay reaches the maximum (~4.8 m) at 12:00 LT on 8 September 2017. We assume a space weather event like the 8-11 September 2017 one to occur in the future. We will study the elevated satellite-based positioning errors resulting from such a space weather event, and the consequent impact on the operational capacity at HKIA.
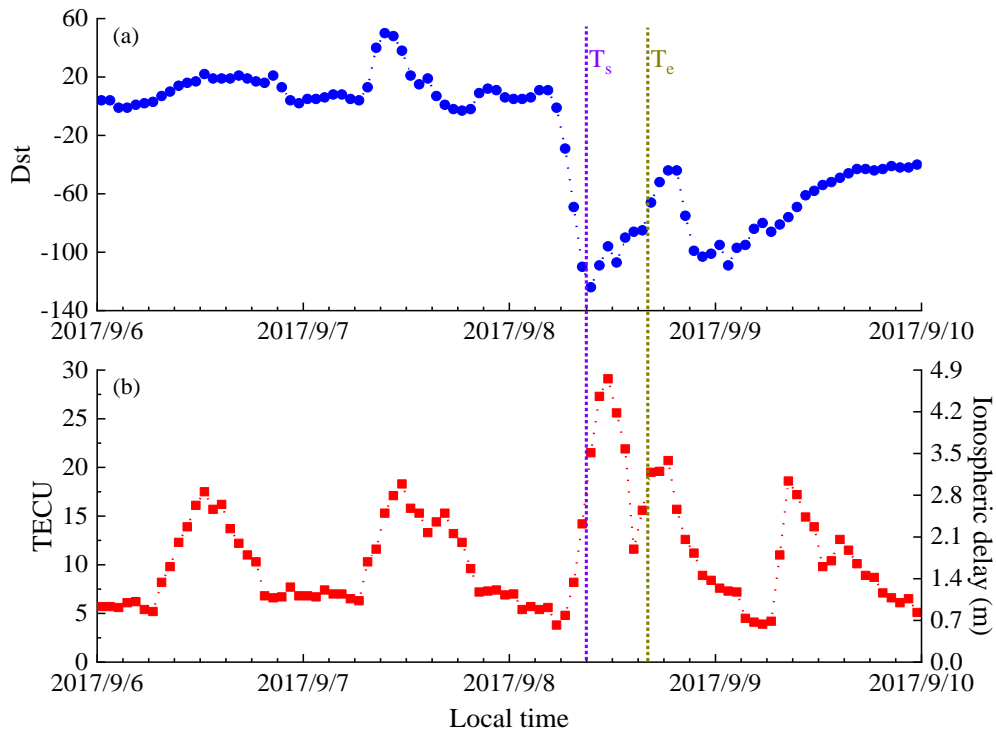
Figure 3.9. (a) The provisional Dst and (b) the TEC variation and ionospheric delay in the Hong Kong area during an intense geomagnetic storm.

We can obtain the flight data during the 8-11 September 2017 geomagnetic storm. However, no data about the aircraft final approach and landing failure caused by GNSS positioning errors are available to us. We will base our study on a projection of the future flight demand at the HKIA, and the steps for simulating the future flight demand are as follows. The hourly arrival flight demand is first captured using flight data from the HKIA on 8 September 2019. Then, based on an annual growth rate of 5% in the Asia Pacific region for passenger air traffic from 2019 to 2040 (Mazareanu, 2021), the hourly arrival demand in 2030 is estimated.

Considering the landing separation standards, the landing time of arrival flights is simulated together with other information, such as callsign, scheduled departure time, planned enroute time, scheduled landing time, etc. Figure 3.10 depicts the historical and predicted hourly arrival demand of the HKIA.
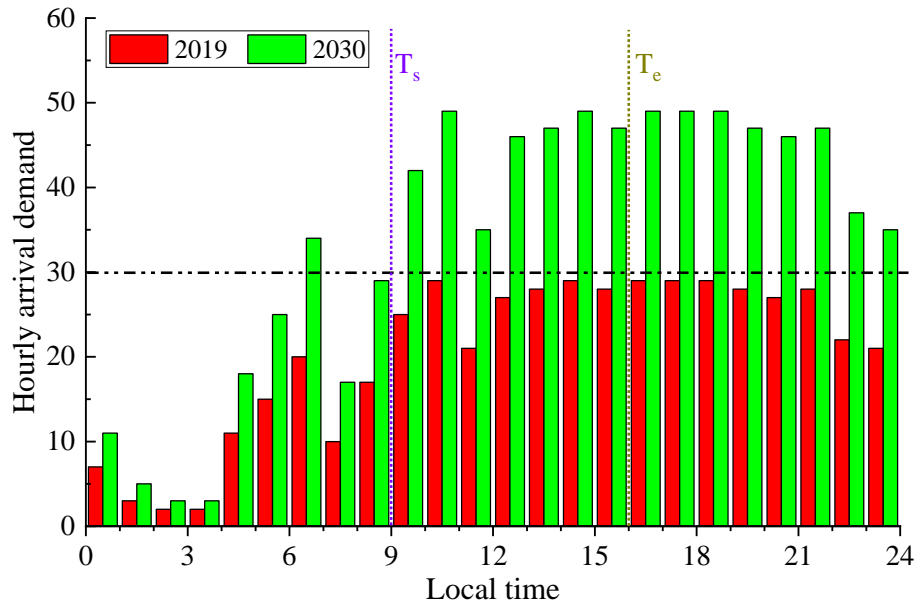
Figure 3.10. The red histograms denote the hourly arrival demand of the HKIA on 8 September 2019. The green histograms denote the predicted hourly arrival demand in the year 2030.

Currently, the airport acceptance rate (AAR), which is defined as the number of flights allowed to land at a given airport within one hour (Mukherjee et al., 2012), is 30, i.e. two-minute arrival slot interval for a single-runway airport (ICAO, 2016a). This is based on the ground navigation system such as the ILS. Considering the limitation of AAR based on ground navigation and booming flight demand, the ICAO introduced satellite navigation to boost airspace capacity and flight efficiency by lowering minimum separation standards. With satellite navigation, the AAR is assumed to be 60, with a one-minute arrival slot interval.

We assume that ground navigation will be used to replace satellite navigation during the final approach and landing phases between T_s=09:00 and T_e=16:00 LT during such a geomagnetic storm when the space weather impact is substantial. Thus, AAR will be reduced from 60 to 30 during the period T_s to T_e. Figure 3.10

43

shows that during peak hours, the estimated arrival demand exceeds 30 flights per hour, implying that some arrival flights may need to be rescheduled (including delay, cancellation, and diversion). The assumptions for the simulated scenario are summarized in Table 3.3. In our study, we also assume the departure flights from the airport will not be affected by space weather, since the aircraft does not rely on GNSS navigation to take off.

Table 3.3. Summary of key assumptions.

Index	Explanation
Arrival flight demand	Predicted arrival demand in green histograms of Figure 3.10.
Airport arrival rate	60 per hour based on satellite navigation.
Satellite navigation failure time	09:00-16:00 LT.

There will be an imbalance between arrival flight demands and airport capacity when the navigation mode switches from satellite navigation (AAR=60) to ground navigation (AAR=30). Ground Delay Programs (GDP) (Glover and Ball, 2013), which is a safe and cost-effective means of shifting predicted airborne delay to ground delay, is the most comprehensive traffic flow management strategy for solving such an imbalance problem. From the standpoint of fairness among different airlines, the arrival time for each flight is assigned in the ascending order of the Original Time of Arrival (OTA) (Vossen and Ball, 2006), i.e., flights having earlier OTAs receive an earlier Controlled Time of Arrival (CTA) than flights with later OTAs. Figure 3.11 demonstrates the change in the arrival flight schedule.
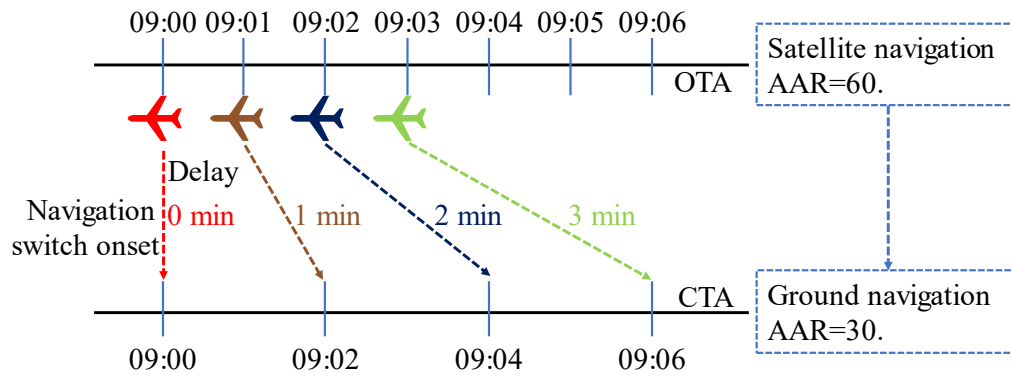
Figure 3.11. Switch from satellite-navigation-based arrival flight schedule (upper time axis: every one minute) to ground-navigation-based arrival flight schedule (lower time axis: every two minutes).

We design a revised air traffic management rule based on whether or not the ionospheric delay can be forecast. This can also be interpreted as whether or not the duration of satellite navigation failure can be forecast.

Condition 1: without ionospheric delay forecast.

If we are unable to forecast the large ionospheric error caused by space weather events, air traffic controllers (ATCs) are informed only when the space weather event commences at T_s. The rescheduling rules are thus as follows.

(1) Flights with OTD/OTA (OTD: Original Time of Departure) before T_s depart from their original airports and land at HKIA as scheduled.

(2) Because airborne flights have a higher priority of landing than the ones on the ground, ATCs assign CTA for each airborne flight in ascending order of their OTA considering the available landing slots. If the CTA minus the OTA for a specific airborne flight is longer than 40 minutes, this flight will be diverted to an alternate airport due to the fuel consumption constraint.

(3) ATCs will then assign the CTA (remaining landing time slots) to each flight on the ground in ascending order according to their OTA. If the difference between CTD (Controlled Time of Departure) and OTD for a specific flight on the ground is more than 100 minutes, this flight will be canceled, and the corresponding time slot will be available for other flights.

(4) At T_e, ATCs are informed that the AAR of HKIA recovers to 60, and then ATCs reschedule flights based on the updated information.

Condition 2: with ionospheric delay forecast.

If we can forecast the ionospheric delay with a forecast lead time (FLT) of δ ($\delta \neq$ 0, in the unit of hours), ATCs will determine the flight arrivals ahead of the development of a space weather event, i.e., at $(T_s - \delta)$ ATCs will be informed that the AAR will decrease to 30 starting from T_s. According to the availability of the common inputs of space weather forecast models and their computational capabilities, we assume four different specific cases with δ=1, 2, 4, and 24 hours, denoted as FLT1, FLT2, FLT4, and FLTL, respectively. Note that FLTL (with "L" denoting "long hours") represents the case with a 24-hour forecast lead time. Lead time longer than 24 hours has not been considered as no civil flight flies longer than 24 hours. The rescheduling rules are as follows.

(1) Flights with OTD/OTA before $(T_s - \delta)$ depart from their original airports and land at HKIA as scheduled. ATCs will assign CTA for each airborne flight, whose OTA is later than T_s.

(2) to (3) are the same as described for **Condition 1**.

(4) At $(T_e - \delta)$, ATCs are informed that the AAR will recover to 60 from T_e on, and ATCs will reschedule flights based on the updated information.

Let I be the set of airborne flights in the ascending order of their OTA indexed by i and let J be the set of flights on the ground in the ascending order of their OTA indexed by j. In the ATM rules, each airborne flight i may be assigned some airborne delays ($x_i^A = 1$) or divert to land at an alternate airport ($x_i^D = 1$). Similarly, each flight j on the ground may be assigned some ground delays ($x_j^G = 1$) or be canceled ($x_j^C = 1$). Just as shown in Figure 3.12, the detailed steps of solution methodology for ATM during space weather are presented. When satellite navigation is out of work and AAR reduces from 60 to 30, the assignments for these airborne flights will be conducted first because airborne fights receive a priority of landing. For each airborne flight i, the OTA and CTA are denoted by a_i and a_i', respectively. If the assigned airborne delay time $T_i^A = a_i' - a_i \leq 40$, this

46

flight i will accept the assigned airborne delay and will land at the HKIA at a_i', $\Longrightarrow$ $x_i^A = 1$; otherwise, i.e. $T_i^A > 40$, flight i will land at an alternate airport without any airborne delay, $\Longrightarrow x_i^D = 1$.

After giving directions to airborne flights, the assignments for flights on the ground will then be carried out. For each flight j on the ground, the OTA, CTA, OTD, and CTD are denoted as a_j, a_j', d_j, and d_j', respectively. ATCs would assign a_j' to each flight j on the ground using the rest of the available arrival time slots. Assuming that the enroute flight time L_j is known and deterministic, the CTD can be calculated by $d_j' = a_j' - L_j$ and the assigned ground delay is $T_j^G = d_j' - d_j$. If $T_j^G \leq 100$, this flight j will accept the assigned ground delay and will depart from the origin airport at d_j', $\Longrightarrow x_j^G = 1$; otherwise, i.e. $T_j^G > 100$, flight j will be canceled without any ground delay, $\Longrightarrow x_j^C = 1$.

Start

Satellite navigation failure

$i = 1$ | $j = 1$

$a_i' - a_i \leq 40\,?$ | $d_j' - d_j \leq 100\,?$

Y / N | Y / N

$x_i^A = 1$ | $x_i^D = 1$ — $x_j^G = 1$ | $x_j^C = 1$

$i = i + 1$ | $j = j + 1$

$i \in I\,?$ (Y / N) | $j \in J\,?$ (Y / N)

End
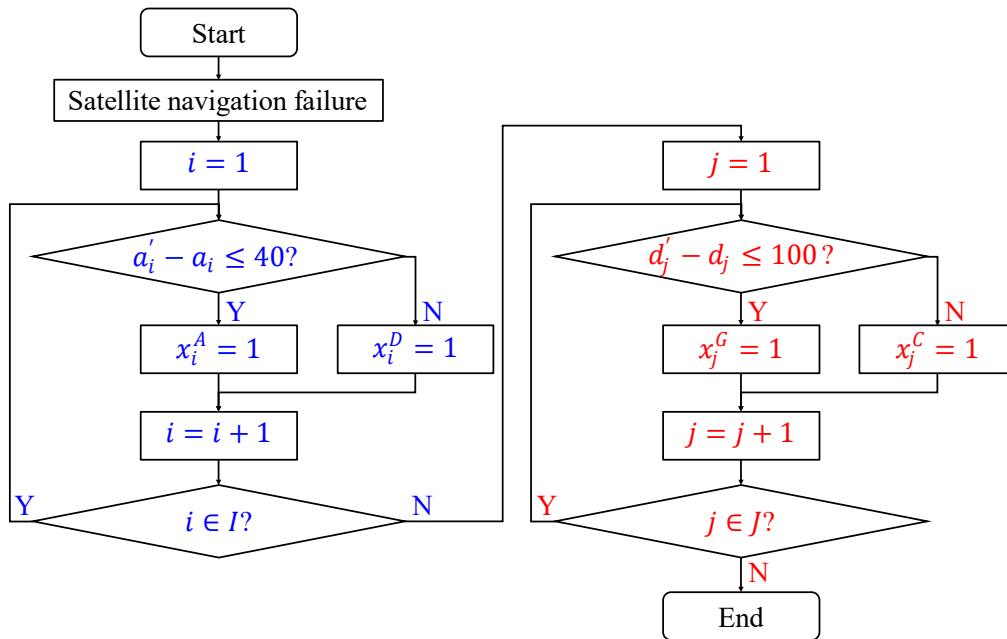
ATM rules				
(1) Assignments for airborne flights				
Callsign	OTA	CTA	Status	Delay
HDA485	13:46	13:46	$x_i^A = 1$	0 min
CPA503	14:13	14:14	$x_i^A = 1$	1 min
(2) Assignments for flights on the ground				
Callsign	OTD	CTD	Status	Delay
AAR721	12:31	14:10	$x_j^G = 1$	99 min
KAL613	12:33	14:12	$x_j^G = 1$	99 min
JNA113	12:34	X	$x_j^C = 1$	0 min
KAL613	12:35	X	$x_j^C = 1$	0 min
EVA867	12:36	14:16	$x_j^G = 1$	100 min

Figure 3.12. Flowchart for the calculation of landing times in ATM (above flowchart and results of calculation examples (below table)). Please note that the landing time 14:14 is not available in the second step of ATM rules (flights on the ground assignments), as this time (14:14) has already been assigned to the airborne flight CPA503 due to the landing priority of CPA503.

Table 3.4. Defined notations and explanations.

Notation	Explanation
I	Set of airborne flights in the ascending order of their OTA (indexed by i).

J	Set of flights on the ground in the ascending order of their OTA (indexed by j).
a_i	The original time of arrival of airborne flight i.
a_i'	The control time of arrival of airborne flight i.
a_j	The original time of arrival of flight j on the ground.
a_j'	The control time of arrival of flight j on the ground.
d_j	The original time of departure of flight j on the ground.
d_j'	The control time of departure of flight j on the ground.
L_j	The enroute flight time of flight j, $L_j = a_j - d_j = a_j' - d_j'$.
T_j^G	Ground delay time (in the units of minutes), $T_j^G = d_j' - d_j$.
T_i^A	Airborne delay time (in the units of minutes), $T_i^A = a_i' - a_i$.
W_C	The average cost of a canceled flight.
W_D	The average cost of a diverted flight.
W_G	The average cost of ground delay per minute.
W_A	The average cost of airborne delay per minute.
x_i^A	$x_i^A = 1$, if $T_i^A \leq 40$; $x_i^A = 0$, otherwise.
x_i^D	$x_i^D = 1$, if $T_i^A > 40$; $x_i^D = 0$, otherwise.
x_j^G	$x_j^G = 1$, if $T_j^G \leq 100$; $x_j^G = 0$, otherwise.
x_j^C	$x_j^C = 1$, if $T_j^G > 100$; $x_j^C = 0$, otherwise.

Given the notations listed in Table 3.4, the total airborne delay time is $\sum_{i \in I} x_i^A T_i^A$; the number of diverted flights is $\sum_{i \in I} x_i^D$; the total ground delay time is $\sum_{j \in J} x_j^G T_j^G$; the number of canceled flights is $\sum_{j \in J} x_j^C$. Thus, the financial costs related to airlines induced by space weather can be expressed below:

$$\text{cost} = \sum_{i \in I}(W_A x_i^A T_i^A + W_D x_i^D) + \sum_{j \in J}(W_G x_j^G T_j^G + W_C x_j^C) \qquad (3.3)$$

s.t.

$$T_j^G = d_j' - d_j \qquad (3.4)$$

$$T_i^A = a_i' - a_i \tag{3.5}$$

$$x_i^A + x_i^D + x_j^G + x_j^C = 1 \tag{3.6}$$

$$x_i^D = 1 | T_i^D > 40 \tag{3.7}$$

$$x_i^A = 1 | T_i^A \le 40 \tag{3.8}$$

$$x_i^D + x_i^A = 1 \tag{3.9}$$

$$x_j^C = 1 | T_j^G > 100 \tag{3.10}$$

$$x_j^G = 1 | T_j^G \le 100 \tag{3.11}$$

$$x_j^C + x_j^G = 1 \tag{3.12}$$

The ground delay and airborne delay can be calculated by (3.4) and (3.5), respectively. Constraint (3.6) ensures that each flight can only have one assignment case. Constraints (3.7) and (3.8) illustrate the conditions of diverted flights and airborne delay flights. For each airborne flight i, it may be a diverted flight ($x_i^D = 1$) or an airborne delay flight ($x_i^A = 1$), expressed in constraint (3.9). Similarly, constraints (3.10) and (3.11) illustrate the conditions of canceled flights and ground delay flights. For each flight j on the ground, it may be a canceled flight ($x_j^C = 1$) or a ground delay flight ($x_j^G = 1$), expressed in constraint (3.12).

3.4.2 Impact of forecast lead times

Figure 3.13(a) shows the simulated landing time of each flight corresponding to various forecast lead times based on the above-defined ATM rules. Although the satellite navigation failure duration is from 09:00 LT to 16:00 LT, the recovery time is actually after 22:00 LT, indicating the long-time effect of space weather. In theory, the CTA of a specific flight would have a longer delay if the forecast lead time is shorter. This is because air traffic would be more jammed when space weather information is obtained with a shorter lead time. In addition, flights with OTA before $(T_s - \delta)$ would depart from their original airports as scheduled. Therefore, there would be more flights taking off if the forecast lead time δ is shorter, causing more airborne delays. A trend of longer airborne delay can be seen at the beginning of the peak hour (Figure 3.13(b)), with simulated flights in FLT0

scenario generally experiencing the longest delays, followed by flights in FLT1, FLT2, FLT4, and FLTL scenarios. FLT0 denotes the scenario in condition 1, i.e., no forecast. Herein, we did not calculate the results under FLT3. Such a trend is more remarkable in Figure 3.13(c) when the delay effects are accumulating. The simulated CTA distribution is more complicated than the ideal case, considering that different flights have different origins and thus different enroute times. Figure 3.13(b) illustrates that the number of canceled flights decreases as the forecast lead time grows. The canceled flights predominantly cluster during peak hours (13:00-15:00 LT). This is because the assigned ground delay for each flight starts to accumulate after 09:00 LT. A substantial number of flights are delayed on the ground for more than 100 minutes during peak hours, which will be canceled. If ATCs are unable to get information on the upcoming space weather, they prefer to canceling the flights. Note that a few flights are canceled before 11:00 LT under scenarios FLT0 and FLT1. Some flights still on the ground with short enroute times can also be delayed or canceled. This is a result of a substantially reduced number of available landing slots because landing intervals are increased from 1 minute to 2 minutes, and airborne flights receive a priority of landing.
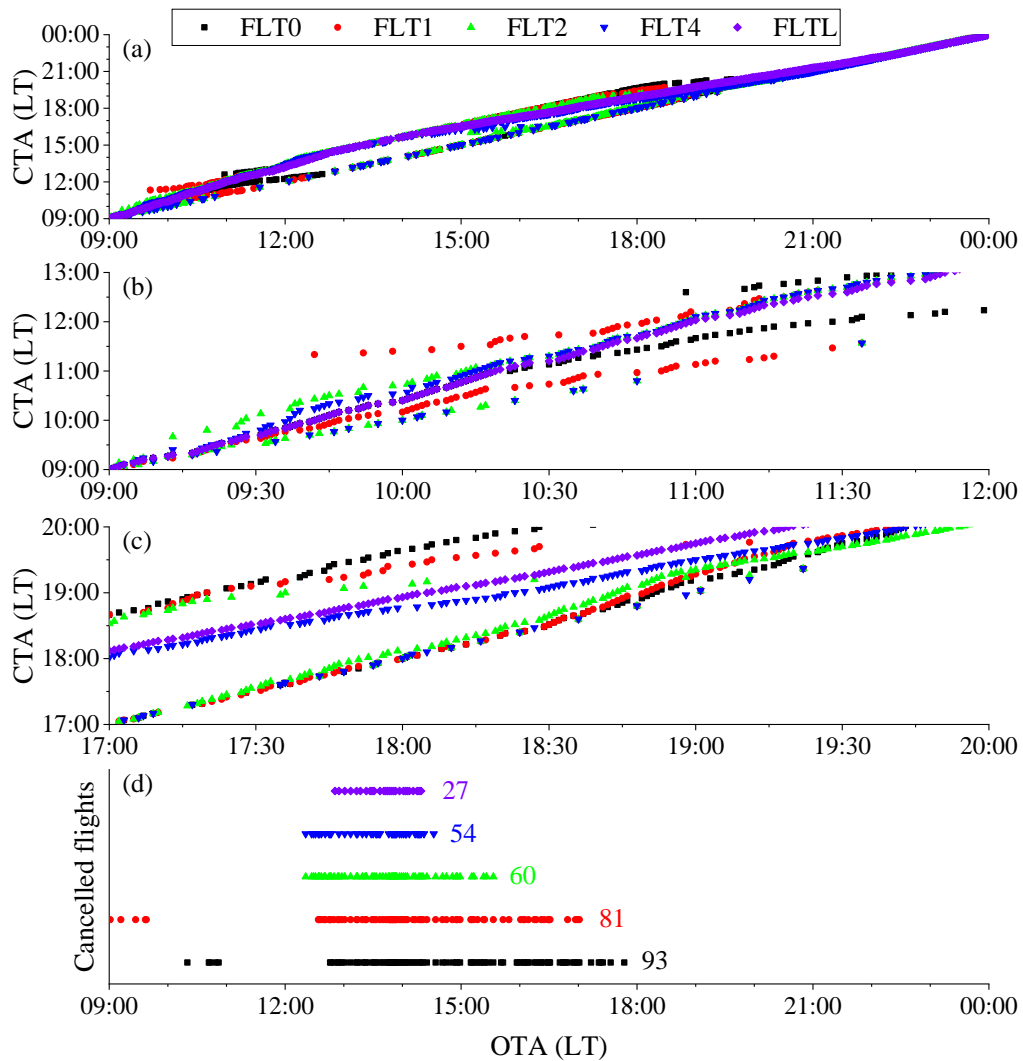
Figure 3.13. (a) The CTA under different forecast scenarios. Each dot represents one flight. (b) The detailed CTA distribution at the beginning of space weather. (c) The detailed CTA distribution after space weather. (d) The distribution of the total number of canceled flights versus OTA.

3.4.3 Economic cost of different forecast lead times

The direct costs related to airline flight delays, cancellations, and diversions resulting from space weather events are also estimated. The average cost of flight cancellation is W_C= €18,570; the average cost of flight diversion is W_D=€7,800; the average cost of ground delay is W_G=€16/min; and the average cost of airborne delay is W_A= €74/min (EUROCONTROL, 2020). Figure 3.14 shows the impact of different forecast lead times on flight assignments and extra financial costs related to airlines. As indicated in Figure 3.14(a), with the increase in forecast lead

time, the airborne delays drop dramatically from 2,558 minutes (FLT0) to 0 minutes (FLTL); while the ground delays increase dramatically from 17,324 minutes (FLT0) to 31,950 minutes (FLTL). Ground delay is defined as the difference between the CTD and OTD for a grounded flight and airborne delay is defined as the difference between the CTA and OTA for an airborne flight. Because ATCs have enough time to make decisions under scenario FLTL, flights will be rescheduled well ahead of the occurrence of the space weather event and thus they are delayed on the ground. However, without a forecast (FLT0), significant air traffic congestion will result in massive airborne delays. In addition, if there is no forecast (FLT0), 5 diverted flights will land at other alternate airports near Hong Kong. This is because more flights will depart from their origin airports before T_s in the case of no forecast FLT0, compared to the case with a forecast, which increases the possibility of flight diversion. In our simulation, there is no flight diversion under other forecast scenarios because there are not too many flights in the air during this event. Figure 3.14(b) indicates that as forecast capabilities improve, the number of canceled flights decreases. ATCs have less confidence in the future AAR when the forecast lead time is shorter. Therefore, they prefer to cancel flights to avoid unexpected problems like airborne holding or flight diversions. If a flight is canceled, there will be no ground delay for this flight, and the time slot associated with this flight can be utilized by other planes. This also helps to explain why, in Figure 3.14(a), the overall ground delays are lower when the forecast lead time is smaller. Figure 3.14(c) shows that without space weather forecasting the extra financial cost related to airlines is 2.23 million Euros and that the cost decreases as the forecast lead time grows.

In addition, the cost associated with the time delay for each passenger is estimated to be about €35.0/hour (Ball et al., 2010). Hence, assuming 200 seats in a typical B757 configuration with an occupancy factor of 80%, the unit delay cost for all passengers is $200 * 80\% * 35.0/60 = 93 \text{ €/min}$. Based on the ground delay time and airborne delay time in Figure 3.14a, the passenger delay cost can be 1.85 million Euros (FLT0), 1.81 million Euros (FLT1), 1.76 million Euros (FLT2), 2.13 million Euros (FLT4), and 2.97 million Euros (FLTL) (shown in Figure 3.14c). On an aggregate basis, the adverse effects of flight delays can be various such as

reducing passenger demand and changing airline scheduling plans (Britto et al., 2012), which may introduce additional indirect economical loss and affect the aggregate economy.
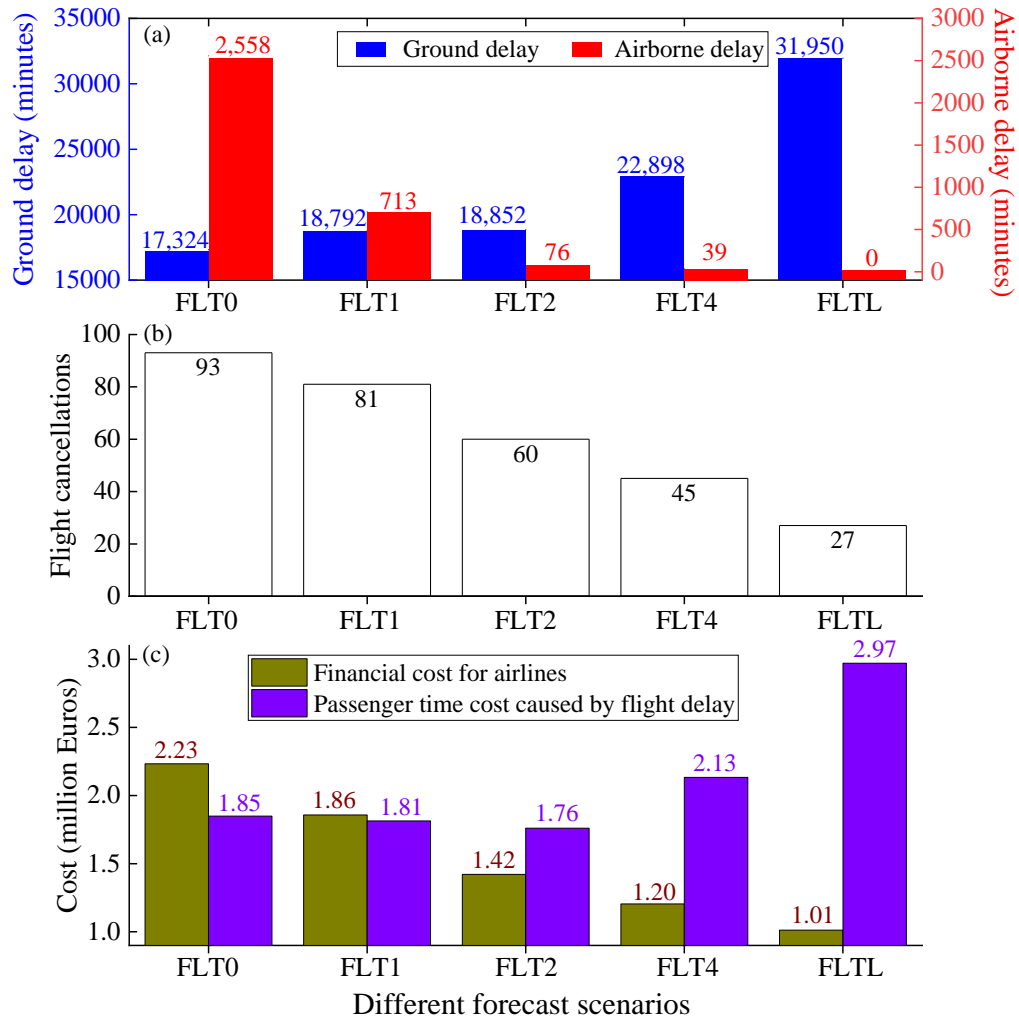
Figure 3.14. The impact of different forecast scenarios on the total ground delay time, total airborne delay time, the number of flight cancellations, extra financial costs for airlines, and passenger time costs caused by flight delays.

3.4.4 Accuracy of satellite navigation failure forecast effects

We also investigate how forecast accuracy affects air traffic management by simulating two more scenarios. In the optimistic forecast, we assume that the adverse event would end two hours earlier than it does, i.e. T_s=09:00 and T_e=14:00. In the pessimistic forecast, we assume that an adverse event would end two hours later than it does, i.e. T_s=09:00 and T_e=18:00. We also assume the

forecast capabilities are set to FLTL. As shown in Table 3.5, the optimistic forecast results in much fewer ground delays than the accurate forecast, but significantly more airborne delays, flight cancellations, and diversions. The induced cost for airlines (1.85 million Euros) is about 83% more than the accurate forecast (1.01 million Euros). Because more flights will be optimistically scheduled to be in the air if the space weather event is expected to end earlier than it does, generating traffic congestion and hence flight diversion. On the other hand, the pessimistic forecast results in more ground delays and more flight cancellations than the accurate forecast. The induced cost (1.72 million Euros) is 70% more than the accurate forecast. If the space weather event is predicted to linger longer than it does, more flights will be grounded pessimistically. The findings show that reliable forecasting is crucial for air traffic management and cost savings. It also implies that an optimistic forecast has a more harmful impact than a pessimistic forecast. The cost resulting from an optimistic forecast is 1.08 times of that from a pessimistic forecast.

Table 3.5. Comparison of the impact of the accuracy of the forecast.

	Optimistic forecast: 09:00-14:00 (LT)	Pessimistic forecast: 09:00-18:00 (LT)	Accurate forecast: 09:00-16:00 (LT)
Ground delay (minutes)	12,739	38,000	31,950
Airborne delay (minutes)	4,184	0	0
No. of canceled flights	56	60	27
No. of Diverted flights	38	0	0
Cost for airlines (million Euros)	1.85	1.72	1.01

3.5   Summary

During the final approach and landing phases, aircraft navigation now primarily relies on ground facilities. To meet the growing need for civil aviation, the ICAO promotes satellite navigation to increase airspace capacity and flight efficiency.

As a result, aircraft will navigate using the GNSS. However, due to the considerable increase in total electron contents and irregularities in the ionosphere, GNSS positioning accuracy will be degraded significantly during severe space weather, which can impact satellite-based aircraft operations.

To explore the impact of GNSS positioning errors on satellite-based air traffic management and induced economic costs, we made two studies. To be specific, we selected the historical Halloween storm in 2003 to quantify the effects on the Continental United States (CONUS) flights from the perspective of CDA failure and RNAV failure. It is estimated that 2,705 flights would be affected during the whole space weather event, causing an economic cost of €2.43 million.

Then, we evaluated the future effects on Hong Kong flights in 2030 by simulating a certain satellite navigation failure period caused by ionosphere storms. In the analysis, the factors such as distribution of arrival flight demand, the duration of satellite navigation failures, and space weather forecast capabilities, have been considered. Our simulation results suggest that if the ionospheric impact on GNSS navigation cannot be predicted, the cost related to airlines incurred to arrival flights at HKIA would be more than €2 million. This cost is reduced to €1 million if the ionospheric impact is precisely predicted. In addition, the time costs for passengers caused by flight delays can reach nearly €3 million. We also show that the cost of an optimistic forecast and a pessimistic forecast is 1.83 times and 1.70 times of an accurate forecast, respectively. The cost related to airlines reduces as forecast lead time increases. Therefore, improving the accuracy and extending the lead time of ionospheric impact forecast on GNSS navigation are crucially important for the aviation industry to reduce impacts and costs during space weather events.

Chapter 4

ADS-B Failure Effects on Air Traffic Management

ADS-B is a digital surveillance technology, which is primarily based on GNSS technology. Taking advantage of ADS-B, flight efficiency can be improved significantly. However, space weather can degrade GNSS performance and consequently cause ADS-B failure. This chapter introduces the difference in air traffic control methods. Then a heuristic algorithm based on ADS-B advantages is proposed to assign landing times for arrival flights. To estimate the ADS-B failure effects on economic cost, an ADS-B failure scenario is simulated using the Hong Kong International Airport as an example.

4.1 Introduction

Traditional surveillance methods for air traffic management include Primary Surveillance Radar (PSR) and Secondary Surveillance Radar (SSR). An emerging surveillance technology is ADS-B.

4.1.1 Primary Surveillance Radar

The radar antenna of PSR revolves (often between 5 and 12 revolutions per minute) and emits a radio pulse. When the wave reaches an aircraft (or another object), it is reflected, and a portion of its energy is returned to the antenna. Figure 4.1 depicts the schematic diagram of the PSR operation principle. PSR is the first civil aviation surveillance sensor that does not require any onboard equipment for aircraft location. In addition, unlike SSR or ADS-B, PSR can detect an aircraft with transponder failure or an intruder. However, PSR still has many drawbacks such as flight altitude data missing, difficult automatic correlation, and the minimum range limit.
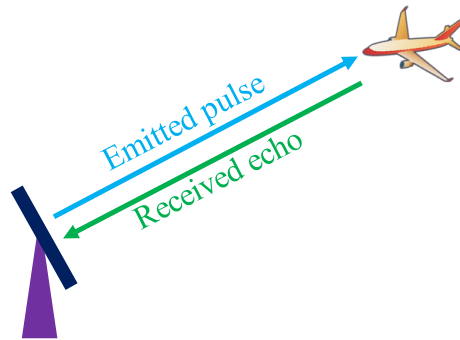
Figure 4.1. Schematic diagram of PSR operation principle.

4.1.2 Secondary Surveillance Radar

The SSR radar antenna revolves (often at 5 to 12 revolutions per minute) and transmits a pulse that is received by onboard electronics (transponder). The transponder returns a reply comprising at least a code (if operating in Mode A), but this is more commonly combined with level (Mode C) or other data, such as aircraft identity, flight level, etc. (Mode S). Figure 4.2 depicts the schematic diagram of the SSR operation principle. SSR takes significantly less power to accomplish the desired range than PSR, as the signal simply needs to reach the aircraft. In addition to the range and heading information from the antenna, SSR can also offer flight-level data. In addition, SSR is immune to interference since its interrogation (1030 MHz) and response frequencies are distinct (1090 MHz). The limitations of SSR include heavily relying on onboard equipment, fake detection, and shadowed onboard antenna.
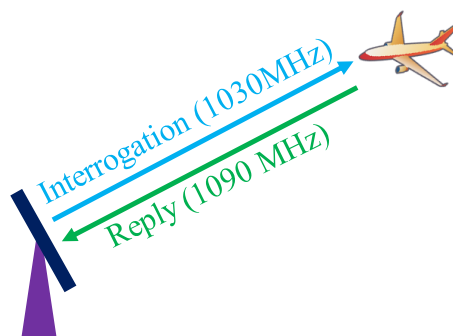
Figure 4.2. Schematic diagram of SSR operation principle.

4.1.3 Automatic Dependent Surveillance-Broadcast

As an indispensable part of the Next Generation Air Transportation System, ADS-

58

B as a surveillance technology determines aircraft real-time positions via the GNSS (Li et al., 2020). ADS-B can replace traditional radar systems such as Primary Surveillance Radar (PSR) and Secondary Surveillance Radar (SSR) because the onboard ADS-B Out system can broadcast their real-time positions together with other information in 1090 MHz with an update rate of 0.5-2 seconds.

As shown in Figure 4.3(a), an aircraft with ADS-B capability determines its position using the GNSS (Asari et al., 2020). The Mode S transponder at the frequency 1090 MHz then continually broadcasts aircraft position, identity, velocity, and other information, which can be received by other aircraft equipped with ADS-B In systems and ADS-B receivers at the ground station (Jheng et al., 2020). After that, ADS-B data are relayed to the air traffic control center for precise tracking of the aircraft, as in Figure 4.3(b) (Chen et al., 2020). In the space segment, GNSS signals propagate from satellites to aircraft to determine aircraft positions. In the air segment, many aircraft share airspace and periodically broadcast ADS-B messages using the same frequency. Hence, ADS-B messages may suffer severe collisions and crowdedness in the channel (Su et al., 2020). In the ground segment, ADS-B receiver performance varies with different manufacturers and system designs, which also affects the quality of received ADS-B messages. The description of ADS-B data is shown in Table 4.1.
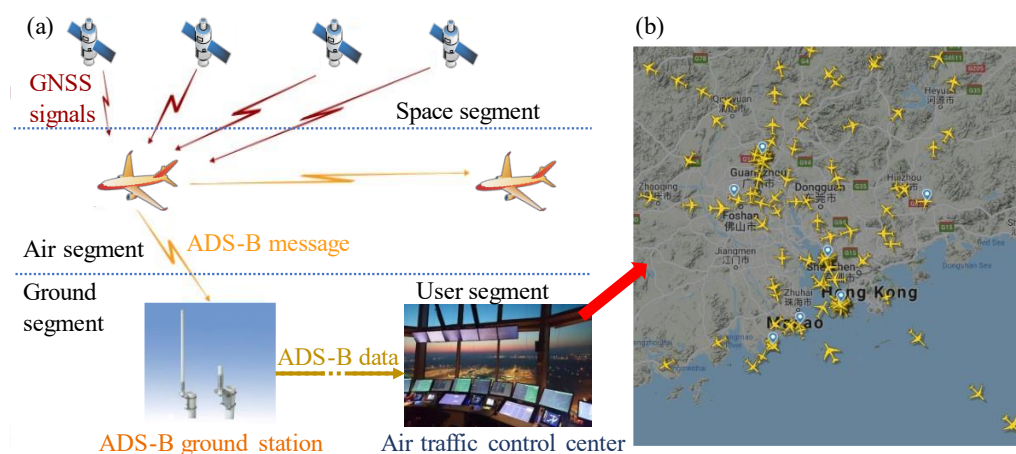
Figure 4.3. Schematic diagram of ADS-B application to ATM.

Table 4.1. ADS-B data description.

Notation	Description

ALT	Barometric altitude (ft)
SPD	Ground Speed (kt)
LON	Longitude (-180º to 180º)
TIM	Universal Time Coordinated
VRT	Vertical Rate (ft/min)
DAT	Date in UTC
LAT	Latitude (-90º to 90º)
TRK	True track (0º to 360º)
FLI	Flight identification
DIS	Distance to ADS-B receiver (km)

Air traffic control stations can receive ADS-B information and monitor real-time flight situations. Figure 4.4 depicts the context diagram exhibiting the data sources, elements, and data flow (Ali et al., 2016).
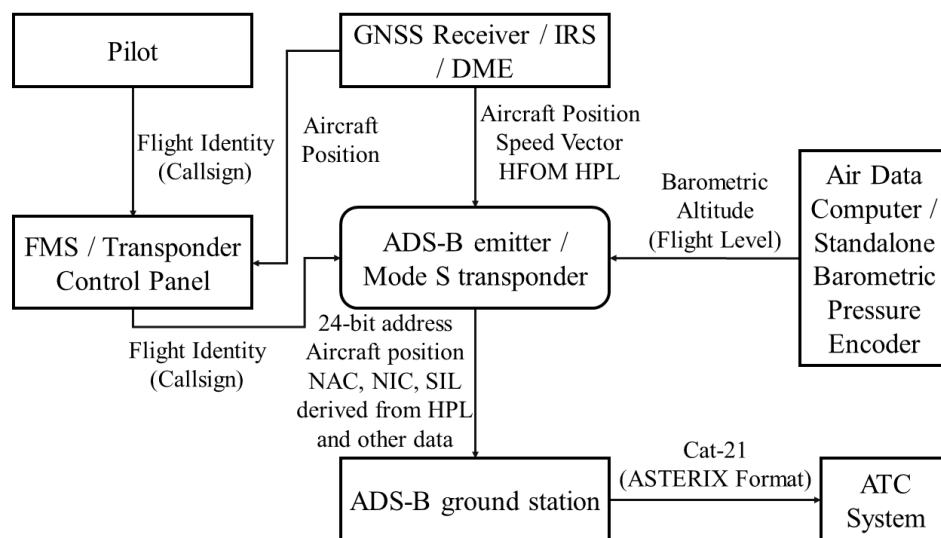
Figure 4.4. Context diagram for ADS-B working principle (Ali et al., 2016).

ADS-B performance parameters are summarized by Ali (2013).

- ADS-B accuracy is defined as the difference between the reported aircraft position in the ADS-B messages and the true position.

- ADS-B integrity is the level of trust that errors will be correctly detected.

- ADS-B continuity is the probability that the system achieves its desired

performance without unexpected interruptions, given the system is ready when the procedure starts.

- ADS-B availability is the system ability to achieve the desired functions at the start of the anticipated operation.

- ADS-B latency denotes the time difference between the time when aircraft position is determined by GNSS and the time when ADS-B signal is received by the ground ADS-B station. Figure 4.5 shows the functional architecture of a transmitting aircraft and a ground ADS-B receiver. Based on the notations, the total latency can be represented as $TL = TOA_E - TOA_A$ ([RTCA, 2009](#)), and total latency can and should be limited to 1.5 seconds ([Levitt, 2012](#)).
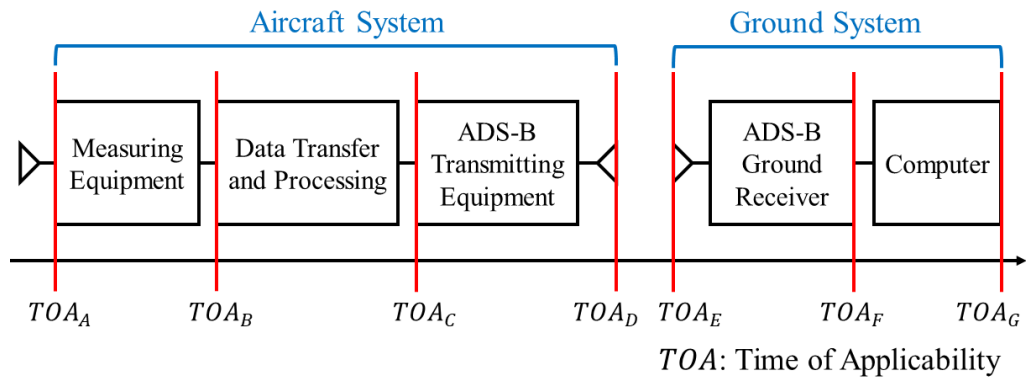
Figure 4.5. Functional architecture diagram of TOA. TOA_A: aircraft positions are determined by GPS. TOA_B: GPS receiver outputs aircraft positions. TOA_C: aircraft position information reaches ADS-B transponder. TOA_D: ADS-B transponder broadcasts signals. TOA_E: ADS-B signal is received by ground receiver. TOA_F: ground receiver outputs ADS-B information. TOA_G: aircraft positions are displayed on the computer.

4.2 Surveillance failure

4.2.1 Radar failure

In the afternoon of 4 November 2015, an extraordinarily powerful solar burst at radio wavelengths of approximately 1 GHz occurred, causing severe disturbances to those air traffic control radars whose antennas were aimed at the Sun in Sweden and other European countries ([Marqué et al., 2018](#)). This occurrence finally

necessitated the deployment of a bulk of radars. Figure 4.6 shows the false echoes observed in the direction of the Sun at a Belgian A/C radar station. Consequently, the entire southern Swedish airspace was forced to close to arrival flights and departure flights for nearly two hours (Opgenoorth et al., 2016). Other systems in other European countries also experienced some radio disturbances during this extraordinary event, although the effects were not as severe as those in Sweden.
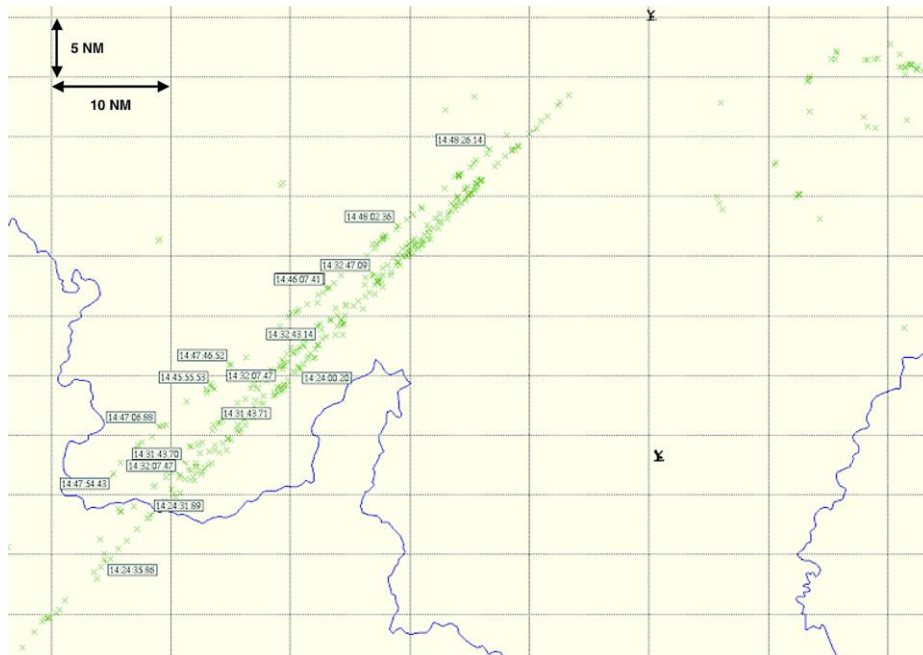
Figure 4.6. False echoes (in green) observed at a Belgian radar station in the upper right corner (Marqué et al., 2018).

4.2.2 ADS-B failure

Each part of the ADS-B system shown in Figure 4.4 may experience failure. A thorough understanding of each failure mode is necessary to ensure flight safety. Ali et al. (2017a) summarized the potential reasons for ADS-B system failure as follows.

The causes of the corruption of ADS-B data for all aircraft are illustrated in Figure 4.7, which can mainly be attributed to the degradation and reduced integrity of ADS-B ground stations and airborne systems. The total causes can be summarized into environmental impact, lack of maintenance, errors in GPS, etc. The corruption of ADS-B data for one single aircraft in Figure 4.8 is explained by the deterioration

and low integrity of airborne equipment of a particular aircraft. The deterioration and low integrity of the onboard navigation system, which provides the aircraft position information to the ADS-B transponder, can lead to the corruption of position data for one single aircraft in Figure 4.9. If there are some problems related to the ground station, the ADS-B data source from all aircraft can be affected, which is shown in Figure 4.10. The loss of ADS-B data from one aircraft is due to human errors (by the pilot) and failure of onboard ADS-B equipment. Detailed information is illustrated in Figure 4.11. At last, the reasons for the failure of ADS-B In in Figure 4.12 include the failure of ADS-B In applications and the failure of ADS-B Out service from other aircraft.
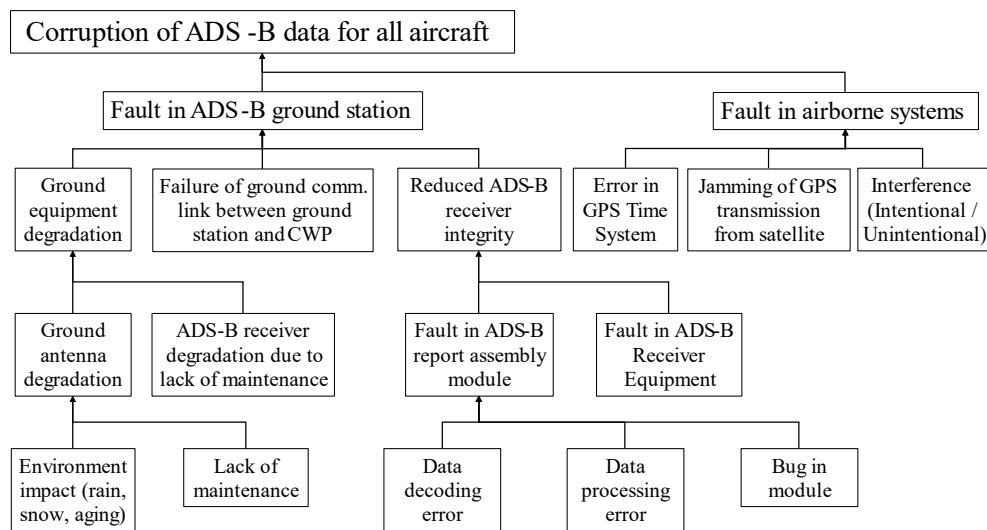
Figure 4.7. Analysis of corruption of ADS-B data for all aircraft. The ADS-B signals from all the aircraft can be received by the ground ADS-B receiver but the data are corrupted.
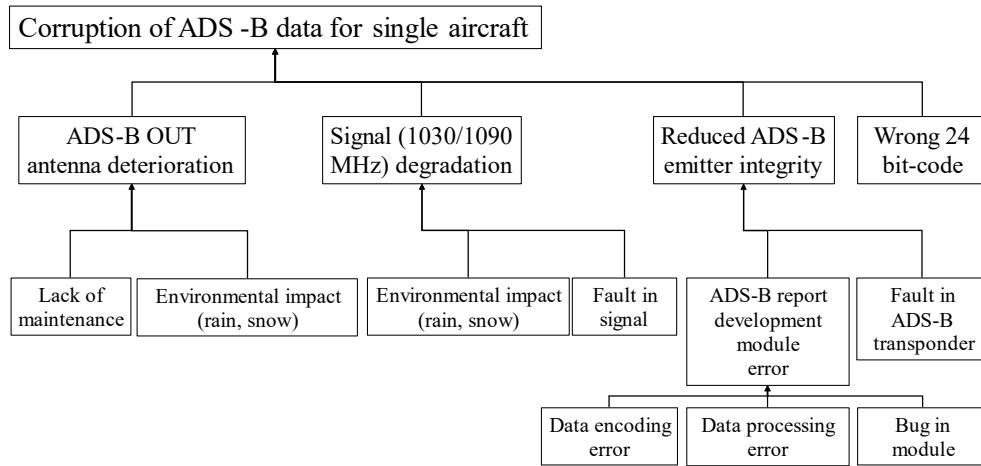
Figure 4.8. Analysis of corruption of ADS-B data for single aircraft. Only the ADS-B signals from single aircraft are corrupted although the data can be received by the ground ADS-B receiver.
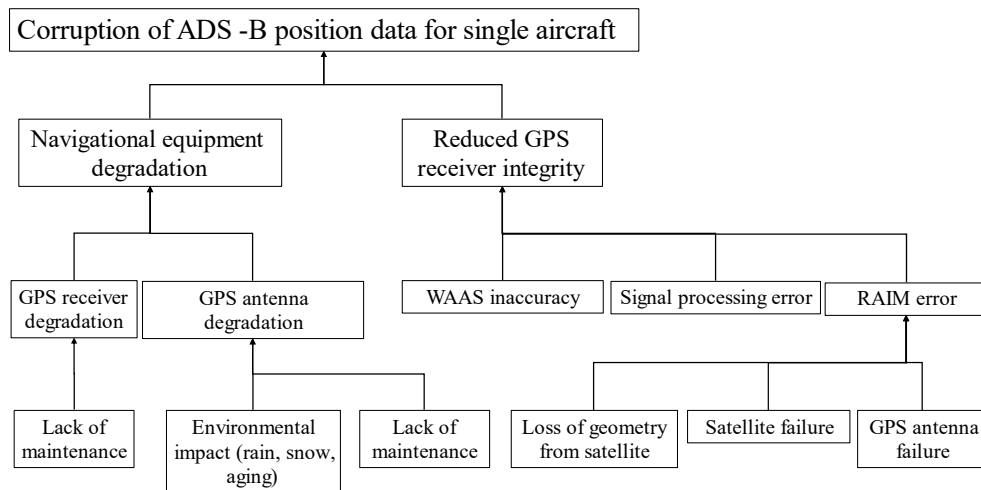
Figure 4.9. Analysis of corruption of ADS-B position data for single aircraft. The position data (longitude, latitude, and altitude) in ADS-B signals from single aircraft are corrupted although the data can be received by the ground ADS-B receiver.
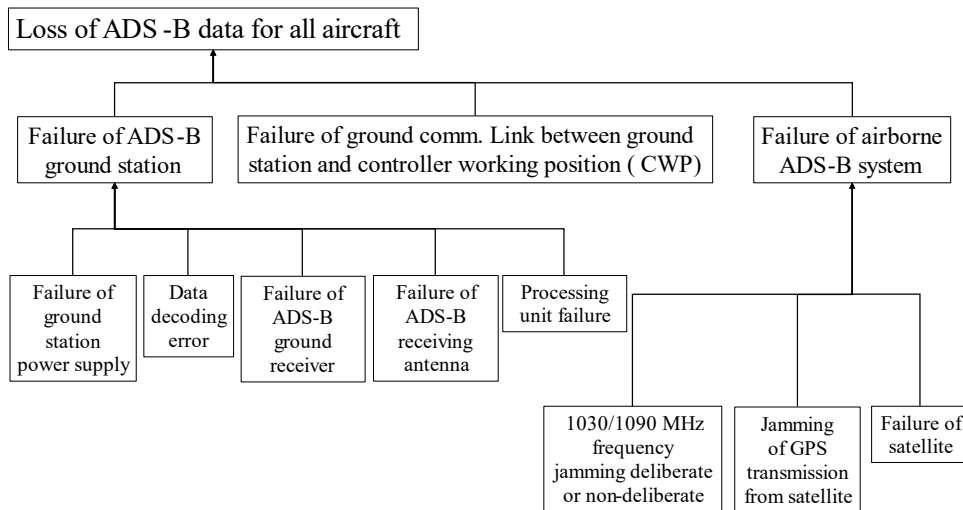
Figure 4.10. Analysis of loss of ADS-B data for all aircraft. The ADS-B signals from all aircraft cannot be received by the ground ADS-B receiver.
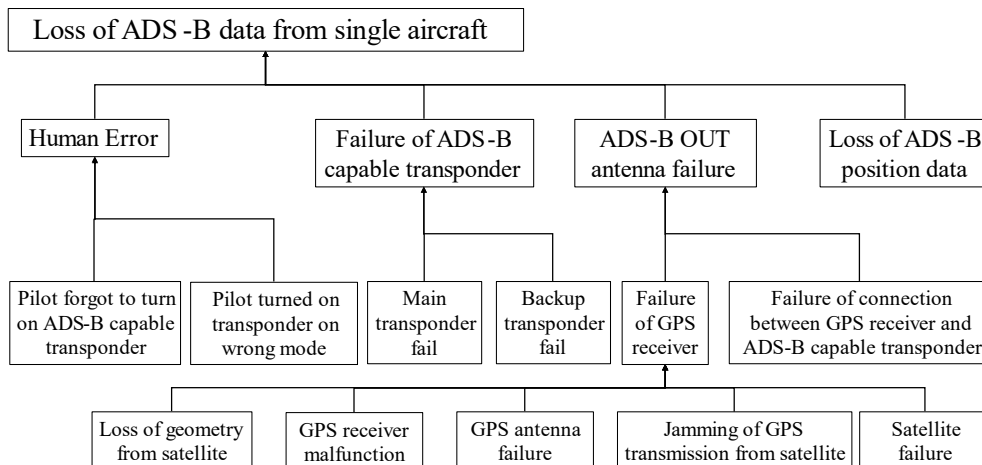
Figure 4.11. Analysis of loss of ADS-B data from single aircraft. The ADS-B signals from single aircraft cannot be received by the ground ADS-B receiver.
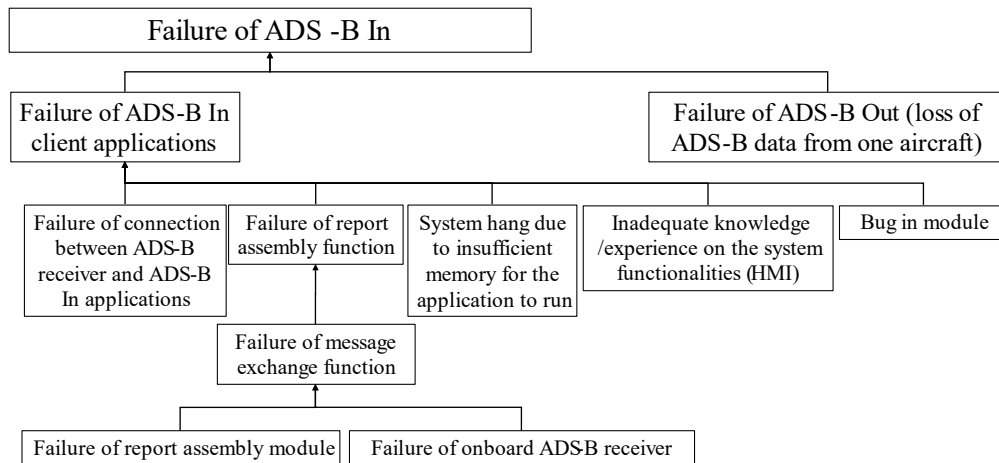
Figure 4.12. Analysis of failure reasons of ADS-B In system.

4.3 Air traffic control method

4.3.1 Radar control

ADS-B is expected to reduce aircraft separation standards, but the current aircraft separation standards based on ADS-B are still the same as those based on radar. By definition, radar control is a technique to deliver air traffic control services utilizing radar and ADS-B (Strohmeier et al., 2014). The risk of aircraft collisions in air traffic control is managed by implementing separation regulations. These regulations stipulate that aircraft must be separated by either a minimum vertical distance or by a minimum horizontal distance determined by a variety of techniques, which is known as radar separation. Standard radar separations are 3 nm in terminal airspace and 5 nm in enroute airspace. In airspace with less traffic, controllers will demand pilots to follow published routes that have been established to separate aircraft. To maintain separation between aircraft on these routes, controllers may require pilots to fly their aircraft at specific speeds.

4.3.2 Procedural control

Procedural control is a method of controlling air traffic without using radar or ADS-B. It is particularly used in the areas out of radar coverage, such as sparsely inhabited land and ocean areas. Additionally, it may also be employed at airports with extremely little traffic flows, e.g. at night or as a backup system in the event of radar failure.

For aircraft that are not vertically separated, procedural control is performed by establishing horizontal separations based on time intervals, the geography of predetermined routes, or aircraft position reports based on ground navigation aids. When procedural control is performed, ATCOs are required to maintain a mental picture of the position of each aircraft based on the flight progress strip.

The most obvious difference between procedural control and radar control is the difference in the minimum horizontal spacing allowed between aircraft. A schematic is illustrated in Figure 4.13. Radar and ADS-B are utilized in a very similar manner. ADS-B equipped aircraft may maintain a minimum separation of 5 nautical miles, on condition that the integrity value must essentially ensure that the aircraft is within 0.5 miles of where it reports. On the basis of satellite geometry, the position integrity is also offered. In the absence of ADS-B, procedural separation will be used.

Within the area control, the procedure control requires a minimum horizontal interval of 10 minutes between the same route and the same altitude (equivalent to a distance of about 150 km for large and medium-sized aircraft), while the interval based on radar control is only 20 km. A smaller minimum allowable interval can achieve better utilization of airspace, a larger airspace capacity, a more conducive to maintaining smooth air route command, and more conducive to improving flight safety rate and flight normality rate.
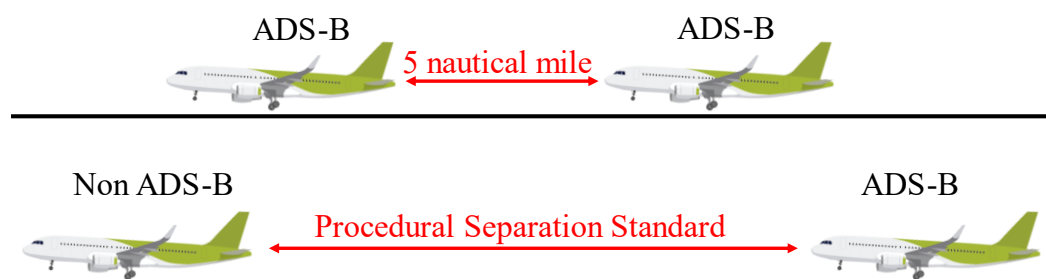
Figure 4.13. The difference in separations between ADS-B surveillance and procedural control.

4.4   Potential benefits of ADS-B in aircraft landing scheduling

Currently, ATCOs rely on the aircraft's radar contacts on the radar screen (Argyle

et al., 2018; Ruffner et al., 2003) to maintain safe separation between aircraft. According to (ICAO, 2007), "*a minimum of 300 m vertical separation or a minimum of 5.6 km radar separation shall be provided between aircraft during turn-on to parallel ILS localizer courses and/or microwave landing system (MLS) final approach tracks in the terminal area airspace*". However, radar performance is related to the power density at the target position, the reflected power, and the antenna gain (Zhang and Mahadevan, 2017), causing high uncertainty in aircraft positions. If the aircraft's positions cannot be obtained accurately, ATCOs would enlarge the separation distance between aircraft to ensure safe operation. Consequently, there will be a reduction in airspace capacity and flight efficiency (Ng et al., 2020). Besides, ATCOs suffer from eye fatigue after focusing on the eye-tracking system for a long time (Wee et al., 2019). In light of potential human failures and operational errors, virtual assistance systems have appeared in the cockpit and on the ground (Ng et al., 2017) to provide tactical decision support and alert potential aircraft conflicts.

Therefore, the use of ADS-B can increase ATCOs' confidence in aircraft's real-time positions, reducing the separation between aircraft without compromising flight safety, which can optimize airspace capacity and improve flight safety (Kunzi, 2013). Nowadays, pilots are required to report to ATCOs when entering a new airspace sector, such as "*CCA101, 9,500 meters maintaining, squawk 1234, 6 miles to FYG*". After that, ATCOs will need to acknowledge said report (Li et al., 2019), replying with "*CCA101, Shanghai control, radar contact*". In contrast, this communication procedure can be eliminated by using ADS-B, which can save time and energy for both ATCOs and pilots.

The transformation to using ADS-B can allow close monitoring of real-time flight activities in the Terminal Maneuvering Area (TMA). This modern design application supports both the separation distance measurement between aircraft and runway schedule displacement under dynamic situations (Ng et al., 2018). One crucial issue is that the flight speed and arrival time on the waypoints and runway is subjected to wind direction and intensity, leading to uncertain ground speed measurements of approaching flights (Huo et al., 2020). Therefore, it is necessary to combine ATM with contemporary technologies and digital-

technology enablers for flight tracking with information from the aircraft's avionic system. With accessibility to real-time flight information using ADS-B, data-driven decisions and flight safety can be significantly improved (Lee et al., 2020).

The real-time position information is more accurate than that from current radar-based systems with an update rate of 4-12 seconds. With more accurate information, Air Traffic Control Officers (ATCOs) can guide aircraft into and out of crowded airspace with smaller separation standards without compromising flight safety. By reducing separation standards between aircraft, airspace capacity can be increased even with safer, more efficient, and more predictable flying. The broadcast ADS-B information can also be received by the aircraft equipped with ADS-B In system, which can achieve improved situational awareness and allow self-separation.

ADS-B data provides the real-time geodetic positions (LLA: Longitude, latitude, and Altitude) positions with ground speed (v in km/h), vertical rate (ρ in ft/min), and flight heading (θ in degree). The LLA coordinate system is first converted to the Earth-Centered Earth-Fixed (ECEF) coordinate system, and then the ECEF coordinate is converted to the ENU (East, North, Up) coordinate system, achieving all aircraft in a unified coordinate system (ENU) (Drake, 2002; King, 2003). The geodetic positions (LLA) of flights are determined by the GNSS and denoted by (lon, lat, h). Using below formulation, (X, Y, Z) in ECEF can be obtained.

$$\begin{cases} X = (N + h)\cos(lon)\cos(lat) \\ Y = (N + h)\cos(lon)\sin(lat) \\ Z = (N \times (1 - e^2) + h)\sin(lon) \end{cases} \tag{4.1}$$

where e is the first eccentricity of the earth, $e^2 = (a^2 - b^2)/a^2$, $N = a/\sqrt{1 - e^2 sin^2(lon)}$, a and b are the equatorial radius and polar radius, respectively. The local aerodrome center is denoted by (lon_0, lat_0, h_0) in LLA and can be converted to ECEF (X_0, Y_0, Z_0) using Eq. (4.1). We set the aerodrome as the origin point $(0, 0, 0)$. The observation vector can be expressed as:

$$\begin{bmatrix} \Delta x \\ \Delta y \\ \Delta z \end{bmatrix} = \begin{bmatrix} X \\ Y \\ Z \end{bmatrix} - \begin{bmatrix} X_0 \\ Y_0 \\ Z_0 \end{bmatrix} \tag{4.2}$$

The observation vector is then transferred into the ENU coordinate system (unit in m) based on the following equation. The ENU coordinate system is illustrated in Figure 4.14.

$$\begin{bmatrix} x \\ y \\ z \end{bmatrix} = \begin{bmatrix} -\sin(lon_0) & \cos(lon_0) & 0 \\ -\sin(lat_0)\cos(lon_0) & -\sin(lat_0)\sin(lon_0) & \cos(lat_0) \\ \cos(lat_0)\cos(lon_0) & \cos(lat_0)\sin(lon_0) & \sin(lat_0) \end{bmatrix} \begin{bmatrix} \Delta x \\ \Delta y \\ \Delta z \end{bmatrix} \tag{4.3}$$
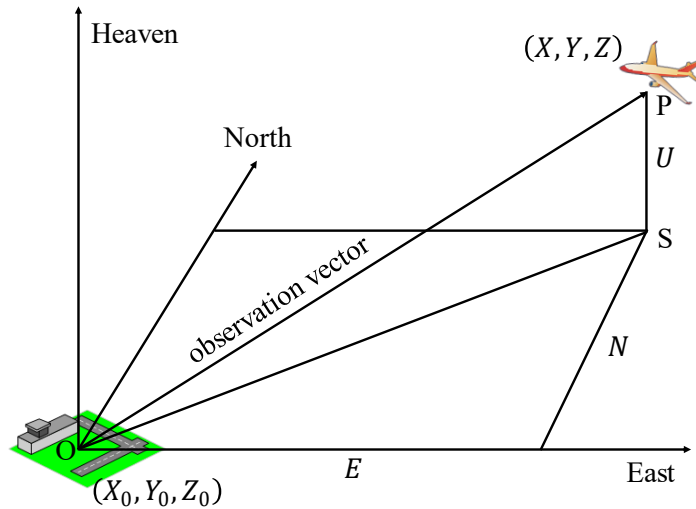
Figure 4.14. The ENU coordinate system.

4.4.1   Problem definition

Aircraft Landing Problem (ALP) is a dynamic problem at the tactical level which involves sequencing the optimal landing order for arriving flights. Lieder et al. (2015) indicated that "*To date, no efficient methods have been proposed in the reviewed literature for the multi-runway ALP that is capable of solving large problem instances*" and summarized the related works before 2015. Therefore, this thesis provides an overview of related articles from 2015, which is listed in Table 4.2. The most common objectives can be classified into four parts: (1) minimizing

the total deviation time from target time; (2) minimizing the total flight delay; (3) maximizing the total airport throughput; (4) minimizing the makespan for all landing aircraft.

Table 4.2. Overview of ALP articles from 2015.

Source	Objective	Solution method
Lieder et al. (2015)	min total delay	Dynamic programming
Ng and Lee (2016)	min makespan	Artificial bee colony algorithm
Rodríguez-Díaz et al. (2017)	min total delay	Simulated annealing algorithm
Xu (2017)	min makespan	Ant colony algorithm
Hong et al. (2018)	min total flight time	Particle swarm optimization
Mahmud and Jeberson (2018)	min total deviation time	Flower pollination algorithm
Prakash et al. (2018)	max total throughput	Data-splitting algorithm
Ikli et al. (2019)	min total deviation time	Mixed-integer programming
Lu et al. (2019)	min total delay	Genetic algorithm
Wu et al. (2019)	min total waiting time	Ant colony algorithm
Salehipour (2020)	min total deviation time	Heuristic solution method
Vincent et al. (2021)	min total delay	Mixed-integer programming

As mentioned above, previous articles about ALP mainly focus on optimizing algorithms without considering aircraft conflict detection or the common operational failure events such as missed approach. Although there is some research on Unmanned Aerial Vehicles (UAV) using ADS-B (Pierpaoli and Rahmani, 2018; Zhang et al., 2018), research gaps exist in ADS-B application to civil aviation. To better understand digital transformation (Vial, 2019; Zheng et al., 2019) and satisfy the rapid evolution of new service systems (Wang et al., 2017), a novel heuristic search method based on ADS-B technology is proposed to achieve continuous and real-time aircraft landing time updates and assignments considering the minimum time separation standards induced by wake turbulence.

71

When a new flight enters the Terminal Maneuvering Area (TMA), the heuristic search method can immediately generate an aircraft landing time with the objective of minimizing the total flight time. Based on the novel and powerful digital technologies, digital platforms, and digital infrastructures, three contributions are summarized as follows:

- Leverage ADS-B data: ADS-B is adopted to solve ALP by reducing communication time and monitoring aircraft's real-time positions.

- Continuous and dynamic scheduling for schedule displacement: The heuristic search method is a fast and effective method for continuous and real-time ALP updates.

- Consideration of operational failure events: The heuristic search method can update landing time when an aircraft is assigned a higher landing priority due to operational failure.

The proposed heuristic search for ALP is illustrated herein with some of its basic properties. We have considered a single-runway ALP model, which can be applied to a multi-airport TMA, on the condition that flight altitude regulations in flight routes are issued. The scheduling assignment for each flight is determined using the proposed heuristic, considering the hard constraint of sufficient time separation. The following three assumptions are made. First, all flights approach using the standard terminal arrival routes. Second, all flights descend in altitude by a standard rate of descent, aiming to keep a vertical separation between flights and guarantee no conflicts among different flight routes. Third, there is no conflict between arrival flights and departure flights.

For ease of explanation, a schematic diagram of ALP is presented in Figure 4.15 (Toratani, 2019). There are three arrival routes from entry points to the runway. The target is to sequence all flights and assign their respective landing time considering the sufficient time separation constraint between two adjacent flights. After detecting flights entering TMA from the entry points using ADS-B, the heuristic solves ALP based on the current flight situation and updates aircraft landing time for all flights within the TMA. The detailed instructions generated from the heuristic are conveyed to pilots to manage air traffic flow.
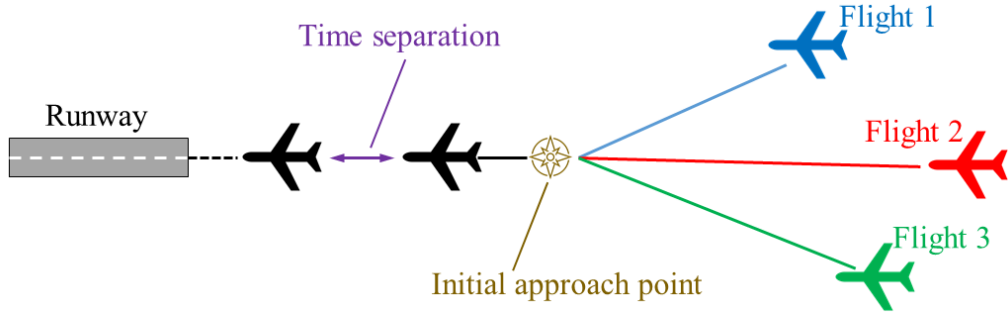
Figure 4.15. The schematic diagram of single-runway ALP.

The ALP mathematical model takes the following input data. Let I be the set of aircraft, and two neighboring flights are indexed by i and j, respectively. The number of flights landing on a single runway is denoted by $|N|$. According to ICAO regulations, there should be a minimum time separation (S_{ji}) between two consecutive flights (preceding flight j and following flight i) to avoid the wake turbulence effect generated by the preceding aircraft. According to the Maximum Take-off Weight (MTOW), aircraft categories are divided into light aircraft ($\text{MTOW} \leq 7\,\text{t}$), medium aircraft ($7\,\text{t} < \text{MTOW} < 136\,\text{t}$), and heavy aircraft ($\text{MTOW} \geq 136\,\text{t}$) (Tobisová et al., 2018). The minimum time separation standard S_{ji} relies on the aircraft types and the values indicated in Table 4.3. The arrival route of flight i is predefined according to the flight plan, and the flight time F_i is related to flight speed and the distance from the entry point to the runway. From the historical data, F_i is between F_i^{min} and F_i^{max}, where F_i^{min} is the shortest flight time and F_i^{max} is the longest flight time. The time when flight i arrives at the entry point (T_i) can be obtained from ADS-B. Therefore, the assigned landing time is $t_i = T_i + F_i$, which should be within the earliest landing time ($t_i^e = T_i + F_i^{min}$) and the latest landing time ($t_i^l = T_i + F_i^{max}$). Every time when a new flight enters the TMA, the proposed heuristic would solve the ALP and output the updated landing time for each flight, so the decision valuable (t_i) may change several times. The binary decision variable y_{ji} represents the sequence of the schedule. If the landing time of flight j is before flight i, y_{ji} is equal to 1; otherwise y_{ji} is equal to 0.

Table 4.3. The minimum time separation standard between two consecutive landing flights (in minutes) ([ICAO, 2007](#)).

		Following aircraft		
		Heavy	Medium	Light
Preceding aircraft	Heavy	2	2	3
	Medium	2	2	3
	Light	2	2	2

Table 4.4. Notations and decision variables.

Sets with indices	Explanation
I	A set of approaching flights (index i, j)
Parameters	Explanation
i, j	Flight ID $i, j \in N$
F_i	Flight time of flight i from an entry point to landing.
F_i^{min}	The shortest flight time of flight i from an entry point to landing.
F_i^{max}	The longest flight time of flight i from an entry point to landing.
T_i	The arrival time at the entry point for flight i.
M	Large artificial variable.
e_i	The earliest landing time.
l_i	The latest landing time.
S_{ji}	The minimum time separation between aircraft j and i.
Decision variables	Explanation
t_i	The landing time of flight i, $t_i \geq 0, \forall\, i \in N$.
y_{ji}	1, if flight j lands before flight i (not necessarily immediately); 0, otherwise.

Given the notations for parameters and decision variables listed in Table 4.4, we presented the nominal formulation of ALP and assumed all parameters to be deterministic. The objective function (4.4) is to minimize the total landing time of

all arrival flights.

$$\min \sum_{i \in I} t_i \qquad (4.4)$$

$s.t.$

$$F_i = t_i - T_i, \forall i \in N \qquad (4.5)$$

$$t_i \geq t_j + S_{ji} - M(1 - y_{ji}), \forall\, i,j \in N, i \neq j \qquad (4.6)$$

$$y_{ji} + y_{ij} = 1, \forall\, i,j \in N, i \neq j \qquad (4.7)$$

$$e_i \leq t_i \leq l_i, \forall\, i \in N \qquad (4.8)$$

$$t_i \geq 0, \forall\, i \in N \qquad (4.9)$$

$$y_{ji} \in \{0,1\}, \forall\, i,j \in N, i \neq j \qquad (4.10)$$

Flight time from entry points to the runway is calculated using constraint (4.5). Inequality equation (4.6) indicates that the landing time of the following aircraft i must be larger or equal to the summation of the preceding time t_j and the minimum time separation requirement S_{ji}. Constraint (4.7) ensures either $y_{ji} = 1, y_{ij} = 0$ or $y_{ji} = 0, y_{ij} = 1$. The landing time t_i of each flight must be in the time window ($[e_i, l_i]$) in constraint (4.8). Constraints (4.9) and (4.10) express three decision variables for t_i and y_{ji}.

4.4.2 Solution approach

As expressed above, the ALP is a real-time dynamic problem, necessitating a continuous and efficient solution approach. However, it always takes a relatively long time to locate an ALP solution because ALP is an NP-hardness (non-deterministic polynomial-time hardness) problem (Kwasiborska, 2017; Lieder et al., 2015; Rodríguez-Díaz et al., 2017). In mathematical programming, a heuristic algorithm can determine near-optimal solutions to an optimization problem, and therefore a novel heuristic search algorithm is proposed to solve the ALP efficiently. The heuristic workflow is shown in Figure 4.16, containing the initialization step and continuous update step.
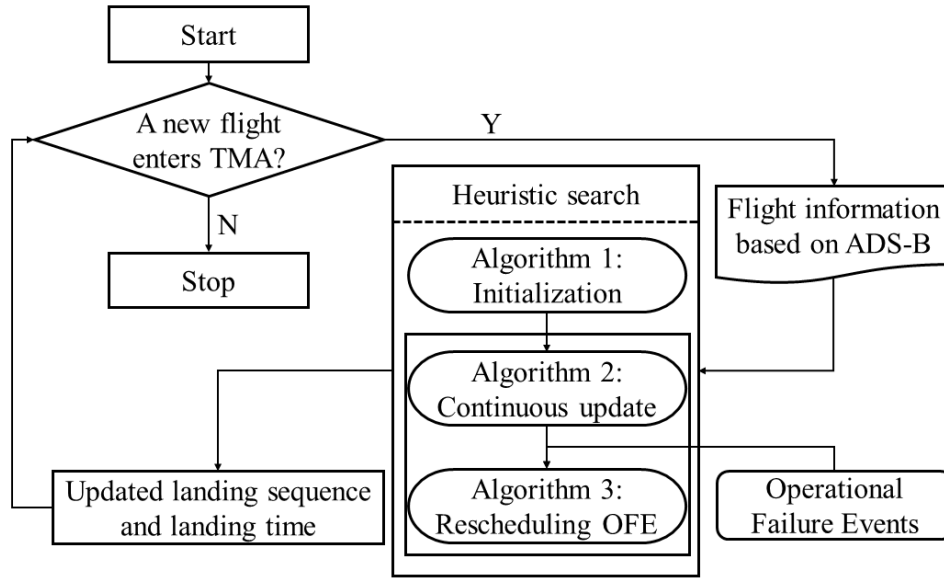
Figure 4.16. Heuristic search workflow for aircraft landing schedule.

This section introduces the algorithm of the aircraft landing problem in detail. Firstly, the initialization of the first two flights is introduced, followed by the continuous update of the heuristic algorithm.

Algorithm 1. Initialization of the first two flights in the decision horizon.

Input	Information of the first two flights j' and i' in the decision horizon: $T_{j'}$, $T_{i'}$, $j' = 1$ and $j' = i$.
Output	Assigned landing time $t_{i'}, t_{j'}$
1	The 1st flight enters TMA at T_j.
2	Calculate $e_{j'} = T_{j'} + F_{j'}^{min}$, and set $t_{j'} = e_{j'}$.
3	The 2nd flight enters TMA at $T_{i'}$.
4	Calculate $e_{i'} = T_{i'} + F_{i'}^{min}$, and compare $e_{i'}$ and $e_{j'}$.
5	If $e_{j'} < e_{i'}$, set $t_{j'} = e_{j'}$, and $t_{i'} = \max\{e_{i'}, t_{j'} + S_{j'i'}\}$.
6	If $e_{i'} < e_{j'}$, set $t_{i'} = e_{i'}$, and $t_{j'} = \max\{e_{j'}, t_{i'} + S_{i'j'}\}$.

After initialization, we introduce the continuous update algorithm for ALP when a new flight i enters TMA at the time T_i. Figure 4.17 shows the schematic diagram.

76

Algorithm 2. Continuous update heuristics.

Input	Information of a new coming flight i: T_i
Output	Assigned landing time on t_i
1	Flight i enters TMA at T_i. Calculate $e_i = T_i + F_i^{min}$.
2	There are two conditions, i.e. (1) or (2). Please see Figure 4.17.
3	Condition (1): find a landing time interval (t_j, t_{j+1}) satisfying $t_j < e_i < t_{j+1}$; set $t_i = \max\{e_i, t_j + S_{ji}\}$. Re-schedule the landing time for flights $m + 1$ to n, if the landing time separations between two adjacent flights are less than the minimum time separation standards.
4	Condition (2): if $e_i > t_j$, set $t_i = \max\{e_i, t_j + S_{ji}\}$.
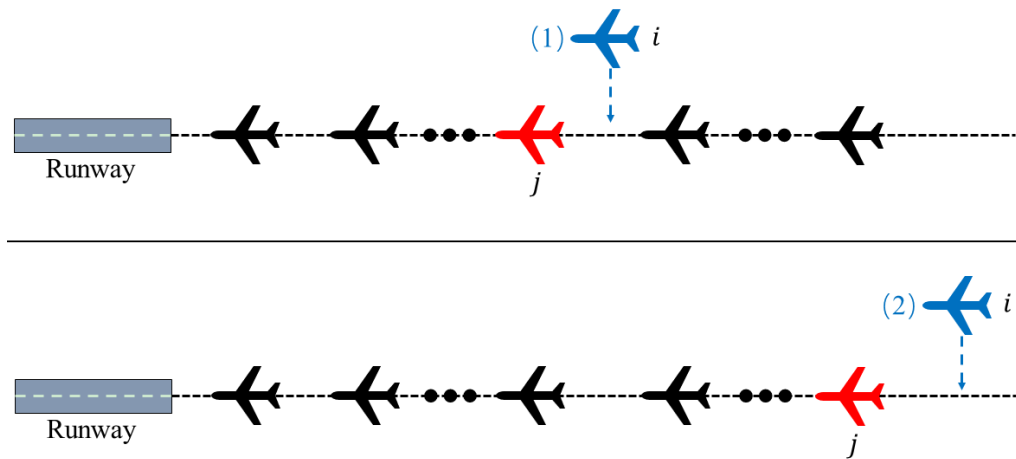
Figure 4.17. Schematic diagram of continuous update heuristics.

In this part, we introduce the ALP algorithm with operational failure events (OFE), e.g., aircraft missing approach. If a flight i cannot land on the runway due to some operational failure problems at T, we will give this flight a higher priority. Based on its current position and speed limit, the earliest landing time is denoted as $\hat{t}_i$. The optimal scheduled landing time in the deterministic solution t_i will now be landing time $\hat{t}_i$ in the rescheduling heuristics. $\hat{t}_i$ will then be updated when an operational failure event occurs. We define the real-time landing sequence decision as $\hat{y}_{ji}$, where $\hat{y}_{ji}=1$, if flight j lands before flight i (not necessarily

immediately); $\hat{y}_{ji} = 0$, otherwise.

Algorithm 3. Rescheduling heuristics under operational failure events (OFE).

Input	The earliest landing time of OFE-flight (*): $\hat{t}_i$
Output	Landing time for all flights.
1	Find an interval satisfying: $\underline{\tau} \leq \hat{t}_i \leq \overline{\tau}$, where $\underline{\tau} = \max\{t_j y_{ji}, \forall j \in I, j \neq i \mid y_{ji} = 1\}$ and $\overline{\tau} = \max\{t_j y_{ij}, \forall j \in I, j \neq i \mid y_{ij} = 1\}$.
2	If $\underline{\tau} + S_{ji} \leq \hat{t}_i$, insert flight i after flight j. The schematic diagram is shown in Figure 4.18 condition (1).
3	The landing time of the upcoming flights will be set as $\hat{t}_i = \min\{\hat{t}_i, \underline{\tau} + S_{ji}\}$ for all the subsequence flights.
4	If $\underline{\tau} \leq \hat{t}_i \cap \underline{\tau} + S_{ji} \geq \hat{t}_i$, swap the positions of flights j and i, and thus, y_{ji} sets to be 0 and $\hat{y}_{ij} = 1$. The updated landing time $\hat{t}_i$ of a certain flight i remains unchanged and the updated landing time of flight j will be $\hat{t}_j = \underline{\tau} + S_{ji}$. The schematic diagram is shown in Figure 4.18 condition (2). Update all the subsequence flights in rules 3 and 4.
5	Check until no violation of minimum time separation standards.
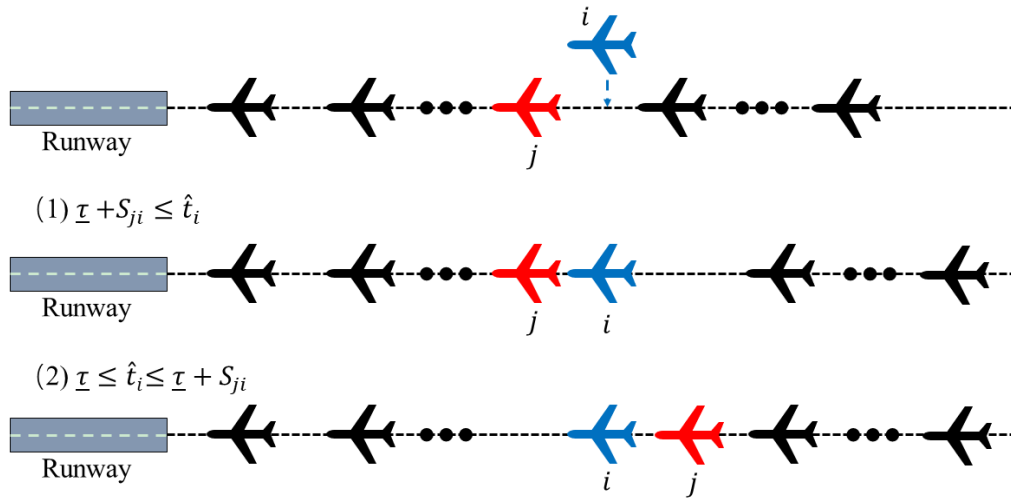
Figure 4.18. Schematic diagram of rescheduling heuristics under OFE.

As mentioned above, some operational failure events may occur during practical operations and cause flights not to be in the expected position, which increases the risk of violating aircraft separation requirements. Taking advantage of ADS-B,

real-time aircraft positions can be monitored. Pilots can then control flight situations to reduce the deviation from target landing time and target flight routes.

4.4.3   Case study results

To test the feasibility and effectiveness of the proposed algorithm, we use the Hong Kong flight data on 5 September 2018 for the study. There were 420 arrival flights at the Hong Kong airport on that day. The layout of arrival routes and waypoints is shown in Figure 4.19. The proposed method implementation is carried out in the personal computer with Intel(R) Core (TM) i7-10510U CPU @ 1.80 GHz 2.30 GHz RAM 4.00 GB and Windows 10 OS. As mentioned in Section 2.2, the method runs and updates once when a new flight enters TMA. Results show that it takes less than one millisecond for each step to update, demonstrating the high efficiency of this method.
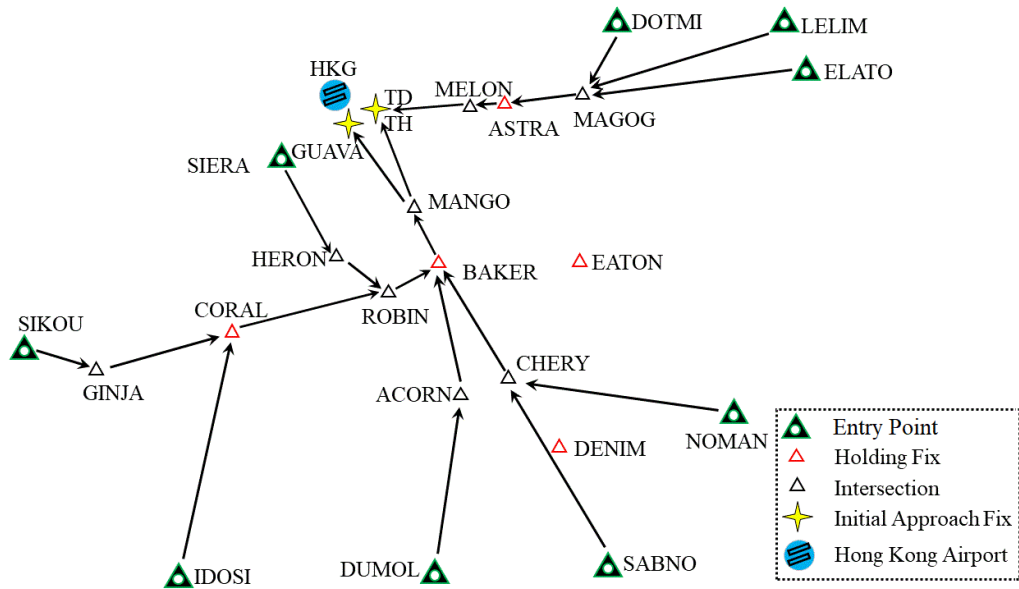
Figure 4.19. Arrival routes of the Hong Kong airport (Jeppesen, 2008).

Based on the numerical results generated from the proposed algorithm, we have compared them with the original historical data and defined an equation below to measure the improvement in flight time.

$$\text{improvement} = \left(\sum_{i \in I} F_i^{ORI} - \sum_{i \in I} F_i^{OPT}\right) \Big/ \sum_{i \in I} F_i^{ORI}$$

where F_i^{ORI} and F_i^{OPT} are the history original flight time and the optimized flight

time of arrival flight i, respectively, calculated by $(t_i - T_i)$. Figure 4.20 shows the saved flight time $(F_i^{ORI} - F_i^{OPT})$ of each flight. It is obvious that most flights can save flight time by 5-15 minutes, except for only six flights enduring longer flight times. These six flights are sacrificed for global objective function optimization. The improvement can be calculated as (16337-11875)/16337=27.3%.
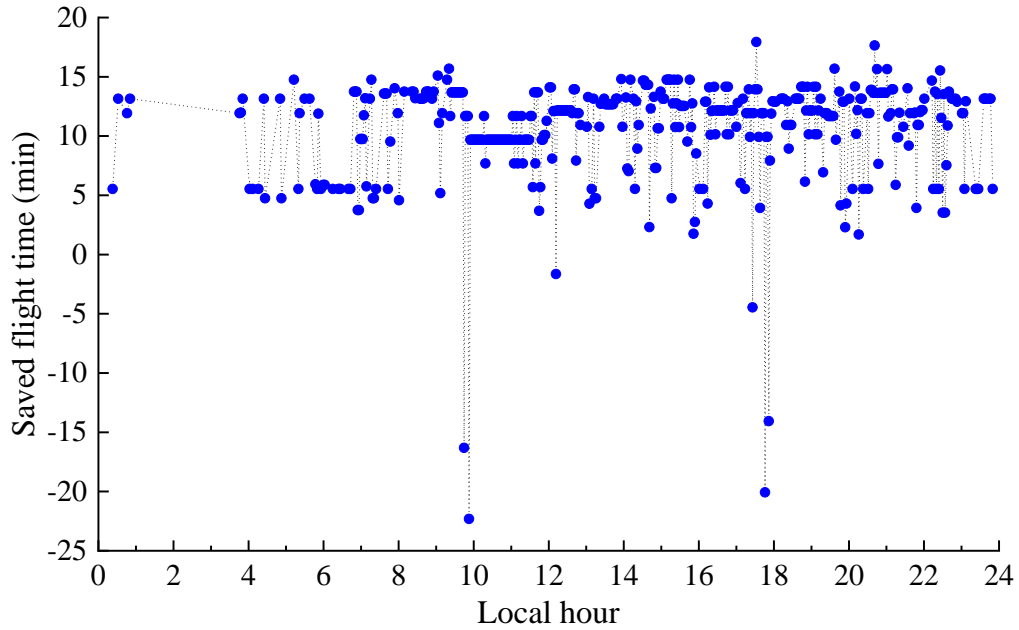
Figure 4.20. The saved flight time of each arrival flight at HKIA in different local hours based on the proposed method for ALP.

Here, we also define another two parameters: (1) delay time of flight i: $D_i = F_i - F_i^{min}$, where F_i and F_i^{min} are the practical and minimum flight time from an entry point to the runway, respectively; (2) landing time interval between flight i and flight $i + 1$: $L_{i,i+1} = t_{i+1} - t_i$, where t_i is the landing time of flight i. Figure 4.21(a) and (b) show delay time distribution and the number of arrival aircraft in terms of local hours, respectively. We can notice that there are more arrival flights during the peak hours (local hour: 10-13), which causes a long delay time if the separation time standard is satisfied. Figure 4.21(c) presents the landing time interval. Most values of $L_{i,i+1}$ range from 3-9 minutes. In theory, thirty flights can land in an hour period with a two-minute separation time interval without any delay time. Figure 4.21 (b) shows that the number of landing aircraft is generally less than thirty, but the delay time still widely exists, which is because many flights

80

are planned to land within a short time slot, which causes the crowdedness of runway allocation. Therefore, some flights are asked to join holding patterns and make circles to maintain safe separation, which causes long flight times and high fuel consumption (Xue et al., 2020a) and pose a threat to flight safety.
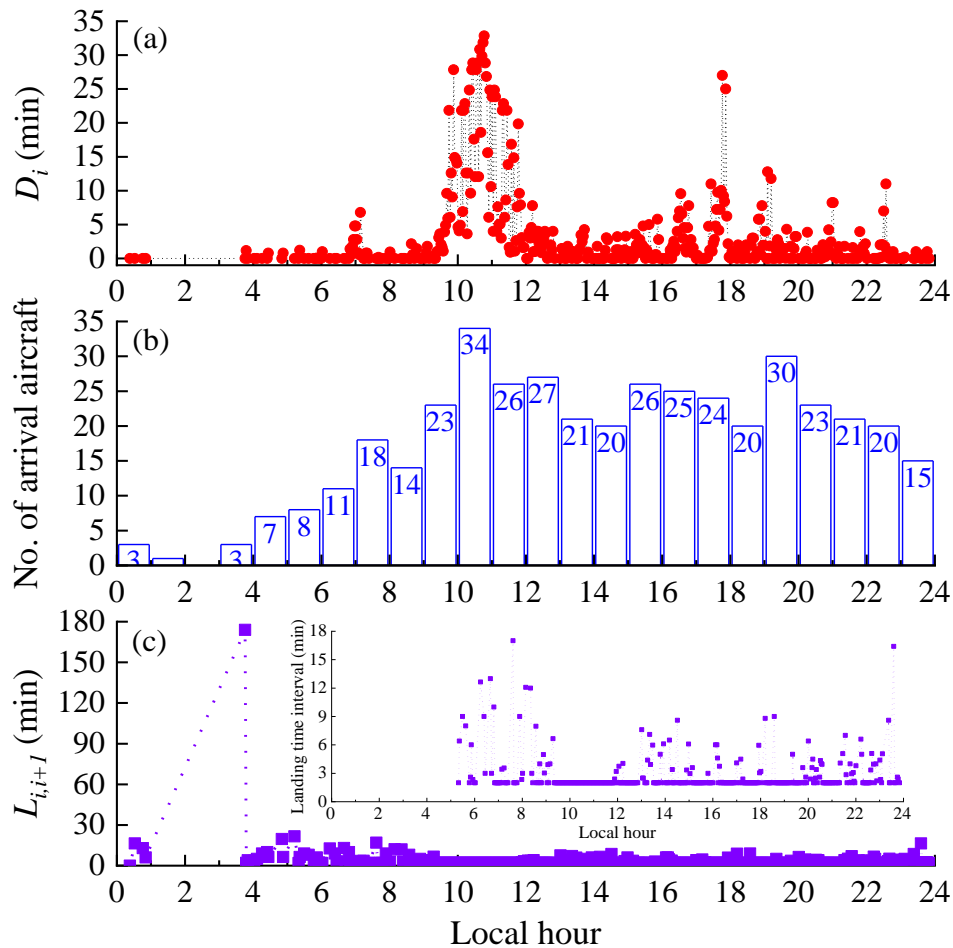
Figure 4.21. Simulation results based on HKIA flight data on 5 September 2018 (a) Delay time of arrival aircraft; (b) the number of arrival aircraft; (c) the landing time interval between two adjacent aircraft.

4.4.4 Discussion

For traditional radar-based ATC, many unnecessary communications commonly exist, increasing the workload of both ATCOs and pilots. ADS-B signals can solve this problem. Except for the graphical information (blips on the screen), ADS-B can provide ATCOs with digital information (longitude, latitude, and altitude), which can increase the confidence level of aircraft positions. On this condition,

ATCOs can reduce the distances among aircraft without violating separation standards, improving situational awareness and airspace capacity utilization (Ali et al., 2017b). Using the historical flight data in Shanghai TMA, we can summarize the relations between ground speed and flight altitude (Figure 4.22(a)). The update rate of ADS-B and radar is assumed to be one second and five seconds, respectively. The average position uncertainty at different flight altitudes can be calculated and is shown in Figure 4.22(b). However, the drawbacks of ADS-B should also be noted. ADS-B performance relies greatly on the GNSS, which can be degraded by space weather and ionospheric scintillation (Xue et al., 2020b), so improving GNSS positioning accuracy is significant (Sun et al., 2020).
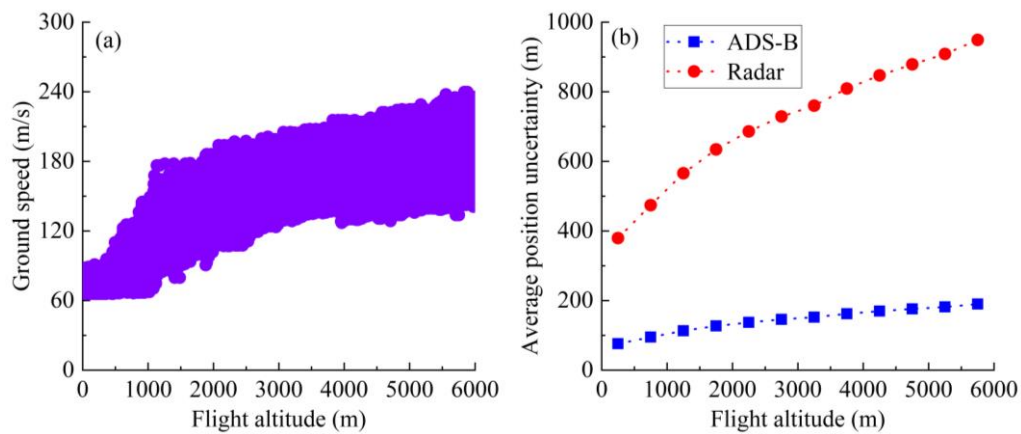
Figure 4.22. (a). Ground speed in terms of different flight altitudes. (b). Average position uncertainty based on a one-second update interval for ADS-B and a five-second update interval for radar.

At the strategic level, ADS-B has a promising applicability. The ground stations can combine the ADS-B data globally and adjust flight plans to avoid unnecessary flight delays and conflicts. As shown in Figure 4.21 (c), many flights are delayed because the landing times of these flights are clustered together without satisfying the time separation standard. To be exact, that is due to the unreasonable arrival time (T_i) at entry point. That is also to say if T_i is assigned reasonably, flight delays can be eliminated. Radar has a limited coverage area (~400 km), so it is challenging to combine real-time flight data in remote, oceanic, and low-altitude areas. On the other hand, ADS-B integration can be achieved based on the ADS-B information-sharing system utilizing receivers in low earth orbit satellites and

on the ground. Herein, we propose a concept based on ADS-B integration to optimize ATM thoroughly, which requires cooperation among ATCs, airlines, and airports. It involves multiple stakeholders and requires further study.

However, in the case of ADS-B failure, the advantages of ADS-B cannot be applied to air traffic management. The increased flight time in each hour due to ADS-B failure is shown in Figure 4.23. Assuming the failure duration time is from 9 LT to 16 LT, the total increased flight time is 1,864 minutes, causing additional fuel of 65.24 tons (35 kg/min×1,864 min) and accordingly CO_2, emission of 205.51 tons. Therefore, the additional economic cost is €333,358, including fuel cost €74,308, CO_2 cost €85,698, and time cost €173,352.
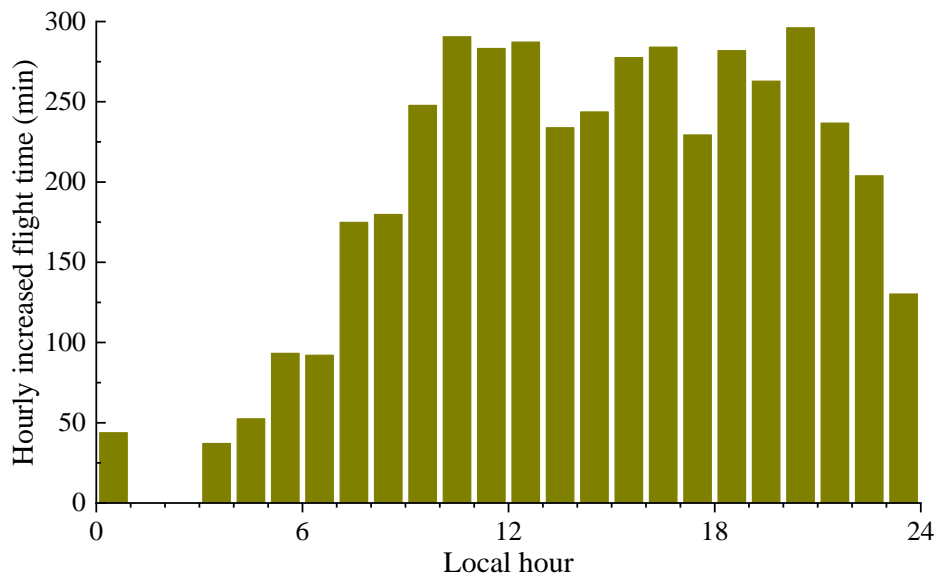
Figure 4.23. The increased flight time in each hour due to ADS-B failure based on the HKIA historical flight data on 5 September 2018.

4.5   Summary

Surveillance technology, including radar and ADS-B, is a significant part of air traffic management, based on which ATCOs can guide aircraft and maintain smooth flight flow. However, space weather events can affect the normal operation of surveillance systems. In the case of ADS-B failure, radar is used for surveillance, although the advantages of ADS-B are unavailable. Likewise, procedure control will be used as a backup system when both radar and ADS-B are unavailable,

which can result in higher aircraft separation standards, less airspace capacity, and more workload for air traffic controllers (ICAO, 2016b). Massive workload during particular work periods may cause fatigue, posing a threat to flight safety (Wingelaar-Jagt et al., 2021).

In order to achieve continuous and real-time aircraft landing time updates and assignments, taking into account the minimum time separation criteria caused by wake turbulence, a unique heuristic search approach based on ADS-B is proposed. The heuristic search approach may instantly provide an aircraft landing time when a new flight reaches the Terminal Maneuvering Area (TMA), to reduce the overall flight time. Compared to radar-based surveillance, ADS-B-based surveillance can reduce flight time for arrival flights significantly. We simulated a scenario by assuming an ADS-B failure duration of 9-16 LT in Hong Kong under the impact of space weather. Using the historical flight data on 5 September 2018, simulation results show that there is an increase in flight time of 1,864 minutes, fuel consumption of 65.24 tons, and CO_2 emission of 205.51 tons. The economic cost caused by ADS-B failure is estimated to be €0.33 million, including fuel cost €74,308, CO_2 cost €85,698, and time cost related to onboard passengers €173,352.

Chapter 5

Elevated Cosmic Radiation Effects on Air Traffic Management

Cosmic radiation poses a threat to the health of aircrew and passengers. As the radiation dose increases with altitude and latitude, one feasible option is to decrease the flight altitude or latitude. Currently, airlines do not fly polar routes during strong radiation storms. These responses to significant cosmic radiation will result in significant costs. This chapter discusses the sources of cosmic radiation and several cosmic radiation systems. Then the cosmic radiation limit for one flight during solar radiation storms is estimated for European airlines. Finally, a multi-objective approach to plan flight altitudes and flight speeds to reduce cosmic radiation and fuel consumption is developed.

5.1   Introduction

5.1.1   Cosmic Radiation Sources

Humans are exposed to a variety of radiation sources with an estimated annual total effective radiation dose of 2.4 mSv per capita, including inhalation (primarily radon) (1.26 mSv), ingestion of food and water (0.29 mSv), cosmic radiation (0.39 mSv), and terrestrial radiation (0.48 mSv) (World Health Organization, 2011). According to the International Commission on Radiological Protection (ICRP), for every 1 Sv increase in effective radiation exposure, the cancer risk increases by 1.65% (Ma et al., 2013).

Cosmic radiation is made up of high-energy protons and atomic nuclei that move through space at nearly the speed of light, originating from the Sun and distant galaxies. Two sources of cosmic radiation are Galactic Cosmic Radiation (GCR) and Solar Energetic Particles (SEP) (Sato et al., 2019). During solar quiet periods, GCR is the primary source of cosmic-ray exposure. The radiation dose rates fluctuate throughout the course of the 11-year solar cycle. In contrast, SEP is an atmospheric incident only when a major solar flare occurs, but the radiation

dosage rates are possibly more than two orders of magnitude higher than those of GCR. National Aeronautics and Space Administration (NASA) has reported that excessive cosmic radiation exposure can potentially induce diseases and biological consequences such as cancer, damage to the central nervous system, and damage to DNA (NASA, 2017). A previous study has found that aircrew members have approximately twice the rate of melanoma as the general population, which could attribute to in-flight exposure to UV rays and cosmic radiation (Sanlorenzo et al., 2015). The guidelines established in NASA-STD-3001 stipulate that the cumulative effective radiation dose for each crew member over their entire spaceflight career should not surpass 600 mSv. Furthermore, in order to mitigate immediate adverse effects, the effective dose limit for short-term radiation exposure resulting from solar particle events is set at 250 mSv per event (Francisco, 2021).

Cosmic radiation can be measured by ground-based neutron monitors. During a powerful Solar Radiation Storm, energetic particles strike our atmosphere and produce secondary particles that may be detected by neutron detectors. When more than three stations detect an increase in radiation, it is classified as a Ground Level Event, which entails an increase in radiation exposure for aircraft in flight. The effect is proportional to height and latitude: the higher the altitude and/or latitude, the greater the impact. Figure 5.1 shows the schematic of the effects of SEP on aviation operations.
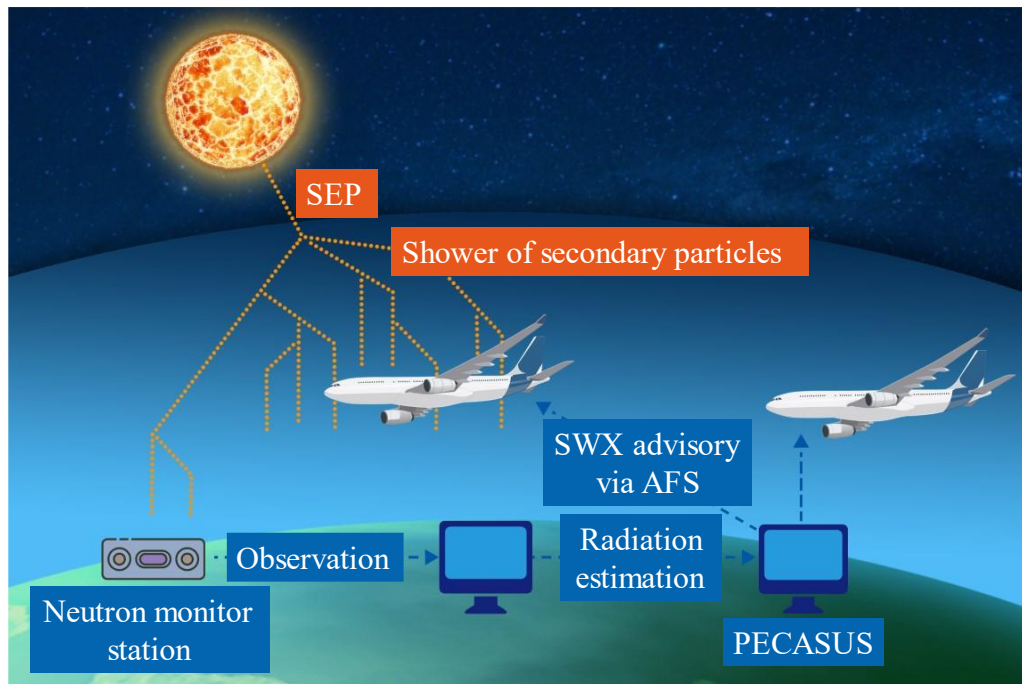
Figure 5.1. Schematic of the effects of SEP on aviation operation.

5.1.2 Cosmic Radiation Calculation Systems

Large Solar Proton Events (SPE) are recognized as a severe hazard to aircrew and passengers in civil aviation (Kataoka, 2011; Tobiska et al., 2015). Thus, the detection and alert of SPE are important. This work can be performed in two approaches: high-energy proton detectors on Geostationary Operational Environmental Satellites (GOES) or neutron monitors on the ground (Sato, 2020). To mitigate exposure to a high level of cosmic radiation, several systems have been developed to issue SEP exposure alerts for the commercial airline industry, such as Warning System for AVIation Exposure to Solar energetic particle (WASAVIES), Aviation Dosimetry (AVIDOS), and Nowcast of Aerospace Ionizing Radiation System (NAIRAS). The detailed descriptions of these three systems are provided as follows.

WASAVIES is a system that assesses the cosmic radiation rate at flight altitudes in real-time and generates an alarm when a rapid increase in the dose rate is observed. WASAVIES was developed by the National Institute of Information and Communications Technology (NICT), Japan Atomic Energy Agency (JAEA), National Institute of Polar Research (NIPR), Hiroshima University, National

Institute of Technology Ibaraki College, and Nagoya University. WASAVIES interpolates the cosmic ray intensity data obtained on the ground and in geostationary orbit using a physical model to calculate the cosmic ray exposure dose at flight altitudes in real time. During quiet space weather days, cosmic radiation intensities do not change significantly. In the case of Ground Level Enhancement (GLE), the data is updated at the interval of 5 minutes (Sato et al., 2014). Figure 5.2 shows the Exposure dose rate map at 12 km altitude at 00:05 UT updated on 12 November 2022 (https://wasavies.nict.go.jp/WorldDose.html).
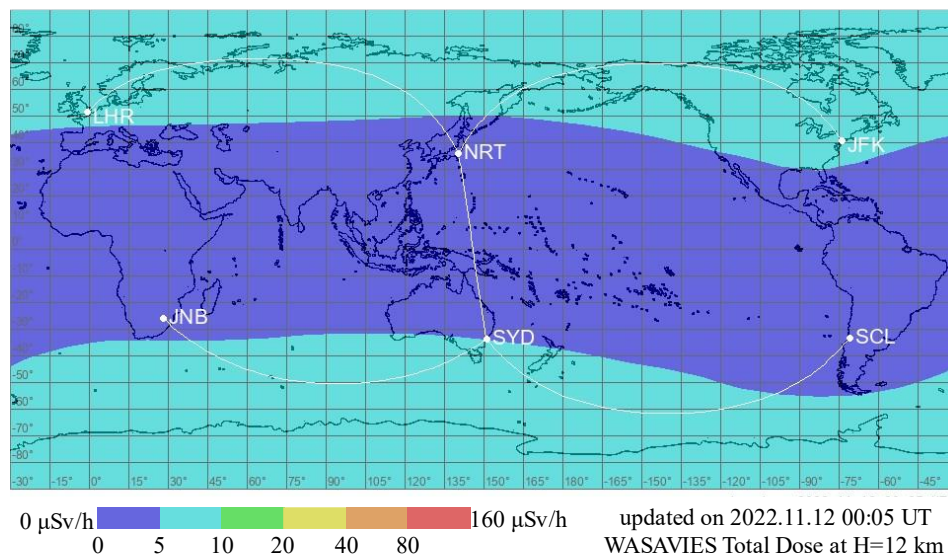
Figure 5.2. Exposure dose rate map at 12 km altitude at 00:05 UT updated on 12 November 2022 from WASAVIES.

AVIDOS is a computer algorithm designed to estimate the exposure of cosmic radiation on aircrew. The algorithm implements a multiparameter model derived from FLUKA (FLUktuierende KAskade) Monte Carlo simulations of cosmic radiation exposure. AVIDOS calculates the ambient dose equivalent and the effective dose. The dose assessment process utilizing AVIDOS has been validated by the Austrian accreditation agency following European laws and is valid across Europe (Latocha et al., 2009). As an example, Figure 5.3 shows the effective dose rate at 11.0 km on 3 November 2022.
(https://www.seibersdorf-laboratories.at/en/products/ionizing-radiation/dosimetry/avidos/current-exposure).
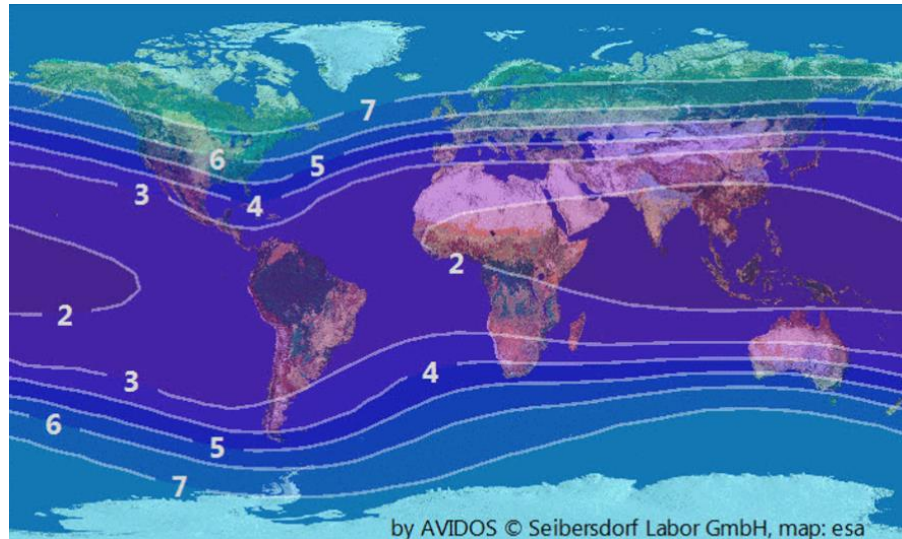
Figure 5.3. The effective dose rate at 11.0 km on 3 November 2022 from AVIDOS.

NAIRAS is a NASA-funded Applied Sciences Program for assessing aviation radiation exposure. The NAIRAS model forecasts atmospheric radiation exposure caused by GCR and SEP. The propagation of GCR particles from space to Earth is modeled based on the Badhwar and O'Neill model (Slaba and Whitman, 2020), with the solar modulation parameterized using high-latitude real-time neutron monitor readings from Oulu, Tomnicki, and Moscow (Ghelfi et al., 2017). During radiation storms, the SEP spectrum is calculated using NOAA/GOES and NASA/ACE satellite ion flux observations. The GCR and SEP transport through the magnetosphere is calculated using the CISM-Dartmouth particle trajectory geomagnetic cutoff rigidity algorithm (Mertens et al., 2013). Figure 5.4 shows the effective dose rate at 11 km at 03:00 UT on 3 November 2022 (https://sol.spacenvironment.net/nairas/Dose_Rates.html).
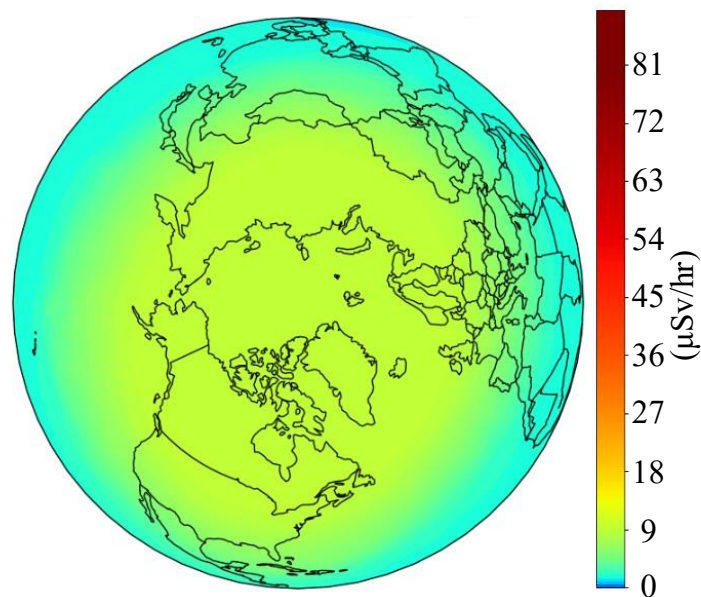
Figure 5.4. The effective dose rate at 11 km at 03:00 UT on 3 November 2022 from NAIRAS.

5.1.3 Aviation Radiation Exposure

Pilots are regarded as occupational radiation workers by the Federal Aviation Administration (FAA) because they can absorb significant cosmic radiation doses when flying high above the Earth with inadequate atmospheric protection (Bagshaw, 2008). Therefore, airline dispatchers are obligated to account for the cumulative cosmic radiation of flight crew while making flight plans. The International Commission on Radiological Protection (ICRP), the FAA, and the Council of the European Union (EU) recommend effective cosmic radiation dose limits for aircrew of 20 mSv/year averaged over five years (a total of 100 mSv in five years) and 1 mSv/year for the general public (Bagshaw, 2008). The ICRP recommends a dose limit of 1 mSv for radiation-related pregnant workers throughout their pregnancy (ICRP, 2016). The National Council on Radiation Protection and Measurements (NCRP) also recommends a monthly radiation limit of 0.5 mSv during pregnancy (NCRP, 2013).

The cosmic radiation intensity is related to altitude, geomagnetic latitude, and solar activity (Yang and Sheu, 2020). The Earth's atmosphere and magnetic field can shield the Earth's surface from cosmic radiation (Parker, 2006), with the

protective effect being greatest at the equator at lower altitudes and weakest towards the poles at higher altitudes. As a result, people on the ground are generally protected against the biological effects of cosmic radiation (Tuo et al., 2012). Due to less protection from the Earth's atmosphere and magnetic field, cosmic radiation rates are stronger at aircraft cruising altitudes and high latitudes than those at low altitudes and low latitudes.

Solar activity is a crucial contributor to the transitory elevation of cosmic radiation (Hapgood et al., 2021; Pesnell, 2012). On a calm space weather day (e.g., 15 March 2013), the total effective cosmic radiation doses along a transequatorial flight (Colombo-Jakarta), a transatlantic flight (Paris-New York), and a transpolar flight (Beijing-Chicago) are estimated to be 9.7, 60 and 82 μSv, respectively (Lochard et al., 2016). During extraordinary Solar Particle Events (SPE), SEP-caused cosmic radiation increases dramatically (Meier and Matthiä, 2014). Table 5.1 lists the total effective doses along specific flight routes on several severe space weather days. Note that the estimated total effective doses for the same flight during the same SPE can be different, e.g. London-New York on 14 July 2000. This is because different cutoff rigidity thresholds are used in different studies. To be specific, the cosmic radiation dose rates decrease with the increase of the cut-off rigidity threshold.

Table 5.1. The total effective doses along specific flight routes under different Ground Level Enhancement (GLE) events. The GLE peak increase rates are from the neutron monitors of the worldwide network (Firoz et al., 2010).

GLE peak increase rate	Date	Flight route	Total effective dose	Source
29.46%	14 July 2000	London-Los Angeles	24 μSv	(Clucas et al., 2005)
	14 July 2000	London-New York	10 μSv	
57.02%	15 April 2001	London-Los Angeles	51 μSv	
	15 April 2001	London-New York	22 μSv	

173.80%	29 September 1989	Continuous 10-hour high-latitude flight at 12 km	570 μSv	([Copeland et al., 2008](#))
269.57%	20 January 2005		390 μSv	
269.57%	20 January 2005	Frankfurt-Los Angeles	168 μSv	([Matthiä et al., 2009](#))
		New York-Beijing	189 μSv	
29.46%	14 July 2000	London-New York	633 μSv	([Anderson et al., 2014](#))
		Paris-San Jose	202 μSv	
5117%	23 February 1956	New York-London	2,670 μSv	([Copeland and Atwell, 2019](#))

According to ICAO Manual on Space Weather Information in Support of International Air Navigation (ICAO Doc 10100) ([ICAO, 2018b](#)), the space weather advisories about radiation are provided as follows.

Inflight or enroute

RAD MOD: Aircraft cannot perform any planned step-climbs. If the current flight level is above the flight level designated in the RAD MOD message, the aircraft are requested to descend to 3,000 ft below that flight level using normal procedures.

RAD SEV: If the current flight level is above the flight level designated in the RAD SEV message, the aircraft are requested to descend to 3,000 ft below that flight level using normal procedures. If no clearance is provided within 30 minutes, aircraft can consider descent to 3,000 feet below the RAD SEV message FL at 1,000-1,500 ft/min.

Dispatch or before departure

RAD MOD: Restrict maximum FL to 3,000 ft below the flight level specified in the RAD MOD message. Apply for 12 hours following the last message.

RAD SEV: There should be no dispatch into RAD SEV areas for 12 hours following the last message.

5.2 Economic Cost Caused by Massive Cosmic Radiation

5.2.1 Cosmic radiation dose

The FAA released a solar radiation alert on 28-29 October 2003, indicating that flights going north or south of 35 degrees latitude were susceptible to high radiation doses (NOAA, 2004). To restrict aviation radiation exposure during the Halloween storm, some polar flights were rerouted to non-polar routes, despite necessitating fuel stops in Japan. Besides, flights between the U.S. and Europe also lowered flight altitudes. The cosmic radiation rates at 11 km from 27 October 2003 to 31 October 2003 were calculated by the Nowcast of Aerospace Ionizing Radiation System (NAIRS), as shown in Figure 5.5. The movie can be found at http://sol.spacenvironment.net/~nairas/Gallery.html.
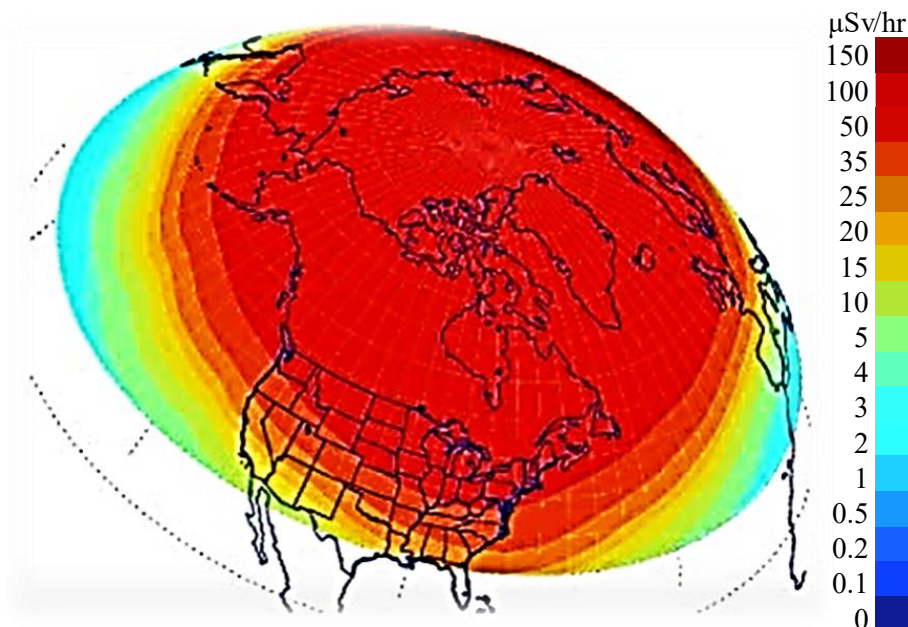
Figure 5.5. Effective dose (galactic cosmic radiation and solar energetic particles) at the altitude of 11 km at UT=12:00 on 28 October 2003. Source: http://sol.spacenvironment.net/~nairas/Gallery.html.

5.2.2 Aviation radiation exposure calculation method

The cosmic radiation rate at a given longitude x and latitude y at time t is denoted by r_{xyt} (in the unit of µSv/min), which is obtained from the NAIRAS. For simplicity, the Great circle routes are assumed to be the real flight routes. We

93

assume that the first and last 30 minutes are used for aircraft climbing and descending, we only consider the cruising period from $T_s = T_d + 30$ to $T_e = T_l - 30$ as the total exposure time of cosmic radiation. Here, T_d and T_l are the departure time at the origin airport and the landing time at the arrival airport, respectively. The total aviation cosmic radiation R_i of a certain flight i is given as

$$R_i = \int_{T_s}^{T_e} r_{xyt} \, dt \qquad (5.1)$$

5.2.3 Economic cost of flight cancellations

We assume that if R_i is above a critical limit, the airlines will choose to cancel the flight, which is one of the most conservative but reliable measures (Jiao et al., 2013). To date, there is still no regulation about the cosmic radiation limits for one flight plan, and it is each airline's responsibility to assess the radiation threat and take appropriate action. We calculated the number of flights whose aviation radiation exposures exceed some specific radiation doses and assumed that airlines would cancel flights in this case. Figure 5.6 shows the number of flight cancellations and corresponding costs for different cosmic radiation limits ranging from 100 μSv to 1,000 μSv. It is obvious the number of flight cancellations during 28-29 October 2003 was higher, which can be explained by the elevated cosmic radiation during these two days. For detailed information about the spatial and temporal distribution of cosmic radiation rates during the Halloween storm, please visit http://sol.spacenvironment.net/~nairas/Gallery.html. To the best of our knowledge, there is still not specific regulation about the cosmic radiation limits for one flight plan. NCRP (2013) mandates that the monthly radiation during pregnancy cannot exceed 0.5 μSv. Consequently, if we set the cosmic radiation limit to 500 μSv, the cancellation costs would be €30.06 million on October 28, €18.56 million on October 29, and €0.35 million on October 30. In contrast, if the limit is set to 1,000 μSv, the total flight cancellation cost would be €2.77 million.
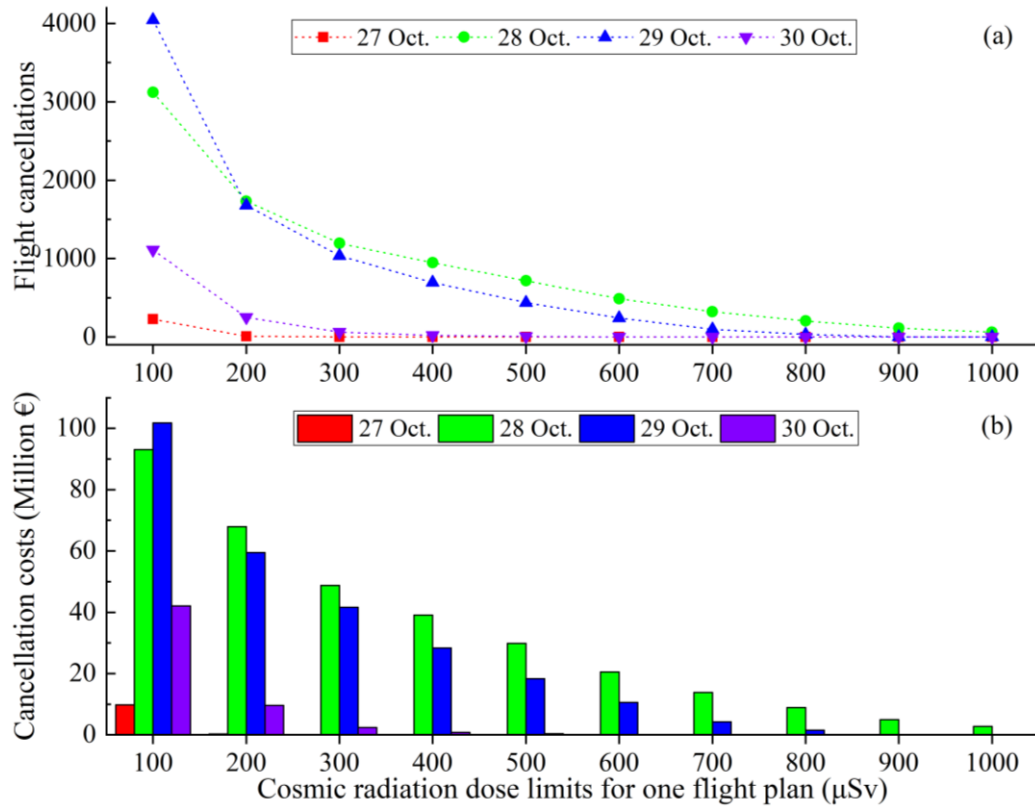
Figure 5.6. The number of canceled flights (a) and the corresponding cancellation costs (b) under different cosmic radiation dose limits for one flight plan.

5.2.4 Economic cost of flight rerouting and lowering altitudes

Apart from canceling flights, airlines can reroute flight paths and lower flight altitudes in reaction to extremely high cosmic radiation (Saito et al., 2021). Rerouting is not considered in this study due to the possibility of increased fuel consumption and possible airspace rights infringement. Lowering flight altitudes is another approach to reduce aviation exposure due to atmosphere protection. Herein, we assume that we do not get cosmic radiation at the height of 9 km. Therefore, we propose a hypothetical scenario and assume that flights can avoid exceeding the cosmic radiation threshold by lowering flight altitude to 9 km. According to Table 5.2, the additional fuel costs caused by lowering flight altitudes would be €5.24 million on October 28, €3.15 million on October 29, and €0.07 million on October 30. It seems that lowering flight altitudes is a better choice because the expenses are much less than canceling flights. However, airspace capacity in each flight level needs to be considered during real operations,

as it may cause air traffic congestion and flight safety problem.

Table 5.2. The nominal fuel consumption at two different Flight Levels (1 FL=100 ft) according to the Base of Aircraft Data (BADA).

Aircraft types	Capacity seats	Fuel consumption rate (kg/min)	
		291 FL	361 FL
A332	250	110.7	91.75
A333	290	108.7	87.75
A350	350	119.4	102.8
A388	520	240.8	213.1
B744	420	179.4	155.9
B763	260	89.1	77.3
B772	360	115.3	104.35
B773	380	125.4	118.7
B788	240	92.9	82.55
B789	195	97.7	88

5.3   Cosmic Radiation Limit Estimation for European Airlines

According to Bundesamt für Strahlenschutz (2022), the occupational group with the highest radiation exposure in 2019 is aircrew, with an average annual effective dose of 1.82 mSv. Comparatively, the average yearly radiation exposure of medical personnel is far lower, at 0.32 mSv. Detailed information is shown in Figure 5.7 (Bundesamt für Strahlenschutz, 2022).
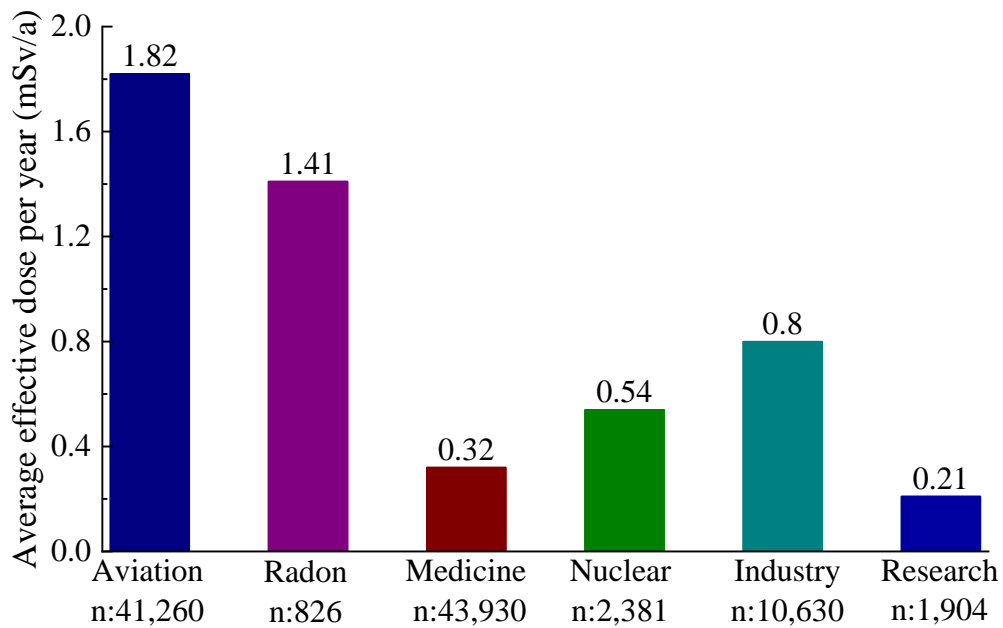
Figure 5.7. Average annual radiation doses in different occupational groups (n: number of radiation-exposed individuals per occupational group) (Bundesamt für Strahlenschutz, 2022).

The EU mandated that aircrew should conduct radiation protection monitoring. With the amendment of the German Radiation Protection Ordinance (Palm, 2002), this requirement has become national law in Germany ever since, which states that aircrew needs mandatory monitoring if they receive more than 1 mSv of effective dose from cosmic radiation during flights. The radiation exposure must be monitored, limited, and reduced based on an individual case. Airlines are required to establish the radiation dose levels and minimize aviation radiation exposure through aircrew scheduling and flight routes. Civil Aviation Research Institute (CARI) series models can calculate the aviation radiation exposure of each flight based on flight data (origin and destination airport, flight duration and altitude, date) and known physical conditions (e.g., neutron flux density) (Copeland, 2017). The variation in the distribution of doses for aircrew is shown in Figure 5.8 (Bundesamt für Strahlenschutz, 2022). Annual dose levels in the interval of 1.5-2.0 mSv are the highest, while the others form a broadly symmetrical distribution around this group. Besides, there is no aircrew with an annual dose of more than 6 mSv.
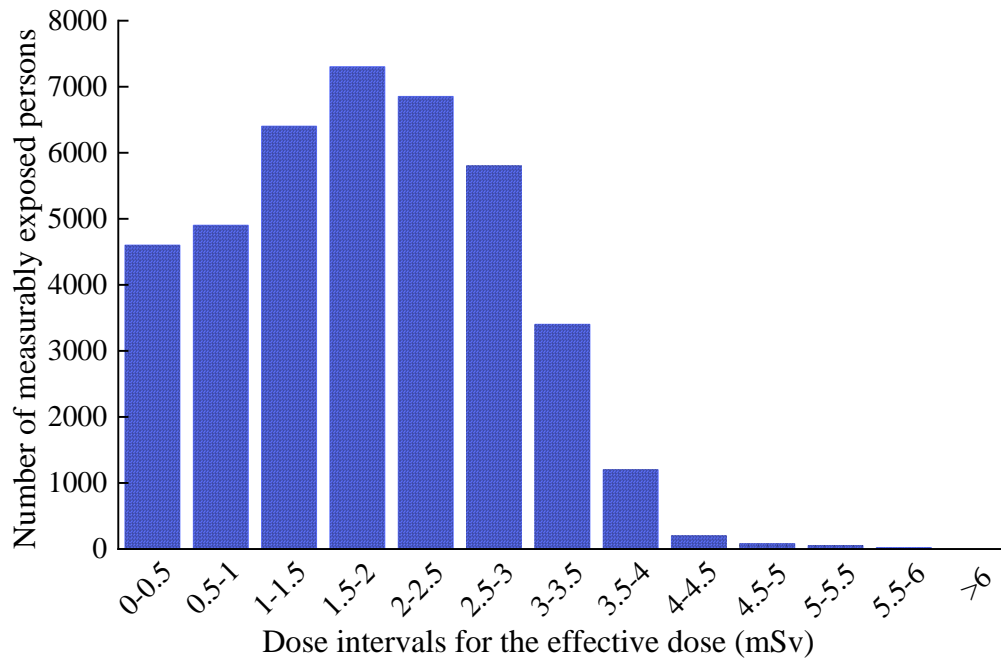
Figure 5.8. The frequency distribution of the annual doses of aviation staff in 2019 in Germany (Bundesamt für Strahlenschutz, 2022).

Cosmic radiation is more severe in Europe due to weaker shielding of the magnetic field in higher latitude regions than in the lower latitude regions. Considering aircrew health, the EU recommends a cosmic radiation control level C^* of 6 mSv per year for aircrew (Bagshaw, 2008; Thierfeldt et al., 2009). Aviation radiation exposure is also related to the total flight time, and it is estimated that the average annual flight time $\mathcal{D}$ for airline pilots is ~700 hours (Flying Staff, 2022). Based on WASAVIES or NAIRAS model, the cosmic radiation rates r in Europe during quiet space weather days can be ~8 μSv/h. Therefore, the cosmic radiation dose limit for one flight trip during the elevated cosmic radiation period is estimated to be $C_{\max} = C^* - \mathcal{D}r$=6,000 μSv-8 μSv/h×700 h=400 μSv. That is to say if the anticipated cosmic radiation dose of one flight trip exceeds $C_{\max}$=400 μSv, the flight should be canceled. We believe the policy recommendations can serve as a criterion for airline decision-makers to assure financial profit meanwhile without jeopardizing aircrew health, by not exceeding the cosmic radiation exposure threshold.

This investigation would greatly benefit the airline industry by protecting airlines from exceeding EU radiation protection standards when extreme space events

occur. Aircrew scheduling is a critical and challenging task for airlines (Quesnel et al., 2020), as aircrew cost is the second-largest component of an airline's total operating cost, just after fuel consumption cost (Wen et al., 2022). If the aircrew is expected to experience massive cosmic radiation for a particular flight route, airlines will have to take certain actions to reschedule flight plans, and sometimes it may disrupt the whole aircrew scheduling. This may hinder airlines to maintain profitability in the competitive market (Lopes et al., 2016; O'Connell et al., 2020).

5.4   Flight Altitude Assignments during Solar Radiation Storm

In response to SPE-caused high cosmic radiation alerts, airlines may lower flight altitudes or reroute flights to lower latitudes (Matthiä et al., 2015), which can result in increased fuel consumption and aircraft emissions (Fujita et al., 2021; Saito et al., 2021). Particularly, flight rerouting is sometimes constrained by air traffic management regulations. Therefore, airlines may inevitably cancel flights, which can cause additional financial costs (Taylor et al., 2021; Yamashiki et al., 2020) and disrupt passenger itineraries (Hu et al., 2021). To the best of our knowledge, the cosmic radiation threshold for any given flight trip has not been established. Considering these issues, we first analyze the cosmic radiation of one flight trip of a European airline during a space weather event. We then propose a multi-objective optimization model based on Mixed-Integer Linear Programming (MILP) to assign the optimal flight altitudes and speed with the objective of minimizing fuel consumption and cosmic radiation. In addition, the Pareto frontier representing the best trade-off between cosmic radiation and fuel consumption is provided as a guideline for tactical ATM based on various preferences and intentions.

5.4.1   Flight Information

A long-distance international flight from Tokyo Narita Airport (NRT) to London Heathrow Airport (LHR) on 6 October 2018 is selected as the case study subject. The historical flight data (https://opensky-network.org/) indicate that: (1) the aircraft type is B787-900; (2) enroute time is ~12.5 hours with a cruising speed of 850 km/h (460 knots); (3) the most representative flight altitude is 12,200 m (40,100 ft); and (4) the great circle route is assumed to represent the actual flight

route with a distance of about 9,600 km (Figure 5.9). We assume the climbing and descending segments are each 300 km and thus set the cruising distance to be 9,000 km and divide it into nine flight segments with 1,000 km for each segment. For example, the first flight segment ($i = 1$) is 300-1,300 km from NRT, and the ninth flight segment ($i = 9$) is 8,300-9,300 km from NRT. Most of the flight route is in high latitude regions and therefore is susceptible to a high level of cosmic radiation.
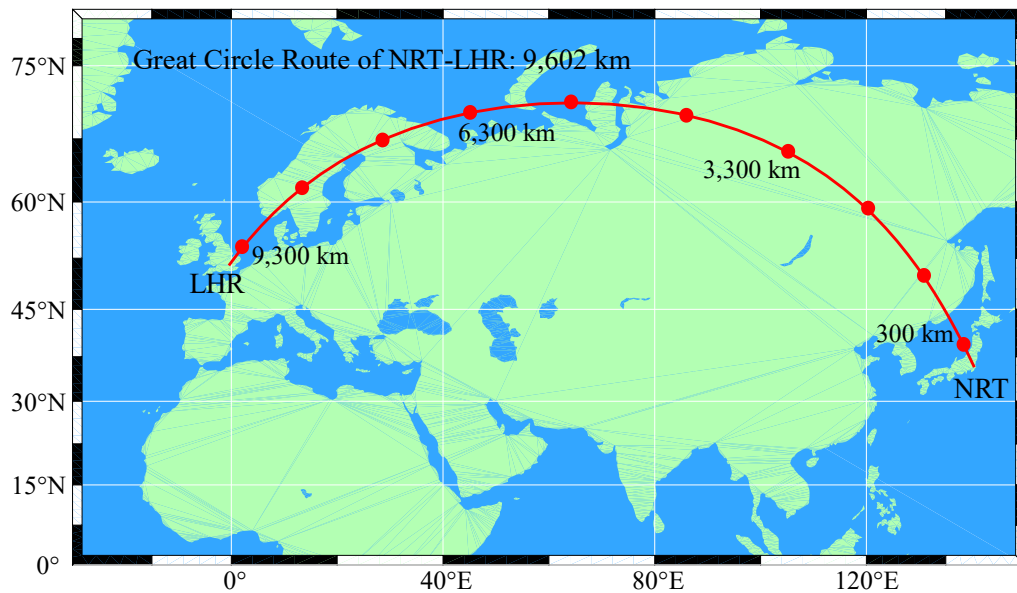
Figure 5.9. The great circle route from NRT (35.765°N, 140.386°E) to LHR (51.477°N, 0.461°W). The cruise phase distance is 9,000 km, and the rest 600 km is for the climbing and descending phases.

5.4.2 Radiation data

The SPE on 20 January 2005 was one of the largest GLE events ever recorded in the neutron monitors of the worldwide network since 1956 (Plainaki et al., 2007; Saito et al., 2021). During this event, the effects of the radiation exposure at altitudes of 12 km were estimated to be ~1.8 mSv/h during 0650-0655 UTC in the Antarctic region and about 0.1 mSv/h at a latitude of 70° in the Northern Hemisphere during 0710-0715 UTC (Matthiä et al., 2009; Mishev et al., 2015). WASAVIES is a physics-based forecast model that computes global cosmic radiation dose rates at different altitudes (Kataoka et al., 2014; Kataoka et al., 2018;

Sato et al., 2018). We use their modeling results to estimate the cosmic radiation information along NRT-LHR during this strong space weather event when a remarkable increase in cosmic radiation rate is obtained in the simulation (Figure 5.10a). For comparison, the radiation is significantly lower during a quiet space weather day on, e.g. 16 March 2022 (Figure 5.10b). Constrained by flight altitude regulation (ICAO, 2016a), six flight altitudes from 301 FL to 401 FL (1 FL=100 ft) with a vertical separation of 20 FL are considered and are indexed by $j = 1, 2, \dots, 6$. For example, $j = 1$ indicates 301 FL, and $j = 6$ indicates 401 FL. Based on WASAVIES simulation results, cosmic radiation rates c_{ij} in flight segment i at flight altitude j are shown in Table 5.3. If the aircraft flies as usual at the altitude of 401 FL without any response to the increased cosmic radiation on 20 January 2005, the total effective cosmic radiation dose would be over 700 μSv assuming that the global effective dose rate distribution in Figure 5.10(a) lasted over the entire flight time. Consequently, the radiation dose for this flight journey will exceed the $C_{\max}$=400 μSv threshold.
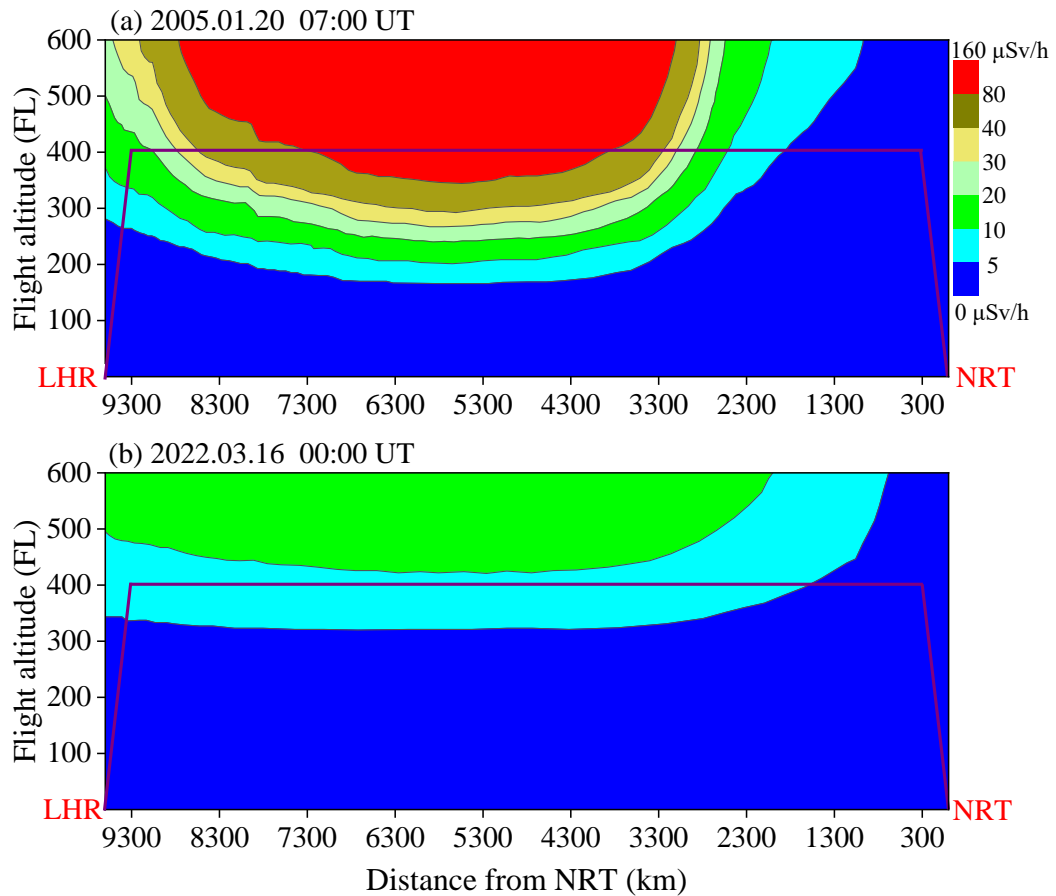
Figure 5.10. WASAVIES simulation results of radiation dose rate along the NRT-LHR flight route on (a) a severe space weather day like 20 January 2005 and (b) a quiet space weather day (16 March 2022). Purple lines outline the schematic diagram of the flight profile from NRT to LHR with the cruising altitude at 401 FL.

Table 5.3. WASAVIES simulation results of average effective radiation dose rate (µSv/h) along the NRT-LHR flight route at different flight levels and at different flight segments.

Flight level	Flight segment i								
	9	8	7	6	5	4	3	2	1
401	33.8	60	118	120	120	84	22.1	4.5	2.5
381	25	60	96	120	120	72	20.3	4	2.5
361	21.7	52	78	120	108	56	15	3.5	2.5

341	19	39	60	60	60	49	13.3	3	2.5
321	14.8	28	50	60	60	40	10.4	2.5	2.5
301	12	21	32	52	35	27	9.5	2.5	2.5

5.4.3 Wind speed data

Wind can play an important role in flight time and fuel consumption, and dispatchers in airlines need to consider the effects of wind while making flight plans. In this study, we use wind data from the National Centers for Environmental Prediction (NCEP) of the United States, which can provide national and global weather, water, climate, and space weather guidance, forecasts, and warnings. The adopted wind speed data are at 12 UT on 1 March 2022. The average headwind speeds in each flight segment and flight altitude are shown in Figure 5.11 (https://rda.ucar.edu/datasets/ds083.2/index.html#sfol-fw?g=22022).
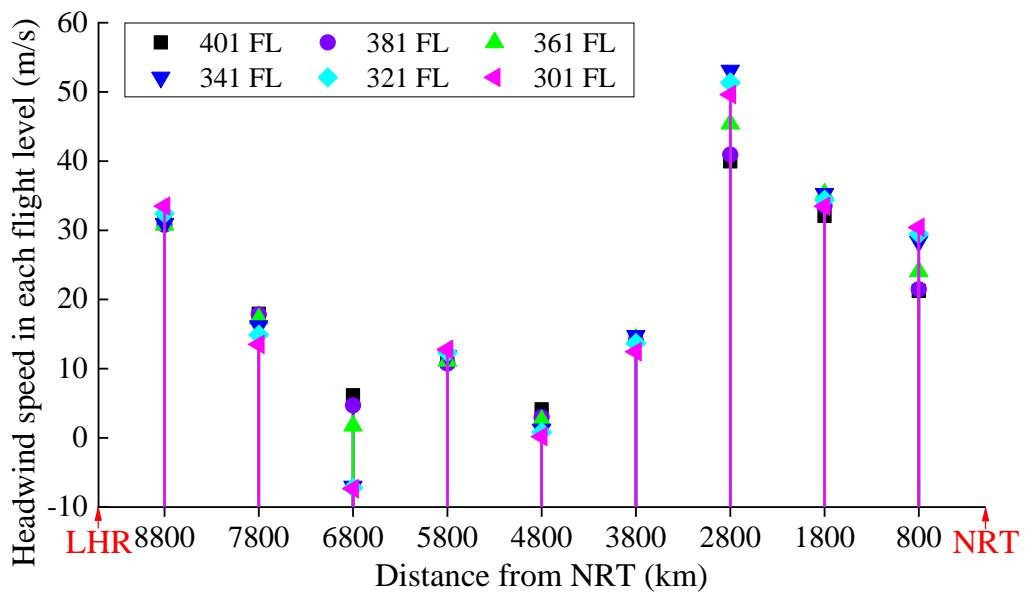
Figure 5.11. The average wind speed at different flight altitudes used for our modelling.

5.4.4 Fuel consumption model

According to the Base of Aircraft Data (BADA) (EUROCONTROL, 2022), the nominal fuel flow f_{ij} (kg/min) in flight segment i at flight altitude j is related to

103

true airspeed (TAS) v_{ij} and the standard air density ρ_{ij}. The wind speed w_{ij} in flight segment i at flight altitude j also plays an important role in flight time and consequently affects fuel consumption. The ground speed g_{ij} vector can be expressed as $g_{ij} = w_{ij} + v_{ij}$. Therefore, the ground speed (km/h) can be expressed by $g_{ij} = |w_{ij} + v_{ij}|$. For a given flight route of distance L (km), the fuel consumption F_{ij} (kg) in flight segment i at flight altitude j can be expressed as:

$$F_{ij} = 60 \cdot f_{ij} \cdot \frac{L}{g_{ij}} \tag{5.2}$$

where the nominal fuel flow f_{ij} (kg/min) in flight segment i at flight altitude j, which is defined as a function of thrust-specific fuel consumption η_{ij} (kg/(min·kN)) and engine thrust T_{ij} (N).

$$f_{ij} = \frac{\eta_{ij} \cdot T_{ij}}{1000} \tag{5.3}$$

where η_{ij} is related to the thrust-specific fuel consumption coefficients C_{f_1}=0.5466, C_{f_2}=1198.1, and the true airspeed (TAS) v_{ij} (km/h).

$$\eta_{ij} = C_{f_1}\left(1 + \frac{v_{ij}}{1.852 \cdot C_{f_2}}\right) \tag{5.4}$$

During the cruise phase, the thrust is assumed to be equal to the drag force D_{ij} (N) in (5.5), and the drag force can be calculated using the formula (5.6)-(5.8) ([EUROCONTROL, 2022](#)).

$$T_{ij} = D_{ij} \tag{5.5}$$

$$D_{ij} = \frac{1}{2}C_{D.ij} \cdot \rho_{ij} \cdot \left(\frac{v_{ij}}{3.6}\right)^2 \cdot S \tag{5.6}$$

$$C_{D.ij} = C_{D_0.CR} + C_{D_2.CR} \cdot \left(C_{L.ij}\right)^2 \tag{5.7}$$

$$C_{L.ij} = \frac{2 \cdot m \cdot g_0}{\rho_{ij} \cdot v_{ij}^2 \cdot S \cdot \cos\theta} \tag{5.8}$$

where $C_{D.ij}$ is the standard drag coefficient; ρ_{ij} is the standard air density (kg/m³); S =360.5 m² is the wing reference area (m²); $C_{D_0.CR}$ =0.021871 and

$C_{D_2.CR}$=0.034141 are drag coefficients; $C_{L.ij}$ is the lift coefficient, which is related to the aircraft mass (m=213,220 kg) and bank angle θ=0°.

5.4.5 Multi-objective optimization model

We use a multi-objective optimization model based on MILP to quantify the optimal values for both flight altitude j and true airspeed v_{ij}. This optimization is performed based on the following assumptions. First, we use the WASAVIES simulation results to specify the distribution of the global effective dose rates. Then we assume that distribution does not change during the whole flight time, which is similar to (Saito et al., 2021). Second, we ignore the impact of altitude-changing phases between 301 FL and 401 FL on final results since these two phases (i.e. climbing from 300 FL to 400 FL and descending from 400 FL to 300 FL) contribute less than 1% to the total effective radiation doses and fuel consumption. Our modeling is to minimize the objective function (5.9) of the total weighted radiation dose and fuel consumption.

$$z = \sum_{i \in I} \sum_{j \in J} \sum_{v \in V_j} x_{ijv} \left(\alpha \frac{\delta C_{ijv}}{C_r} + \beta \frac{F_{ijv}}{F_r} \right) \tag{5.9}$$

where I=9 is the total number of flight segments indexed by i; J=6 is the total number of feasible flight altitudes indexed by j; V_j is the feasible TAS at flight altitude j constrained by the flight envelope; x_{ijv} is a binary decision variable; α and β are the weights of radiation dose and fuel consumption, respectively; δ represents the error in the global cosmic radiation calculation, defined as the ratio of the True cosmic radiation to the Forecast cosmic radiation (RTF); C_{ijv} is the WASAVIES simulated cosmic radiation dose in flight segment i at flight altitude j with TAS v_{ij}; F_{ijv} is the corresponding fuel consumption; C_r=100 μSv is the referential cosmic radiation dose from NRT to LHR; F_r=60 tons is the referential fuel consumption from NRT to LHR. The detailed flowchart of the proposed model is illustrated in Figure 5.12.

The constraints are listed as follows:

$$\alpha + \beta = 1 \text{ with } 0 \leq \alpha \leq 1 \text{ and } 0 \leq \beta \leq 1 \tag{5.10}$$

$$\sum_{j \in J} \sum_{v \in V_j} x_{ijv} = 1, \forall i \in I \tag{5.11}$$

$$\sum_{i \in I} \sum_{j \in J} \sum_{v \in V_j} \delta x_{ijv} C_{ijv} \leq C_{\max} \tag{5.12}$$

$$\sum_{i \in I} \sum_{j \in J} \sum_{v \in V_j} x_{ijv} F_{ijv} \leq F_{\max} \tag{5.13}$$

$$x_{ijv} \in \{0,1\} \tag{5.14}$$

Constraint (5.10) defines the cosmic radiation weight α and fuel consumption weight β. Constraint (5.11) states that each flight segment i should be assigned only one flight altitude j with only one TAS (v_{ij}). Constraint (5.12) indicates that the total cosmic radiation dose cannot exceed $C_{\max}$=400 μSv. Constraint (5.13) indicates that the total fuel consumption cannot exceed $F_{\max}$=90 tons based on aircraft fuel tank capacity. Constraint (5.14) indicates that if a TAS v_{ij} is set for flight segment i and flight altitude j, x_{ijv}=1, otherwise, x_{ijv}=0.
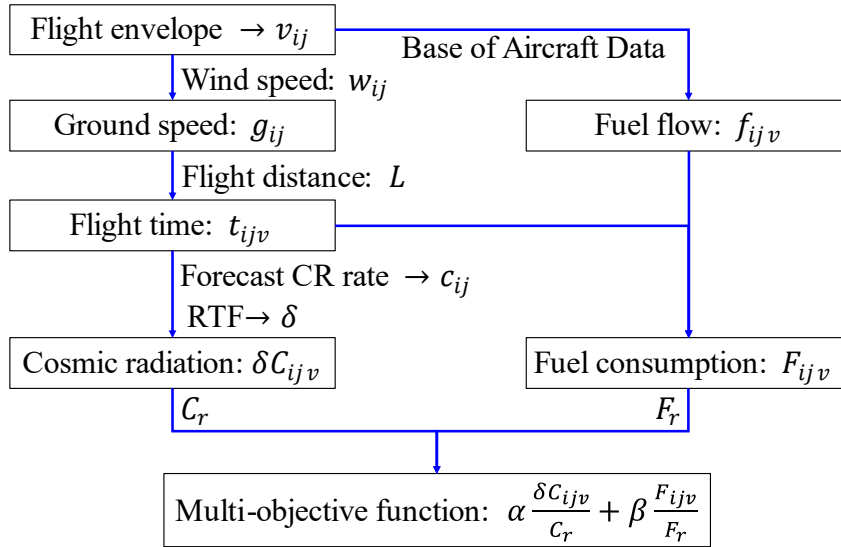
Figure 5.12. Multi-objective optimization model flowchart. Considering the specific TAS v_{ij}, and wind speed w_{ij}, and flight distance L, we can obtain flight time $t_{ijv} = L/g_{ij}$. Then the cosmic radiation dose C_{ijv} in flight section i at flight altitude j can be calculated by $C_{ijv} = \delta c_{ij} t_{ijv}$ based on the WASAVIES simulated cosmic radiation rate c_{ij} and RTF δ. The fuel consumption F_{ijv} in flight segment

i at flight altitude j can be calculated by $F_{ijv} = f_{ijv}t_{ijv}$, where the fuel flow f_{ijv} is based on BADA.

5.4.6 Results

Traditional solutions for reducing cosmic radiation

Similar to the two traditional solutions (lower flight altitude and reroute) proposed in (Saito et al., 2021), the results for this case study are as follows.

(1) Lower flight altitude while maintaining the same flight route and speed as the original flight plan. The new flight altitudes for the test are 301, 321, 341, 361, and 381 FL. Considering different δ, the final results of cosmic radiation dose and fuel consumption are summarized in Table 5.4. The calculated cosmic radiation dose with δ=1.0 is less than $C_{\max}$ only when the flight altitude decreases to 341 FL or below. However, fuel consumption is 66 tons at 341 FL or more at lower altitudes.

(2) Reroute while maintaining the same flight altitude and speed as the original flight plan. Referring to the rerouting method proposed for theoretical analysis in (Saito et al., 2021), Figure 5.13 outlines the new flight route: first from NRT (35.765°N, 140.386°E) to T (35.765°N, 0.461°W) along the same latitude, and then from T (35.765°N, 0.461°W) to LHR (51.477°N, 0.461°W) along the same longitude. The cosmic radiation rates can be estimated using Figure 5.13 and RTF δ. In the first segment, the distance from NRT to T is $2\pi r \times\cos(35.765°)\times(0.461°+140.386°)/360°$=12,708 km, where r is the mean radius of the Earth, equal to 6,371 km. Accordingly, the flight time from NRT to T is 12,708 km/(460×1.852 km/h)=14.91 h. The cosmic radiation is 3δ μSv/h×14.91 h=44.76δ μSv. In the second segment, the distance from T to LHR is $2\pi r\times(51.477°-35.765°)/360°$=1,747 km. The flight time from T to LHR is 1,747 km/(460×1.852 km/h)=2.05 h. The cosmic radiation is about 3δ μSv/h×2.05 h×2/3+15δ μSv/h×2.05 h×1/3=14.35δ μSv. Thus, the total cosmic radiation is 59δ μSv, and the total fuel consumption is (14.91 h+2.05 h)×60 min/h×f=89 tons, where

f=87.66 kg/min is the nominal fuel flow at 401 FL at a cruising speed of 460 kt. Therefore, it can be concluded that rerouting can reduce the cosmic radiation dose to 59δ µSv, unlikely to exceed C_{max}=400 µSv; but it will increase fuel consumption by about 50%, nearly approaching the maximum fuel tank capacity (90 tons), and also produce more aircraft emissions. In practice, Air Navigation Service Providers (ANSPs) can assist with flight rerouting in reaction to such space weather events. However, airlines may also decide not to accept the re-designed flight route based on considerations such as flight duration, aircraft, and crew allocation, and additional crew expenses (Britto et al., 2012).

Table 5.4. Results of fuel consumption and cosmic radiation dose in two traditional solutions: lowering flight altitudes vs. rerouting.

Methods	Flight level	Fuel consumption (ton)	Cosmic radiation dose (µSv)				
			δ=0.8	δ=0.9	δ=1.0	δ=1.1	δ=1.2
Lowering flight altitudes	401	61	579	652	724	796	869
	381	62	531	598	664	730	797
	361	64	469	527	586	645	703
	341	66	319	359	399	439	479
	321	68	278	312	347	382	416
	301	70	199	224	249	274	299
Rerouting	401	89	47	53	59	65	71
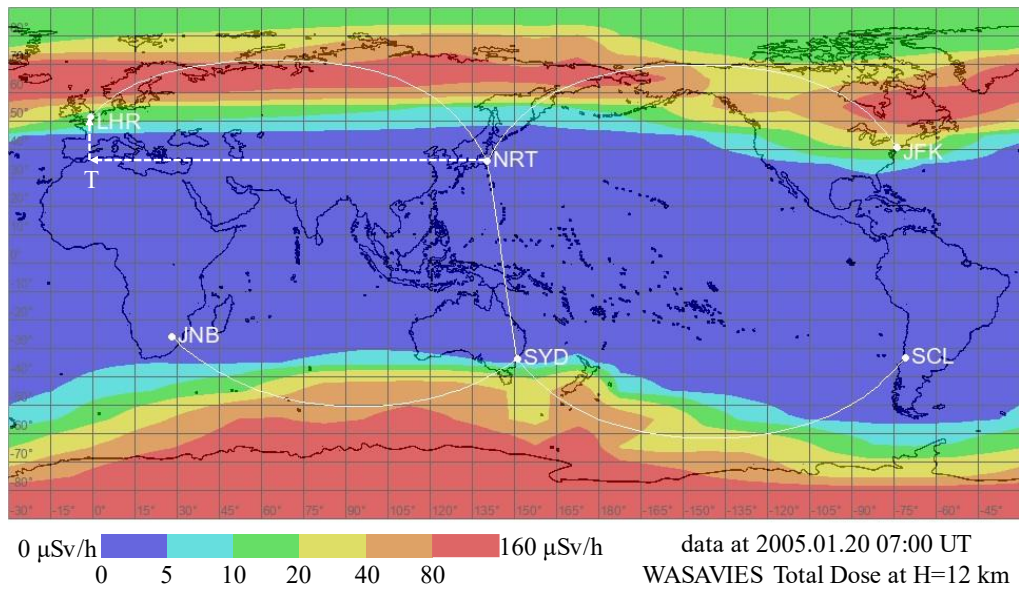
Figure 5.13. Worldwide map of calculated dose rate during GLE69 (7:00 UT, 20 January 2005) from WASAVIES (https://wasavies.nict.go.jp/about_e.html).

Optimized solutions for reducing cosmic radiation

Compared to traditional solutions, this section introduces the advantages of our proposed optimized solutions. In the objective function (equation 5.9), α and β are the weights of cosmic radiation and fuel consumption, respectively. As airlines may have different preferences about cosmic radiation and fuel consumption, airline dispatchers can assign various weights to these two parameters. Sensitivity analysis is conducted to provide dispatchers with sensible decisions about flight planning. Taking the cosmic radiation forecast error into consideration, Table 5.5 lists the detailed results of cosmic radiation and fuel consumption under various weighting values α. For a given α, the fuel consumption increases with the increased δ, because aircraft has to fly at lower altitudes to satisfy the constraint of total cosmic radiation dose. As the accuracy of forecast models will be determined more precisely, airlines may set a more sensible value of δ.

Table 5.5. Results of cosmic radiation (CR) and fuel consumption (FC) under various weighting values α in the case of different RTF δ.

	δ=0.8		δ=0.9		δ=1.0		δ=1.1		δ=1.2	
α	CR	FC	CR	FC	CR	FC	CR	FC	CR	FC

109

0	399.9	60.3	399.9	61.1	399.9	62.0	399.9	62.9	399.8	63.6
0.01	399.9	60.3	399.9	61.1	399.9	62.0	399.8	62.9	399.8	63.6
0.02	399.9	60.3	399.5	61.1	399.9	62.0	397.9	62.9	398.8	63.6
0.03	393.6	60.4	398.3	61.1	399.9	62.0	391.3	63.0	393.2	63.7
0.04	332.2	61.6	373.7	61.6	323.7	63.8	355.6	63.8	365.9	64.3
0.05	259.0	63.8	289.5	63.8	303.5	64.4	331.5	64.4	321.0	65.7
0.06	244.0	64.3	271.2	64.4	266.9	65.7	292.1	65.8	315.6	65.9
0.07	240.2	64.5	239.0	65.8	264.1	65.8	286.9	66.0	310.8	66.1
0.08	212.5	65.8	234.7	66.0	260.8	66.0	281.8	66.3	302.3	66.5
0.09	208.6	66.0	233.6	66.1	254.0	66.4	276.4	66.5	298.9	66.7
0.1	207.6	66.1	228.5	66.4	251.2	66.5	272.5	66.8	295.0	66.9
0.2	176.2	69.5	196.5	69.8	216.2	70.1	235.4	70.4	255.4	70.7
0.3	168.6	71.1	189.4	71.1	210.1	71.2	230.1	71.4	250.4	71.6
0.4	166.9	71.6	187.3	71.8	207.5	72.0	228.2	72.0	248.7	72.1
0.5	165.8	72.1	184.9	73.0	205.3	73.1	225.6	73.2	245.6	73.6
0.6	163.9	73.3	184.4	73.4	204.8	73.4	225.2	73.5	245.4	73.8
0.7	163.7	73.6	184.1	73.7	204.5	73.7	225.0	73.7	245.2	74.0
0.8	163.5	74.0	183.9	74.0	204.4	74.0	224.8	74.0	245.2	74.0
0.9	163.5	74.0	183.9	74.0	204.4	74.0	224.8	74.0	245.2	74.0
1	163.5	74.0	183.9	74.0	204.4	74.0	224.8	74.0	245.2	74.0

Taking $\delta=1.0$ (accurate forecast) as an example, Figure 5.14 illustrates the assigned optimal flight altitudes in the case of C_{max}=400 μSv and F_{max}=90 tons. An obvious trend is that the optimal flight altitudes decrease with the increased α, especially for flight segments i=5, 6, 7 due to these segments in high latitudes with considerable cosmic radiation rates (Figure 5.10a). According to the B789 flight envelope, the feasible TAS at various flight altitudes j may range from 400+(j-1)×10 kt to 550+(j-1)×10 kt. The speeds are assigned in discrete increment of 10 kt to reduce the calculation time of the proposed model, which is reasonable and practical in air traffic management. Thus, the number of available TAS at each flight level is 16. Figure 5.15 shows the optimal assigned TAS v_{ij} in each flight segment under various α. When α is in a lower range, i.e. when the target function

emphasizes more on fuel savings, the aircraft will fly at higher altitudes at fuel-saving speeds. Consequently, the assigned speeds vary greatly when α=0-0.03. When α is larger than 0.2, the priority is to minimize cosmic radiation. Thus, aircraft would fly at greater speeds at lower altitudes. Specifically, the assigned speed at 301 FL is 550 kt.
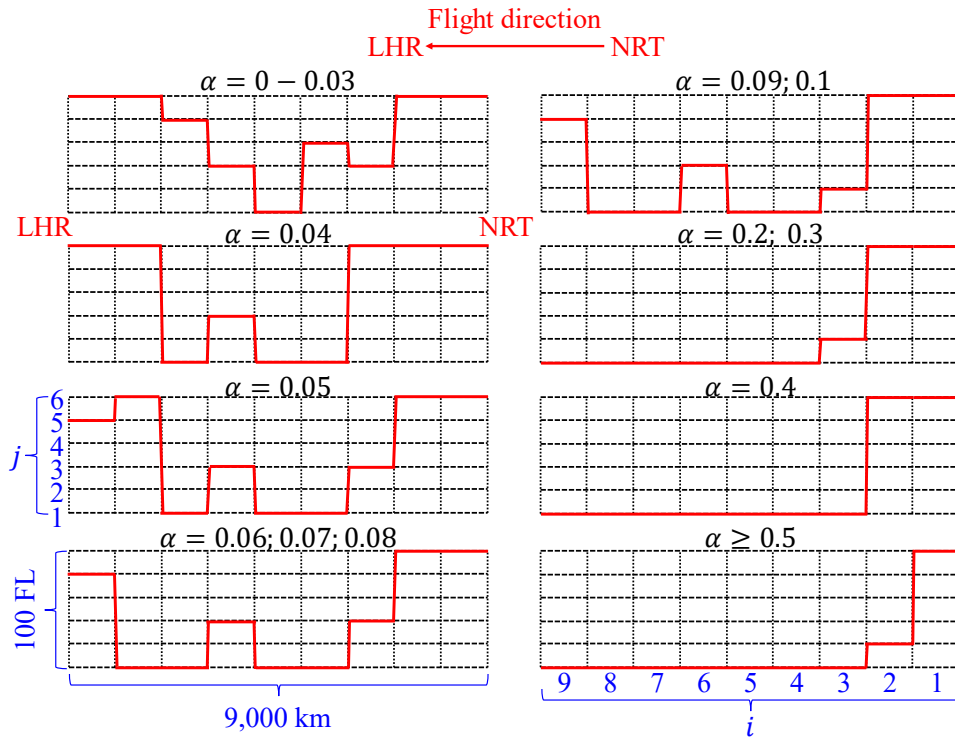
Figure 5.14. The optimal flight altitude assignment in each flight segment under different weights assigned to radiation dose. The flight direction is from NRT to LHR with a cruising distance of 9,000 km, labeled by i. The range of the change of flight altitudes is 100 FL, labeled by j.
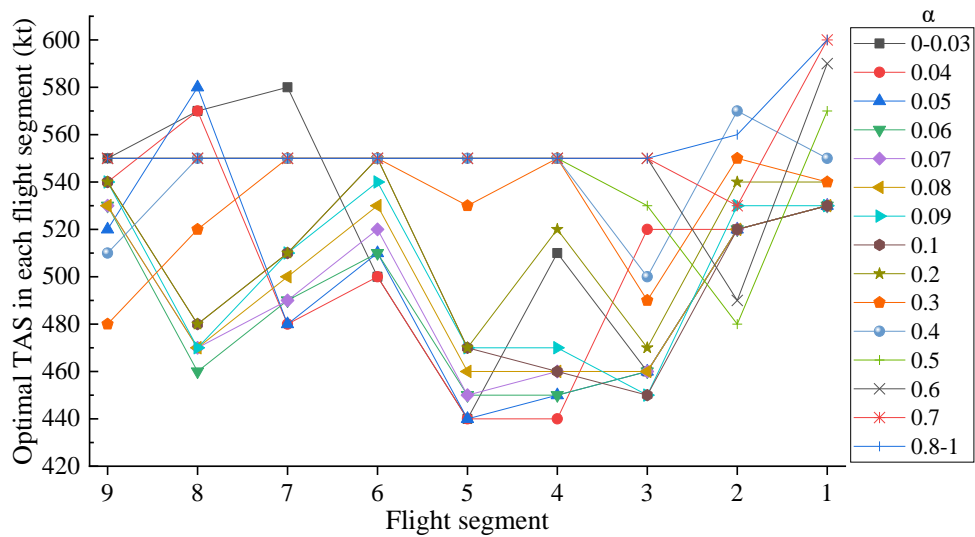
Figure 5.15. The optimal TAS v_{ij} in each flight segment under various weighting values α assigned to cosmic radiation.

Pareto frontier results based on the proposed model

The Pareto frontier representing the best trade-off between the cosmic radiation dose and fuel consumption is presented in Figure 5.16. In multi-objective optimization, the Pareto frontier is the set of all Pareto efficient solutions. Therefore, the selection of the optimal solution is dependent on the criteria of the decision-makers. Rather than evaluate the whole range of every parameter, decision-makers just need to make tradeoffs within this set. To the best of our knowledge, airlines have not yet implemented multi-objective optimization that considers both fuel consumption and cosmic radiation dose. Dispatchers do not make tactical flight plans for fuel consumption or cosmic radiation dose from quantitative perspectives. There may be various preferences among airlines regarding fuel usage and aviation radiation exposure. Consequently, we believe that the Pareto frontier may help airlines make timely and efficient decisions based on their unique operational conditions.

The extreme points at $\alpha = 0$ and $\alpha = 1$ correspond to only considering fuel consumption and only considering cosmic radiation dose, respectively. The cosmic radiation dose decreases from 399.96 μSv to 204.37 μSv with α increasing from 0 to 1. In contrast, fuel consumption shows an opposite trend, increasing

from 67.78 tons to 74.01 tons, which indicates that F_{max} ranging from 75 tons to 90 tons does not affect the final optimal solutions. We divide the weights of cosmic radiation dose into three classes, i.e. lower α (0-0.05), medium α (0.06-0.1), and higher α (0.2-1). Compared to the results at α=0, the cosmic radiation dose at α=0.05 decreases by 24.1%, and fuel consumption increases only by 3.8%. When α increases from 0.2 to 1, fuel consumption increases from 70.1 tons to 74.0 tons, while cosmic radiation doses only decrease from 216.2 μSv to 204.4 μSv.
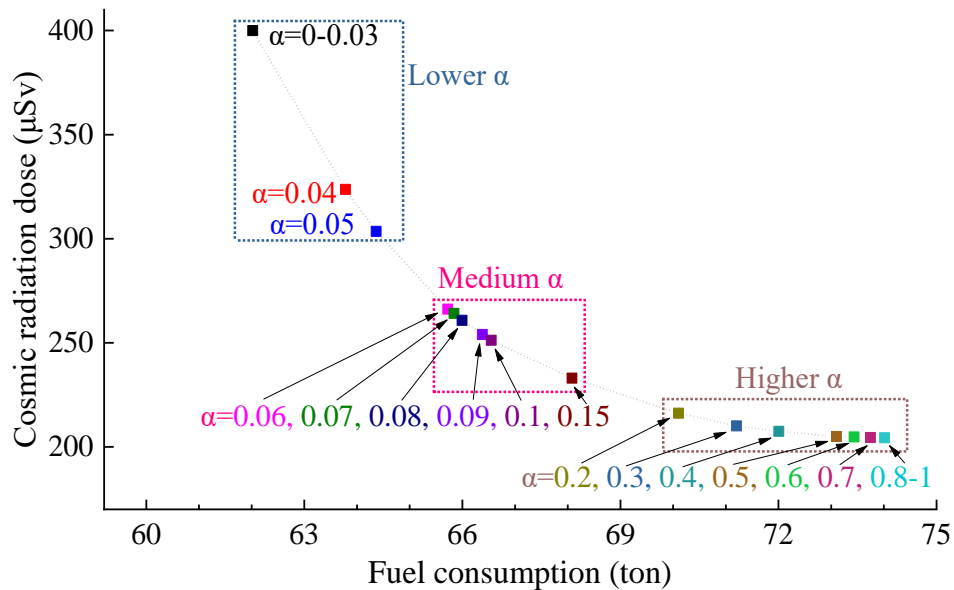
Figure 5.16. Pareto frontier for the cosmic radiation dose versus fuel consumption. The optimized solutions are mainly classified into three classes, i.e., lower α, medium α, and higher α.

Advantages of the proposed model

Supposing that the aircraft just lowers flight altitude to 341 FL in response to high cosmic radiation, fuel consumption is 66 tons and cosmic radiation dose is 399 μSv according to Table 5.4. Obviously, the optimized results under α=0-0.08 in Figure 5.16 can reduce both cosmic radiation and fuel consumption. Specifically, the fuel consumption under α=0-0.03 is only 62 tons, reducing fuel by 4 tons. The cosmic radiation under α=0.08 is 261 μSv, which is only 65.4% of 399 μSv. If the aircraft lowers flight altitude to 321 FL, fuel consumption is 68 tons and cosmic radiation dose is 347 μSv, which is inferior to the optimized results under α=0.04-

0.1. Similarly, if the aircraft lowers flight altitude to 301 FL, fuel consumption is 70 tons and cosmic radiation dose is 249 μSv, while the optimized result under α=0.15 is 68 tons & 233μSv. These positive outcomes validate the value of our work.

Economic Benefits

Assuming a 250-seat B789 aircraft with an occupancy of 80%, there will be 200 passengers. According to www.google.com/travel/flights, the airfare for a one-way direct flight from Tokyo to London in August 2022 is about $2,000 for economy class, which means the total ticket price is $400,000. The B789 flight cancellation cost is $82,730, of which $ 42,740 is allocated to passenger care and compensation (EUROCONTROL, 2020). As space weather is classified as an exceptional occurrence, airlines are not compelled to compensate passengers. Therefore, the cancellation cost is about $0.44 million (400,000+82,730-42,740). If the flight plan is executed, the fuel cost is about $85,425 ($1,139/ton×75 tons) (IATA, 2022). Accordingly, the economic benefit for airlines might be up to $0.44 million-$85,425=$0.35 million compared to flight cancellations. In addition, flight cancellations can change passenger itineraries, and the indirect costs to passengers are considerable. Compared to lowering flight altitudes to 341 FL, the optimized solutions can save fuel at least 4 tons, resulting in a saving of $4,556. Compared to rerouting, the economic benefit is ($1,139/ton×(89-62) tons=$30,753, where 89 tons is from Table 5.4 and 62 tons is from Table 5.5. This is more substantial than lowering flight altitudes.

5.4.7 Discussions

According to average pilot working hours, background cosmic radiation, and regulations of the European Union, we set $C_{\max} = 400$ μSv as the upper threshold of cosmic radiation dose per flight in our case study. Under this threshold, the optimal flight profiles and true airspeed can be obtained by using the proposed multi-objective optimization approach. The basis of scenario generation is mainly based on cosmic radiation forecast models such as WASAVIES and NAIRAS. As a result, the final objective function relies heavily on forecast accuracy. In tactical air traffic management, the forecast lead time is equally crucial. Furthermore, air-

ground communications can also be problematic in high-latitude regions during strong space weather events ([Kubo et al., 2015](#)), which is especially prevalent for polar flights ([Shea and Smart, 2012](#)). Although the issue of communication failure is not considered in this study, it is still important when choosing an alternative flight route.

The assigned flight profiles show that aircraft need to change flight altitude several times during long-distance travel, which may cause passenger discomfort ([Bagshaw and Illig, 2019](#); [Muhm et al., 2007](#)), increase the workload of pilots and air traffic controllers ATC, and affect flight safety ([Bongo and Seva, 2022](#)). However, please note that the distance of each flight segment is 1,000 km, which is equivalent to the distance of typical flight routes such as Beijing-Shanghai, London-Madrid, or Atlanta-Houston. That is to say, the discomfort is not significant.

During a space weather event, cosmic radiation can rise dramatically and pose a threat to aircrew health. To reduce the massive aviation radiation exposure, traditionally airlines may cancel flights, lower flight altitudes, or reroute flights, which can cause increased fuel consumption and financial costs. After investigating a long-distance flight during an extreme cosmic radiation event using the multi-objective optimization approach, our study suggests that: (1) traditional solutions may either exceed the radiological protection recommendations or be uneconomical; (2) a multi-segment flying profile with varying flight altitudes and speed can protect the aircrew and passengers from radiation at a safe radiation dose level and simultaneously have an economically acceptable fuel consumption; (3) the economic benefits of the proposed method may range from \$4,556 to \$0.35 million for a single long-distance flight, e.g. from Tokyo to London.

5.5   Summary

Aircrews receive more cosmic radiation due to their long-term exposure at high altitudes, especially during the severe space weather events when the radiation rates always increase significantly. Currently, it is technically impossible to shield

aircraft from cosmic radiation. Flying at lower altitudes or routing with less radiation is not the most effective in many circumstances as it increases costs, carbon emissions, and other pollution.

To explore the effect of elevated cosmic radiation caused by space weather on aviation, we first calculated the aviation radiation exposure, assuming an extremely strong space weather event like the 2003 Halloween solar storm would have occurred in 2019. The results show that the economic costs of flight cancellations can be from €2.77 million to €48.97 million to prevent massive cosmic radiation exposure, depending on the cosmic radiation dose limits for a given plan. Then we tried to estimate the cosmic radiation dose limit for one flight trip in Europe during space weather, and this limit is estimated to be 400 μSv, which can serve as the policy recommendations for airline decision-makers to assure financial profit meanwhile without jeopardizing aircrew health regulations.

We also presented a multi-objective optimization model to assign flight altitudes and speeds throughout a multi-segment route to minimize both aviation radiation exposure and fuel consumption while maintaining normal aircraft performance. The study is based on a Tokyo-to-London international flight under the assumption that a space weather event comparable to the solar radiation storm on 20 January 2005 occurred. We showed that the proposed flying paths may successfully reduce fuel usage while adhering to cosmic radiation restriction regulations. Our research gives insight into future air transportation decisions amid adverse space weather conditions.

Chapter 6
Discussions and Implications

The economic costs of HF communication blackouts, satellite navigation failure, ADS-B failure, and increased cosmic radiation on aviation industry are related to space weather intensities and the number of flights. This chapter discusses the possibility of space weather events and the economic costs of various disasters. Subsequently, the benefits of GNSS integrity monitoring procedures on air traffic management are presented from the standpoint of real operation.

6.1   Space Weather Possibility

Estimating the probability of a solar storm similar to the Halloween solar storm occurring in a given year involves assessing historical data and statistical analysis. It is important to note that predicting individual solar storms with specific characteristics is extremely challenging due to the complexity and variability of the Sun's behavior. The estimation of probabilities is based on historical data and statistical analysis, which provides a probabilistic assessment of the likelihood of similar events happening in the future. However, the actual occurrence of such events cannot be predicted with certainty.

Space weather forecasts and predictions are regularly monitored by global space weather centers. They analyze data from solar observatories, satellites, and ground-based instruments to assess the probability of space weather events occurring. By analyzing historical data and using predictive models, they can estimate the likelihood of specific space weather events and their potential impact on aviation operations.

Air traffic management and aviation authorities also consider space weather forecasts when planning and managing flights. They may reroute aircraft away from regions with high space weather risk or take other precautionary measures to ensure aviation safety during space weather events. Overall, considering the likelihood and probability of space weather events is essential for ensuring

aviation safety and minimizing potential disruptions caused by space weather phenomena.

The space weather event selected in this study is the Halloween solar storm of 2003, which may occur once each solar cycle (Xue et al., 2023). If a 1-in-100-year solar storm (e.g. 1859 Carrington event) occurs in the future, the economic effects on air traffic will likely be much more significant. During such an event, the majority of satellites, such as navigation satellites and communication satellites, may be inoperable, and widespread power outages may emerge (Eastwood et al., 2017; Ritter et al., 2020). As a result, from the perspective of air traffic management, the number of flight cancellations will likely be substantially greater than those in this study and they are requested to remain on the ground until all systems recover. This is of great interest for future study. It is worth mentioning that our methodology can also be useful for estimating the economic costs of weak and moderate space weather events, as a routine assessment of air traffic.

The solar activity has demonstrated a 11-year cycle. Figure 6.1 shows the annual mean total sunspot number since 1900 (https://www.sidc.be/silso/datafiles#total). The year 2025 is expected to be the upcoming solar maximum in Solar Cycle 25 (Hapgood et al., 2022), with the predicted maximum sunspot number with 122.1 (±18.2) in January 2025 (±6 months) (Okoh et al., 2018). Due to the increasing flight demand after the COVID-19 pandemic (IATA, 2023; Sun et al., 2021b), space weather-caused air traffic disruptions have been a challenging problem.
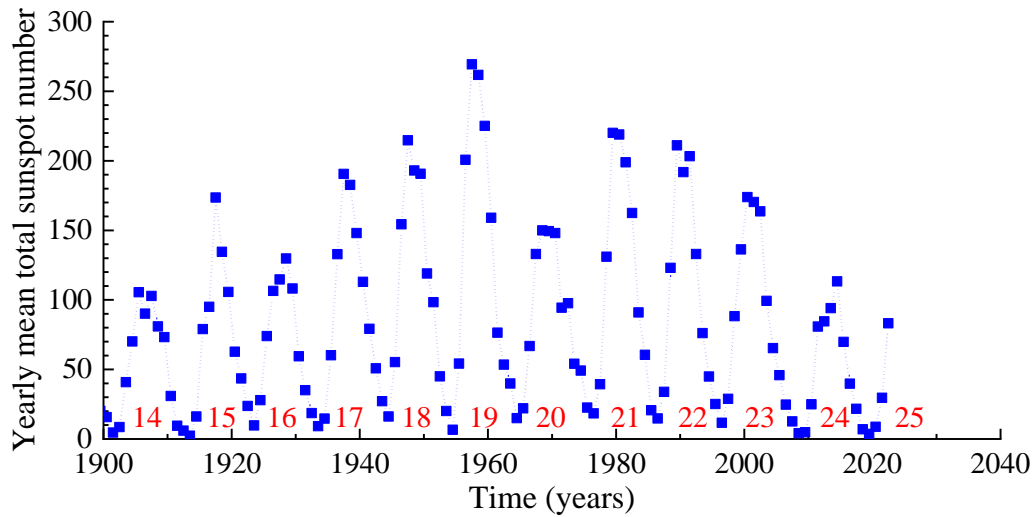
Figure 6.1. Yearly mean total sunspot number denoted by blue squares and the Solar Cycle indexed from 14 to 25 since 1900. Data source: the Sunspot Index and Long-term Solar Observations (SILSO).

To inform the general public about both current and future space weather conditions and their potential impact on individuals and various systems, the space weather intensity is indicated by the Space Weather scales provided by NOAA. Table 6.1 lists the scales of geomagnetic storms (measured by Kp values), solar radiation storms (measured by Flux level $\geq$ 10 MeV particles), and radio blackouts (https://www.swpc.noaa.gov/noaa-scales-explanation). In addition, the average frequency of space weather events in different scales is quantified.

Table 6.1. NOAA space weather scales of Geomagnetic storms, Solar radiation storms, and Radio blackouts (1 cycle=11 years).

Description	Scale	Physical measure	Average Frequency
Extreme	G5	Kp=9	4 per cycle
	S5	10^5	Fewer than 1 per cycle
	R5	X20	Fewer than 1 per cycle
Severe	G4	Kp=8 or 9-	100 per cycle
	S4	10^4	3 per cycle
	R4	X10	8 per cycle
Strong	G3	Kp=7	200 per cycle
	S3	10^3	10 per cycle

119

	R3	X1	175 per cycle
Moderate	G2	Kp=6	600 per cycle
	S2	10^2	25 per cycle
	R2	M5	350 per cycle
Minor	G1	Kp=5	1,700 per cycle
	S1	10	50 per cycle
	R1	M1	2,000 per cycle

With the development of modern models and technologies, if the probability of severe space weather events can be assumed, such information would be highly useful in evaluating the potential space weather effects on air traffic management. Understanding the likelihood of severe space weather events allows air traffic management authorities to proactively prepare and plan for potential disruptions and safety concerns. With this information, air traffic management can take the following actions:

➢ Preemptive Planning: Air traffic management can develop contingency plans and procedures to mitigate the impact of severe space weather events. This includes rerouting flights, adjusting flight altitudes, and coordinating with airlines to ensure the safety of passengers and crew.

➢ Communication and Alerting: Air traffic management can communicate with airlines and pilots, providing them with real-time information on space weather conditions and potential hazards. This enables pilots to make informed decisions and take necessary precautions during flights.

➢ Ground-based Navigation and Communication: Severe space weather events can disrupt global navigation satellite systems (GNSS) and communication systems. Air traffic management can implement alternative ground-based navigation and communication systems to maintain safe and efficient operations during space weather disturbances.

➢ Space Weather Monitoring: Air traffic management can monitor space weather forecasts and real-time data from space weather agencies. This allows them to continuously assess the evolving situation and make dynamic adjustments to flight routes and operations.

➢ Collaborative Decision-Making: Air traffic management can collaborate with space weather agencies, airlines, and other aviation stakeholders to exchange information and coordinate responses to severe space weather events effectively.

By taking these measures, air traffic management can minimize the impact of severe space weather events on aviation operations, enhance safety, and maintain the efficiency of air traffic flow. Early awareness and proactive planning based on the assumed probability of such events are vital for ensuring the resilience and safety of air traffic management systems in the face of space weather challenges.

6.2 Economic Costs of Other Disasters

After evaluating the economic costs due to space weather, this part aims to present to economic costs related to other events or disasters. For example, the direct demand losses of air transportation services induced by the terrorist attack on 11 September 2001 ranged from $214.3 billion to $420.5 billion (Gordon et al., 2007). The 2010 Eyjafjallajökull eruption in Iceland resulted in the closure of over 300 European airports during 15-21 April 2010, which caused an economic loss of 1.7-3.3 billion Euros (Alexander, 2013; Mazzocchi et al., 2010). In the 2001 and 2010 extreme cases, a large number of airports were completely closed, and all flights were cancelled.

Furthermore, Typhoon Mangkhut caused the closure of Hong Kong International Airport, resulting in the cancellation of the majority of scheduled flights. Figure 6.2 shows the Mangkhut trajectory during 7-17 September 2018. It is evident that on 16 September, the typhoon was near Hong Kong. Figure 6.3 shows the daily number of flights landing on and taking off from the Hong Kong International Airport, with an average of 950 flights per day. Notably, the number of flights on 16 September 2018 reduced significantly, with only 45 departure flights and 4 arrival flights. Based on the cancellation costs in Table 2.1, the economic cost of flight cancellations caused by this typhoon is about €36 million.
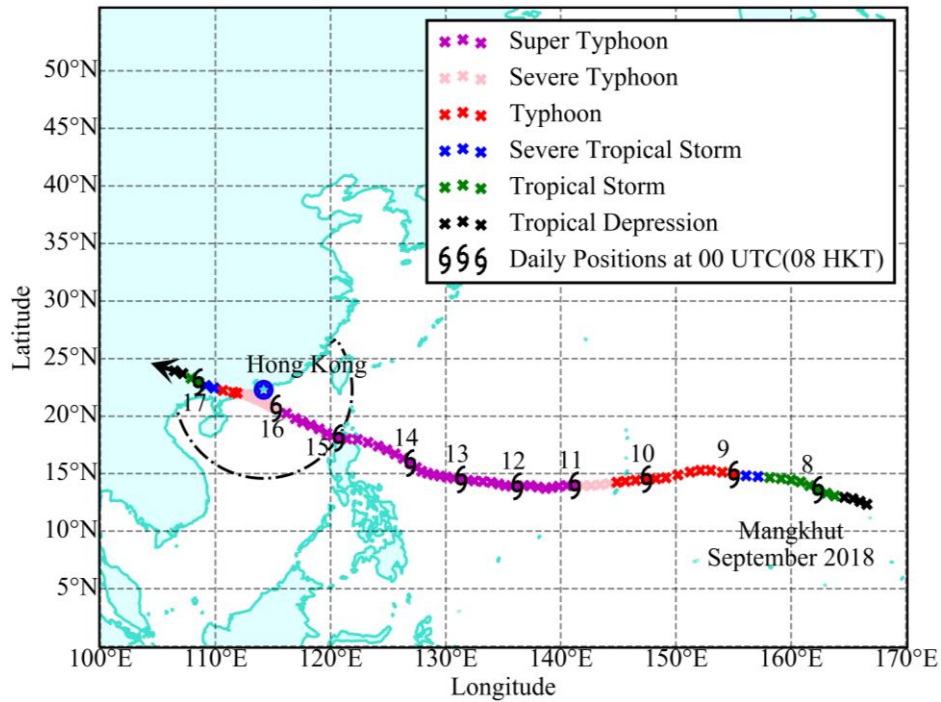
Figure 6.2. Mangkhut path during 7-17 September 2018. The various intensities of typhoon are denoted by different colors.
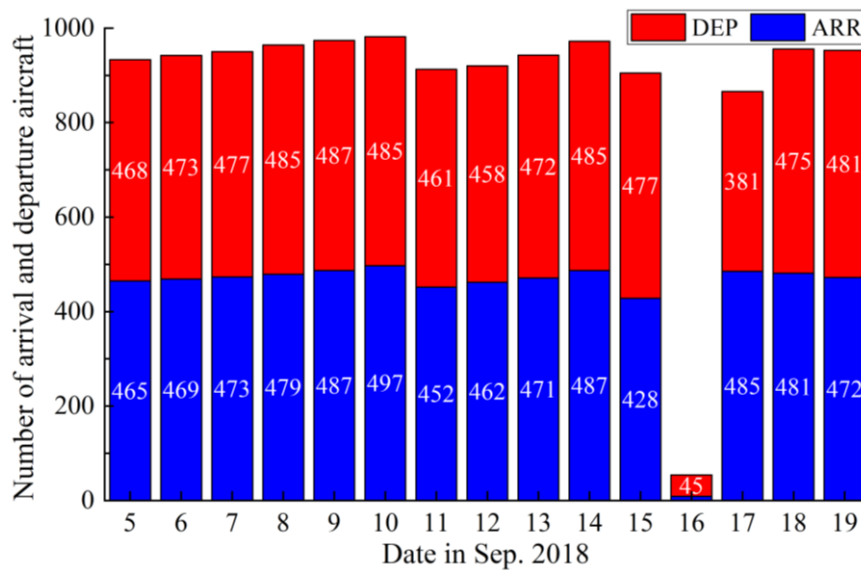
Figure 6.3. The daily number of flights during 5-19 September 2018.

In summary, compared to these three events, it can be concluded that the 2003 Halloween storm would have relatively low economic effects on aviation. That can be explained by the fundamental properties of space weather effects on aviation and the resilience of the air traffic management system. The effects of

space weather include high-frequency communication blackouts, GNSS-based navigation and surveillance failure, and massive cosmic radiation. However, aviation communications rely primarily on VHF (only HF communications in the polar region); aircraft navigation can be accomplished using ground navigation aids, which cover the majority of terminal maneuvering areas; radar systems have always been used for real-time surveillance; the majority of cosmic radiation can be shielded by the Earth's atmosphere and magnetic field, and only a few dozens of flights at high latitudes may be affected.

6.3   Benefits of GNSS Integrity Monitoring Procedures

Considering the harmful effects of space weather on aviation, space weather centers have been providing space weather advisories for the aviation sector. As an example, Table 6.2 shows a space weather advisory for the effect of space weather on GNSS. The forecast indicates that the GNSS-based operations within the High latitudes of the Northern Hemisphere (HNH) spanning from W015° to E015° will not be available for the subsequent 6, 12, 18, and 24 hours.

Table 6.2. An example of space weather advisory for GNSS.

DTG:	20221107/1058Z
SWXC:	PECASUS
ADVISORY NR:	2022/56
SWX EFFECT:	GNSS SEV
OBS SWX:	07/1042Z HNH W015-E015
FCST SWX +6 HR:	07/1700 NOT AVBL
FCST SWX +12 HR:	07/2300 NOT AVBL
FCST SWX +18 HR:	08/0500 NOT AVBL
FCST SWX +24 HR:	08/1100 NOT AVBL
RMK:	Space weather event (ionospheric disturbance) in progress. Impact on GNSS performance possibly leads to loss of GNSS signals and degradation of timing and positioning performance.
NXT ADVISORY	Will be issued by 20221107/1642Z=

However, in a practical situation, the effects of space weather on GNSS may be different from the forecasted information in the advisory, which can cause unnecessary flight delays and flight cancellations, causing additional economic costs. This highlights the importance of GNSS monitoring procedures in aviation for ensuring the accuracy and reliability of satellite-based navigation systems. Two commonly used GNSS integrity monitoring procedures in aviation are Receiver Autonomous Integrity Monitoring (RAIM) and the WAAS.

RAIM is a technique that allows a GNSS receiver to check the integrity of the satellite signals it receives (El-Mowafy et al., 2019; Fu et al., 2015). If any signal anomalies or inconsistencies are detected, the receiver can provide an alert or exclude unreliable satellite signals from navigation calculations. This helps pilots and air traffic controllers ensure the accuracy and reliability of navigation information even in the presence of space weather effects on GNSS signals.

WAAS is another integrity monitoring system used in the United States and other regions (Demyanov et al., 2019; SenthamilSelvan et al., 2022). It provides corrections and integrity monitoring over a wide area, improving the accuracy and reliability of GNSS for aviation. WAAS helps mitigate the effects of space weather events on GNSS by providing augmentation and monitoring services.

Both RAIM and WAAS play crucial roles in ensuring the safety and reliability of GNSS-based navigation in aviation. RAIM is primarily used as an onboard integrity monitoring technique, while WAAS is a ground-based augmentation system that enhances GNSS performance across a broader geographic area. These systems help pilots maintain accurate navigation, especially during critical phases of flight such as takeoff, landing, and approach.

In summary, integrity monitoring procedures designed for aviation can be adapted and utilized in air traffic management during space weather events to monitor and mitigate the impact of GNSS disruptions. These procedures help ensure the safety and efficiency of air traffic operations by providing timely information, alerts, and alternative navigation solutions when space weather events affect GNSS accuracy.

Chapter 7

Conclusions and Future Work

Intense solar activity may result in a variety of space weather events, such as solar flares, coronal mass ejections, and solar energetic particles, which pose a grave threat to the aviation sector and cause a substantial economic cost. This thesis estimates the economic costs associated with four factors: HF communication outages, satellite navigation failure, ADS-B failure, and significant cosmic radiation. This chapter gives a comprehensive conclusion to the thesis. From the perspective of air traffic management, some future work for mitigating space weather effects is presented at the end.

7.1   Conclusions

Technologies on Earth and in orbit may be affected by space weather events such as CMEs and solar flares, which can interact with the ionosphere and magnetosphere. To be specific, GNSS and HF radio signals are disrupted by CMEs and solar flares, and radiation from these events can cause harm to human health and satellite electronics. CMEs and solar flares can also increase the atmospheric drag on satellites. Due to the reliance on these technologies for vital infrastructure and operations, the effect of solar storms on technologies is of great concern in modern society. When combined, interruption of electrical grid services, satellite damage, loss of GPS and HF radio communications, and radiation exposure caused by solar storms would have serious negative effects on the economy, national security, and human health.

Air traffic relies heavily on communication, navigation, and surveillance technologies. Space weather events can degrade the performance of these technologies, and increased cosmic radiation caused by solar radiation storms can harm the health of passengers and aircrew. All of these can impede normal flight operations and necessitate flight plan adjustments. This thesis discusses the effects of space weather on flight operation and quantifies the induced economic costs. Our results provide a benchmark for the community to study the space weather

effects on aviation despite we have made some assumptions and simulations.

We assume that a space weather event as intense as the Halloween solar storm of 2003 would have occurred in 2019. After studying the effects of the Halloween solar storm on flight operations from the perspective of air traffic management, we can get several results. Especially, the potential daily economic losses associated with polar aircraft rerouting and cancellations caused by HF communication blackouts vary from €0.21 million to €2.20 million. In addition, this Halloween solar storm can cause failures in continuous descent approach and area navigation, resulting in a cost of up to €2.43 million. Besides, the economic costs of flight cancellations can be from €2.77 million (if the cosmic radiation dose limit for a given flight plan is 1,000 μSv) to €48.97 million (if the cosmic radiation dose limit for a given flight plan is 100 μSv). These results are from simulation models.

We also simulated a period (9-16 LT) with satellite navigation failure to investigate the potential effects of a moderate ionosphere storm event on Hong Kong flights in 2030. The economic costs can exceed 2 million Euros if the duration of satellite navigation cannot be forecast. In contrast, the cost can decrease to 1 million Euros if the ionospheric impact can be accurately forecasted.

ADS-B can enhance flight efficiency. Thus, we proposed a method to schedule aircraft landings using a heuristic algorithm. Based on the proposed model, the overall flight time for all arriving aircraft can be greatly decreased. We studied one example based on the historical Hong Kong flight data of 2018. We assumed that HKIA experienced an ADS-B failure from 9 LT to 16 LT on 5 September 2018. The total flight duration of all arrival flights at HKIA will increase by 1,864 minutes per day, leading to an increase in fuel consumption of 65.24 tons. The daily economic cost including fuel cost, CO_2 cost, and time cost related to onboard passengers will increase by €0.33 million.

The cosmic radiation dose limit for one flight trip in Europe during space weather is estimated to be 400 μSv, which is used to serve as the policy recommendations for airline decision-making. In addition, a multi-objective optimization model is proposed to assign flight altitudes and speeds to minimize aviation radiation

exposure and fuel consumption. We selected an international flight from Tokyo to London as an example. It was assumed that a space weather event comparable to the solar radiation storm on 20 January 2005 occurred and affected the Tokyo to London flight. The results indicate that the traditional solutions may either violate the radiological protection recommendations or be uneconomic, and the proposed method can reduce fuel consumption efficiently without exceeding cosmic radiation restriction regulations. Additionally, the economic benefits of the proposed method may range from $4,556 to $0.35 million.

The problem caused by space weather can be significant. Space weather events may disrupt regular flight operations and result in significant economic losses. Our work provides a comprehensive estimate of economic costs due to space weather effects on global aviation. To protect technologies from the impacts of solar storms, resilience strategies may be undertaken to safeguard the earth- and space-based systems and infrastructure against the effects of solar storms. Improved solar storm models will aid in the development of more accurate solar storm forecasts and give a deeper knowledge of the effects of solar storms on space and terrestrial technologies.

7.2   Future work

This thesis mainly focuses on the study of space weather effects on air traffic management and quantifies the corresponding economic cost from the perspective of air traffic management based on some proposed models and necessary assumptions. Some related future work can be further conducted to reduce space weather effects and increase the resilience of the air traffic management system.

Propose rerouting model for HF communication blackouts

In this study, the proposed air traffic management response to HF communication blackouts is the cancellation of polar flights. However, in practical terms, canceling polar flights may not be the most optimal solution. Consequently, it becomes imperative to develop a rerouting model for polar flights aimed at avoiding HF communication blackout areas. Moreover, adjusting the schedules of polar flights based on space weather advisories regarding HF communication

blackout durations should also be considered.

Quantify aircraft separation standards in CNS/ATM

Currently, ADS-B separation criteria are identical to radar separation standards. However, it is expected that aircraft separation standard distances based on ADS-B should be reduced compared to those based on radar. CNS/ATM is proposed, and Communication, Navigation, and Surveillance seem to be at the same level, but this is not the reality. Required Communication Performance (RCP), Required Navigation Performance (RNP), and Required Surveillance Performance (RSP) are three essential principles that should be comprehended thoroughly. Another point needing to be considered is ADS-B latency. The relationship may be represented mathematically as follows: $RSP^2 = RCP^2 + RNP^2 + (Latency \times GS)^2$, where GS is the Ground Speed of the aircraft. Therefore, the updated aircraft minimum separation standards will be evaluated and quantified in a variety of circumstances, which is the backbone of CNS/ATM, especially during space weather events.

Evaluate satellite navigation-based flight efficiency

Satellite navigation can enhance flight efficiency and increase airspace capacity. However, it has to be determined how much satellite navigation can improve flight efficiency. Some major airports provide ground navigation aids in the terminal area, so ground navigation can be utilized as a backup if satellite navigation fails. However, to what extent flight efficiency will decline is currently unknown, as it depends on many factors, such as airspace configuration, onboard navigation systems performance, wake turbulence, etc. In our study, there are several assumptions about the AAR based on satellite navigation and ground navigation, which is the benchmark for tactical ATM according to space weather service for aviation.

Assess biological effects of cosmic radiation

Although it is commonly acknowledged that massive cosmic radiation dose is harmful to human health, there are no specific guidelines regarding the consequences of cosmic radiation on human health, particularly aircrew, and passengers. This future study is related to biological sciences, and additional data

about human health and aviation radiation exposure are required for in-depth data analysis, which may serve as a baseline for the study of the biological effects of cosmic radiation.

References

Alberti, T., Carbone, V., Lepreti, F., 2017. Effects of the solar activity on space weather and earth's climate.

Aleshin, I., Arakelov, A., Burov, V., Ivanov, S., Ochelkov, Y.P., Repin, A.Y., Kholodkov, K., 2021. Space Weather Center to Support International Air Navigation: Infrastructure and Software. *Russian Meteorology and Hydrology* 46(3), 200-204.

Alexander, D., 2013. Volcanic ash in the atmosphere and risks for civil aviation: a study in European crisis management. *International Journal of Disaster Risk Science* 4(1), 9-19.

Ali, B.S., 2013. A safety assessment framework for Automatic Dependent Surveillance Broadcast (ADS-B) and its potential impact on aviation safety. Centre for Transport studies, Department of Civil and Environmental.

Ali, B.S., Ochieng, W.Y., Majumdar, A., 2017a. ADS-B: Probabilistic safety assessment. *J. Navig* 70(4), 887-906.

Ali, B.S., Ochieng, W.Y., Zainudin, R., 2017b. An analysis and model for Automatic Dependent Surveillance Broadcast (ADS-B) continuity. *Gps Solutions* 21(4), 1841-1854.

Ali, B.S., Schuster, W., Ochieng, W., Majumdar, A., 2016. Analysis of anomalies in ADS-B and its GPS data. *GPS solutions* 20(3), 429-438.

Almeida Filho, D., Souza-Santos, D., Federico, C., da Silva, F., 2023. Evaluation of neutron doses in Brazilian aircrew by the Monte Carlo method. *Radiation Measurements* 166, 106959.

Andalsvik, Y., Jacobsen, K., 2014. Observed high-latitude GNSS disturbances during a less-than-minor geomagnetic storm. *Radio Science* 49(12), 1277-1288.

Anderson, J.L., Mertens, C.J., Grajewski, B., Luo, L., Tseng, C.-Y., Cassinelli, R.T., 2014. Flight attendant radiation dose from solar particle events. *Aviation, Space, and Environmental Medicine* 85(8), 828-832.

Aquino, M., Monico, J., Dodson, A., Marques, H., De Franceschi, G., Alfonsi, L., Romano, V., Andreotti, M., 2009. Improving the GNSS positioning stochastic model in the presence of ionospheric scintillation. *Journal of*

Geodesy 83, 953-966.

Argyle, E.M., Houghton, R.J., Atkin, J., De Maere, G., Moore, T., Morvan, H.P., 2018. Human performance and strategies while solving an aircraft routing and sequencing problem: an experimental approach. *Cogn Technol Work* 20(3), 425-441.

Asari, A., Alagheband, M.R., Bayat, M., Asaar, M.R., 2020. A new provable hierarchical anonymous certificateless authentication protocol with aggregate verification in ADS-B systems. *Computer Networks*, 107599.

Astafyeva, E., Yasyukevich, Y., Maksikov, A., Zhivetiev, I., 2014. Geomagnetic storms, super-storms, and their impacts on GPS-based navigation systems. *Space Weather* 12(7), 508-525.

Ataç, T., Özgüç, A., 2006. Overview of the solar activity during solar cycle 23. *Solar Physics* 233, 139-153.

Atiq, M., 2018. Historical review of ionosphere in perspective of sources of ionization and radio waves propagation. *Research & Reviews: Journal of Space Science & Technology* 7(2), 28-39.

Bagshaw, M., 2008. Cosmic radiation in commercial aviation. *Travel medicine and infectious disease* 6(3), 125-127.

Bagshaw, M., Illig, P., 2019. The aircraft cabin environment, *Travel medicine*. Elsevier, pp. 429-436.

Bajaja, B., Majumdar, A., 2021. Aviation Safety: An Initial Exploration of the Feasibility of Using Language Engineering Technologies for Reducing Pilot-Air Traffic Control Miscommunications. *Advances in Human Aspects of Transportation: Part I*, 56.

Ball, M., Barnhart, C., Dresner, M., Hansen, M., Neels, K., Odoni, A., Peterson, E., Sherry, L., Trani, A., Zou, B., 2010. Total delay impact study, *NEXTOR Research Symposium, Washington DC*.

Bamford, R., Kellett, B., Bradford, J., Todd, T.N., Benton Sr, M., Stafford-Allen, R., Alves, E., Silva, L., Collingwood, C., Crawford, I., 2014. An exploration of the effectiveness of artificial mini-magnetospheres as a potential solar storm shelter for long term human space missions. *Acta astronautica* 105(2), 385-394.

Barcellos-Hoff, M.H., Blakely, E.A., Burma, S., Fornace Jr, A.J., Gerson, S., Hlatky, L., Kirsch, D.G., Luderer, U., Shay, J., Wang, Y., 2015. Concepts and challenges in cancer risk prediction for the space radiation environment. *Life Sciences in Space Research* 6, 92-103.

Barish, R.J., 2014. In-Flight Radiation: addressing patients' concerns. *Journal of Radiology Nursing* 33(2), 46-52.

Bartlett, D.T., 2004. Radiation protection aspects of the cosmic radiation exposure of aircraft crew. *Radiation protection dosimetry* 109(4), 349-355.

Birolini, S., Antunes, A.P., Cattaneo, M., Malighetti, P., Paleari, S., 2021. Integrated flight scheduling and fleet assignment with improved supply-demand interactions. *Transportation Research Part B: Methodological* 149, 162-180.

Blanch, J., Walter, T., Enge, P., 2012. Satellite navigation for aviation in 2025. *Proceedings of the IEEE* 100(Special Centennial Issue), 1821-1830.

Bolat, A., 2001. Models and a genetic algorithm for static aircraft-gate assignment problem. *Journal of the Operational Research Society* 52(10), 1107-1120.

Bongo, M., Seva, R., 2022. Effect of Fatigue in Air Traffic Controllers' Workload, Situation Awareness, and Control Strategy. *The International Journal of Aerospace Psychology* 32(1), 1-23.

Bothmer, V., Daglis, I.A., Lanzerotti, L.J., 2007. Space weather effects on communications. *Space weather-physics and effects*, 247-268.

Bottollier-Depois, J., Chau, Q., Bouisset, P., Kerlau, G., Plawinski, L., Lebaron-Jacobs, L., 2003. Assessing exposure to cosmic radiation on board aircraft. *Advances in Space Research* 32(1), 59-66.

Britto, R., Dresner, M., Voltes, A., 2012. The impact of flight delays on passenger demand and societal welfare. *Transportation Research Part E: Logistics and Transportation Review* 48(2), 460-469.

Brown, R., 1978. On the poleward expansion of ionospheric absorption regions triggered by sudden commencements of geomagnetic storms. *Journal of Geophysical Research: Space Physics* 83(A3), 1169-1171.

Bubalo, B., Gaggero, A.A., 2021. Flight delays in European airline networks. *Research in Transportation Business & Management*, 100631.

Builta, S., 2016. Assessing fuel burn inefficiencies in oceanic airspace. Purdue

University.

Bundesamt für Strahlenschutz, 2022. Ionizing Radiation Environmental Radioactivity – Medicine – Occupational Radiation Protection – Nuclear Hazards Defence.

Cameron, T., Fiori, R., Themens, D., Warrington, E., Thayaparan, T., Galeschuk, D., 2022. Evaluation of the effect of sporadic-E on high frequency radio wave propagation in the Arctic. *Journal of Atmospheric and Solar-Terrestrial Physics* 228, 105826.

Camps, A., Park, H., Foti, G., Gommenginger, C., 2016. Ionospheric effects in GNSS-reflectometry from space. *IEEE journal of selected topics in applied earth observations and remote sensing* 9(12), 5851-5861.

Cander, L.R., 2019. *Ionospheric space weather*. Springer.

Cannon, P., Angling, M., Barclay, L., Curry, C., Dyer, C., Edwards, R., Greene, G., Hapgood, M., Horne, R.B., Jackson, D., 2013. *Extreme space weather: impacts on engineered systems and infrastructure*. Royal Academy of Engineering.

Cao, Y., Jin, L., Nguyen, N.V., Landry, S., Sun, D., Post, J., 2014. Evaluation of fuel benefits depending on continuous descent approach procedures. *Air Traffic Control Quarterly* 22(3), 251-275.

Cerruti, A.P., Kintner Jr, P.M., Gary, D.E., Mannucci, A.J., Meyer, R.F., Doherty, P., Coster, A.J., 2008. Effect of intense December 2006 solar radio bursts on GPS receivers. *Space Weather* 6(10).

Cesaroni, C., Spogli, L., Aragon-Angel, A., Fiocca, M., Dear, V., De Franceschi, G., Romano, V., 2020. Neural network based model for global Total Electron Content forecasting. *Journal of Space Weather and Space Climate* 10, 11.

Chen, B., Liu, Z., 2015. A comprehensive evaluation and analysis of the performance of multiple tropospheric models in China region. *IEEE transactions on geoscience and remote sensing* 54(2), 663-678.

Chen, L., Yu, S., Chen, Q., Zhao, Y., 2020. Data Reception Analysis of ADS-B on Board the TianTuo-3 Satellite, *Journal of Physics: Conference Series*. IOP Publishing, p. 012030.

Clucas, S.N., Dyer, C.S., Lei, F., 2005. The radiation in the atmosphere during

major solar particle events. *Advances in Space Research* 36(9), 1657-1664.

Copeland, K., 2017. CARI-7A: Development and validation. *Radiation Protection Dosimetry* 175(4), 419-431.

Copeland, K., Atwell, W., 2019. Flight safety implications of the extreme solar proton event of 23 February 1956. *Advances in Space Research* 63(1), 665-671.

Copeland, K., Sauer, H.H., Duke, F.E., Friedberg, W., 2008. Cosmic radiation exposure of aircraft occupants on simulated high-latitude flights during solar proton events from 1 January 1986 through 1 January 2008. *Advances in Space Research* 42(6), 1008-1029.

Corlu, C.G., de la Torre, R., Serrano-Hernandez, A., Juan, A.A., Faulin, J., 2020. Optimizing energy consumption in transportation: Literature review, insights, and research opportunities. *Energies* 13(5), 1115.

Coster, A., Komjathy, A., 2008. Space weather and the global positioning system. *Space Weather* 6(6).

Coster, A.J., Yizengaw, E., 2021. GNSS/GPS Degradation from Space Weather. *Space Weather Effects and Applications*, 165-181.

Dave, G., Choudhary, G., Sihag, V., You, I., Choo, K.-K.R., 2022. Cyber security challenges in aviation communication, navigation, and surveillance. *Computers & Security* 112, 102516.

Delta, 2010. Space Weather and Delta's Polar Routes.

Demyanov, V.V., Zhang, X., Lu, X., 2019. Moderate geomagnetic storm condition, WAAS Alerts and real GPS positioning quality. *Journal of Atmospheric Science Research* 2(1), 10-23.

Di Trolio, R., Di Lorenzo, G., Fumo, B., Ascierto, P.A., 2015. Cosmic radiation and cancer: is there a link? *Future Oncology* 11(7), 1123-1135.

Ding, W., Zhang, Y., Hansen, M., 2018. Downstream impact of flight rerouting. *Transportation Research Part C: Emerging Technologies* 88, 176-186.

Doherty, P., Coster, A.J., Murtagh, W., 2004. Space weather effects of October–November 2003. *GPS Solutions* 8(4), 267-271.

Drake, S.P., 2002. Converting GPS coordinates [phi, lambda, h] to navigation coordinates (ENU).

Dubey, S., Wahi, R., Gwal, A., 2006. Ionospheric effects on GPS positioning.

Advances in Space Research 38(11), 2478-2484.

Durante, M., Kronenberg, A., 2005. Ground-based research with heavy ions for space radiation protection. *Advances in Space Research* 35(2), 180-184.

Eastwood, J., Biffis, E., Hapgood, M., Green, L., Bisi, M., Bentley, R., Wicks, R., McKinnell, L.A., Gibbs, M., Burnett, C., 2017. The economic impact of space weather: Where do we stand? *Risk analysis* 37(2), 206-218.

El-Mowafy, A., Imparato, D., Rizos, C., Wang, J., Wang, K., 2019. On hypothesis testing in RAIM algorithms: Generalized likelihood ratio test, solution separation test and a possible alternative. *Measurement Science and Technology* 30(7), 075001.

Eldredge, L., Enge, P., Harrison, M., Kenagy, R., Lo, S., Loh, R., Lilly, R., Narins, M., Niles, R., 2010. Alternative positioning, navigation & timing (PNT) study, *International civil aviation organisation navigation systems panel (NSP), Working Group Meetings, Montreal, Canada.*

Elmarady, A.A., Rahouma, K., 2021. Studying cybersecurity in civil aviation, including developing and applying aviation cybersecurity risk assessment. *IEEE access* 9, 143997-144016.

Enge, P., Enge, N., Walter, T., Eldredge, L., 2015. Aviation Benefits from Satellite Navigation. *New Space* 3(1), 19-35.

Erlykin, A., Wolfendale, A.W., 2006. The anisotropy of galactic cosmic rays as a product of stochastic supernova explosions. *Astroparticle Physics* 25(3), 183-194.

Eroshenko, E., Belov, A., Boteler, D., Gaidash, S., Lobkov, S., Pirjola, R., Trichtchenko, L., 2010. Effects of strong geomagnetic storms on Northern railways in Russia. *Advances in Space Research* 46(9), 1102-1110.

Eskilsson, S., Gustafsson, H., Khan, S., Gurtov, A., 2020. Demonstrating ADS-B AND CPDLC attacks with software-defined radio, *2020 Integrated Communications Navigation and Surveillance Conference (ICNS)*. IEEE, pp. 1B2-1-1B2-9.

Eufrásio, A.B.R., Eller, R.A., Oliveira, A.V., 2021. Are on-time performance statistics worthless? An empirical study of the flight scheduling strategies of Brazilian airlines. *Transportation Research Part E: Logistics and Transportation Review* 145, 102186.

Eun, Y., Hwang, I., Bang, H., 2010. Optimal arrival flight sequencing and scheduling using discrete airborne delays. *IEEE Transactions on Intelligent Transportation Systems* 11(2), 359-373.

EUROCONTROL, 2020. Standard Inputs for Economic Analyses. *Supporting European Aviation*.

EUROCONTROL, 2022. User manual for the Base of Aircraft Data (BADA) revision 3.16. *https://www.eurocontrol.int/model/bada*.

FAA/William J. Hughes Technical Center, 2004. NSTB/WAAS T&E team. In: WAAS performance analysis, Report #7.

Fajardo, I., Lidtke, A.A., Bendoukha, S.A., Gonzalez-Llorente, J., Rodríguez, R., Morales, R., Faizullin, D., Matsuoka, M., Urakami, N., Kawauchi, R., 2019. Design, implementation, and operation of a small satellite mission to explore the space weather effects in LEO. *Aerospace* 6(10), 108.

Fellner, A., Konieczka, R., 2019. Rotorcraft in the performance based navigation international civil aviation organization implementation. *Transactions on Aerospace Research*.

Firoz, K., Cho, K.S., Hwang, J., Phani Kumar, D., Lee, J., Oh, S., Kaushik, S.C., Kudela, K., Rybanský, M., Dorman, L.I., 2010. Characteristics of ground-level enhancement–associated solar flares, coronal mass ejections, and solar energetic particles. *Journal of Geophysical Research: Space Physics* 115(A9).

Flying Staff, 2022. How Many Hours Do Pilots Work? *Flying Magazine*.

Francisco, D., 2021. Human Spaceflight Standards Health and Medical Technical Authority (HMTA). *https://www.nasa.gov/sites/default/files/atoms/files/ochmo_standards_overview_sept_15_2021_francisco.pdf*.

Friedberg, W., Copeland, K., Duke, F.E., O'Brien III, K., Darden Jr, E.B., 2000. Radiation exposure during air travel: guidance provided by the Federal Aviation Administration for air carrier crews. *Health physics* 79(5), 591-595.

Fu, L., Zhang, J., Li, R., Cao, X., Wang, J., 2015. Vision-aided RAIM: A new method for GPS integrity monitoring in approach and landing phase.

Sensors 15(9), 22854-22873.

Fujita, M., Sato, T., Saito, S., Yamashiki, Y., 2021. Probabilistic risk assessment of solar particle events considering the cost of countermeasures to reduce the aviation radiation dose. *Scientific Reports* 11(1), 1-9.

Gaisser, T.K., Engel, R., Resconi, E., 2016. *Cosmic rays and particle physics*. Cambridge University Press.

Ghelfi, A., Maurin, D., Cheminet, A., Derome, L., Hubert, G., Melot, F., 2017. Neutron monitors and muon detectors for solar modulation studies: 2. ϕ time series. *Advances in Space Research* 60(4), 833-847.

Glaser-Opitz, H., Glaser-Opitz, L., 2015. Evaluation of CPDLC and voice communication during approach phase, *2015 IEEE/AIAA 34th Digital Avionics Systems Conference (DASC)*. IEEE, pp. 2B3-1-2B3-10.

Glenn Lightsey, E., Humphreys, T.E., Bhatti, J.A., Joplin, A.J., O'Hanlon, B.W., Powell, S.P., 2014. Demonstration of a space capable miniature dual frequency GNSS receiver. *Navigation: Journal of The Institute of Navigation* 61(1), 53-64.

Glover, C.N., Ball, M.O., 2013. Stochastic optimization models for ground delay program planning with equity–efficiency tradeoffs. *Transportation Research Part C: Emerging Technologies* 33, 196-202.

Gonzalez, W.D., Tsurutani, B.T., Clúa de Gonzalez, A.L., 1999. Interplanetary origin of geomagnetic storms. *Space Science Reviews* 88(3), 529-562.

Goodman, J.M., 2005. Operational communication systems and relationships to the ionosphere and space weather. *Advances in Space Research* 36(12), 2241-2252.

Gopalswamy, N., Yashiro, S., Liu, Y., Michalek, G., Vourlidas, A., Kaiser, M., Howard, R., 2005. Coronal mass ejections and other extreme characteristics of the 2003 October–November solar eruptions. *Journal of Geophysical Research: Space Physics* 110(A9).

Gordon, P., Moore, J.E., Park, J.Y., Richardson, H.W., 2007. The economic impacts of a terrorist attack on the US commercial aviation system. *Risk Analysis: An International Journal* 27(3), 505-512.

Gulati, I., Tiwari, R., Johnston, M., Dlay, S., 2019. Impact of Solar Flares on HF Radio Communication at High Latitude, *2019 International Conference*

on Automation, Computational and Technology Management (ICACTM).
IEEE, pp. 550-554.

Guo, J., Geng, J., 2018. GPS satellite clock determination in case of inter-frequency clock biases for triple-frequency precise point positioning. *Journal of Geodesy* 92(10), 1133-1142.

Guo, N., Kou, Y., Zhao, Y., Yu, Z., Chen, Y., 2014. An all-pass filter for compensation of ionospheric dispersion effects on wideband GNSS signals. *GPS Solutions* 18, 625-637.

Gurtov, A., Polishchuk, T., Wernberg, M., 2018. Controller–pilot data link communication security. *Sensors* 18(5), 1636.

Gwiggner, C., Nagaoka, S., 2014. Data and queueing analysis of a Japanese air-traffic flow. *Eur J Oper Res* 235(1), 265-275.

Hapgood, M., 2017. Satellite navigation—Amazing technology but insidious risk: Why everyone needs to understand space weather. *Space Weather* 15(4), 545-548.

Hapgood, M., 2022. Ionospheric Science: An Example of the Importance of Diversity in Approaches to Scientific Research. *Atmosphere* 13(3), 394.

Hapgood, M., Angling, M.J., Attrill, G., Bisi, M., Cannon, P.S., Dyer, C., Eastwood, J.P., Elvidge, S., Gibbs, M., Harrison, R.A., 2021. Development of space weather reasonable worst‑case scenarios for the UK national risk assessment. Wiley Online Library.

Hapgood, M., Liu, H., Lugaz, N., 2022. SpaceX—Sailing close to the space weather? *Space Weather* 20(3), e2022SW003074.

Haynes, B.D., 2015. Technology candidates for air-to-air and air-to-ground data exchange.

Hong, Y., Choi, B., Kim, Y., 2018. Two-stage stochastic programming based on particle swarm optimization for aircraft sequencing and scheduling. *IEEE Transactions on Intelligent Transportation Systems* 20(4), 1365-1377.

Hoque, M.M., Jakowski, N., 2011. Ionospheric bending correction for GNSS radio occultation signals. *Radio Science* 46(06), 1-9.

Hoque, M.M., Jakowski, N., 2012. Ionospheric propagation effects on GNSS signals and new correction approaches. *Global Navigation Satellite*

Systems: Signal, Theory and Applications, 381-405.

Horne, R., Glauert, S., Meredith, N., Boscher, D., Maget, V., Heynderickx, D., Pitchford, D., 2013. Space weather impacts on satellites and forecasting the Earth's electron radiation belts with SPACECAST. *Space Weather* 11(4), 169-186.

Horne, R.B., Thorne, R.M., Shprits, Y.Y., Meredith, N.P., Glauert, S.A., Smith, A.J., Kanekal, S.G., Baker, D.N., Engebretson, M.J., Posch, J.L., 2005. Wave acceleration of electrons in the Van Allen radiation belts. *Nature* 437(7056), 227-230.

Hu, Y., Zhang, P., Fan, B., Zhang, S., Song, J., 2021. Integrated recovery of aircraft and passengers with passengers' willingness under various itinerary disruption situations. *Computers & Industrial Engineering* 161, 107664.

Huang, Z., Yuan, H., 2013. Analysis and improvement of ionospheric thin shell model used in SBAS for China region. *Advances in Space Research* 51(11), 2035-2042.

Hudson, H.S., 2011. Global properties of solar flares. *Space Science Reviews* 158(1), 5-41.

Hundhausen, A., 1999. Coronal mass ejections, *The many faces of the sun*. Springer, pp. 143-200.

Huo, J., Keung, K., Lee, C., Ng, K.K., Li, K., 2020. The Prediction of Flight Delay: Big Data-driven Machine Learning Approach, *2020 IEEE International Conference on Industrial Engineering and Engineering Management (IEEM)*. IEEE, pp. 190-194.

IATA, 2022. Jet Fuel Price Monitor. *International Air Transport Association*.

IATA, 2023. Air Passenger Numbers to Recover in 2024.

ICAO, 2007. Doc 4444–Procedures for Air Navigation Services: Air Traffic Management. International Civil Aviation Organization Montréal.

ICAO, 2008. Manual on Air Traffic Management System Requirements. *International Civil Aviation Organization*.

ICAO, 2016a. Doc 4444-Procedures for Air Navigation Services: Air Traffic Management. International Aviation Civil Organization Montreal.

ICAO, 2016b. Procedures for Air Navigation and Air Traffic Management Pans-atm Doc 4444.

ICAO, 2018a. ICAO Annex 10 Volume 1 Radio Navigation Aids. *International Civil Aviation Organization*.

ICAO, 2018b. Manual on space weather information in support of international air navigation. International Civil Aviation Organization.

ICRP, 2016. Radiological Protection from Cosmic Radiation in Aviation. *Annals of the ICRP*.

Ikli, S., Mancel, C., Mongeau, M., Olive, X., Rachelson, E., 2019. An optimistic planning approach for the aircraft landing problem, *EIWAC 2019:, 6th ENRI International Workshop on ATM/CNS*.

Ishii, M., 2017. Japanese space weather research activities. *Space Weather* 15(1), 26-35.

Jeppesen, 2008. Airport Information VHHH (Hong Kong Intl). *http://www.fly-sea.com/charts/VHHH.pdf*.

Jheng, S.-L., Jan, S.-S., Chen, Y.-H., Lo, S., 2020. 1090 MHz ADS-B based wide area multilateration system for alternative positioning navigation and timing. *IEEE Sensors Journal*.

Jiao, Y., Morton, Y.T., 2015. Comparison of the effect of high-latitude and equatorial ionospheric scintillation on GPS signals during the maximum of solar cycle 24. *Radio Science* 50(9), 886-903.

Jiao, Y., Morton, Y.T., Taylor, S., Pelgrum, W., 2013. Characterization of high-latitude ionospheric scintillation of GPS signals. *Radio Science* 48(6), 698-708.

Kataoka, R., 2011. Predicting radiation dose on aircraft from solar energetic particles. *Space Weather* 9(8).

Kataoka, R., Sato, T., Kubo, Y., Shiota, D., Kuwabara, T., Yashiro, S., Yasuda, H., 2014. Radiation dose forecast of WASAVIES during ground-level enhancement. *Space Weather* 12(6), 380-386.

Kataoka, R., Sato, T., Miyake, S., Shiota, D., Kubo, Y., 2018. Radiation dose nowcast for the ground level enhancement on 10–11 September 2017. *Space Weather* 16(7), 917-923.

Kelly, M.A., Comberiate, J.M., Miller, E.S., Paxton, L.J., 2014. Progress toward forecasting of space weather effects on UHF SATCOM after Operation

Anaconda. *Space Weather* 12(10), 601-611.

Kim, E., Choi, D., 2016. A UWB positioning network enabling unmanned aircraft systems auto land. *Aerospace science and Technology* 58, 418-426.

Kim, J., Kim, Y., Song, J., Kim, D., Park, M., Kee, C., 2019. Performance improvement of time-differenced carrier phase measurement-based integrated GPS/INS considering noise correlation. *Sensors* 19(14), 3084.

King, C.-Y., 2003. Virtual instrumentation-based system in a real-time applications of GPS/GIS, *International Conference on Recent Advances in Space Technologies, 2003. RAST'03. Proceedings of*. IEEE, pp. 403-408.

Kintner, P., Humphreys, T., Hinks, J., 2009. GNSS and ionospheric scintillation. *Inside GNSS* 4(4), 22-30.

Kintner, P.M., Ledvina, B.M., De Paula, E., 2007. GPS and ionospheric scintillations. *Space weather* 5(9).

Kistan, T., Gardi, A., Sabatini, R., Ramasamy, S., Batuwangala, E., 2017. An evolutionary outlook of air traffic flow management techniques. *Progress in Aerospace Sciences* 88, 15-42.

Knipp, D.J., Ramsay, A., Beard, E., Boright, A., Cade, W., Hewins, I., McFadden, R., Denig, W., Kilcommons, L., Shea, M., 2016. The May 1967 great storm and radio disruption event: Extreme space weather and extraordinary responses. *Space Weather* 14(9), 614-633.

Kress, B., Mertens, C., Wiltberger, M., 2010. Solar energetic particle cutoff variations during the 29–31 October 2003 geomagnetic storm. *Space Weather* 8(5).

Kubo, Y., Kataoka, R., Sato, T., 2015. Interplanetary particle transport simulation for warning system for aviation exposure to solar energetic particles. *Earth, Planets and Space* 67(1), 1-13.

Kunzi, F., 2013. Reduction of Collisions Between Aircraft and Surface Vehicles Conflict Alerting on Airport Surfaces Enabled by Automatic Dependent Surveillance-Broadcast. *Transportation Research Record*(2325), 56-62.

Kwasiborska, A., 2017. Sequencing landing aircraft process to minimize schedule length. *Transportation research procedia* 28, 111-116.

Langley, R.B., Teunissen, P.J., Montenbruck, O., 2017. Introduction to GNSS, *Springer handbook of global navigation satellite systems*. Springer, pp. 3-

23.

Latocha, M., Beck, P., Rollet, S., 2009. AVIDOS—A software package for European accredited aviation dosimetry. *Radiation Protection Dosimetry* 136(4), 286-290.

Lee, H., Li, G., Rai, A., Chattopadhyay, 2020. Real-time anomaly detection framework using a support vector regression for the safety monitoring of commercial aircraft. *Advanced Engineering Informatics* 44, 101071.

Lee, J., Nam, U.W., Pyo, J., Kim, S., Kwon, Y.J., Lee, J., Park, I., Kim, M.H.Y., Dachev, T.P., 2015. Short-term variation of cosmic radiation measured by aircraft under constant flight conditions. *Space Weather* 13(11), 797-806.

Lee, J., Pullen, S., Datta-Barua, S., Lee, J., 2016. Real-time ionospheric threat adaptation using a space weather prediction for GNSS-based aircraft landing systems. *IEEE Transactions on Intelligent Transportation Systems* 18(7), 1752-1761.

Levitt, I., 2012. Modeling ADS-B out system latency, *Ieeeaaia Digit Avion*. IEEE, pp. 5D6-1-5D6-7.

Li, F., Lee, C.-H., Chen, C.-H., Khoo, L.P., 2019. Hybrid data-driven vigilance model in traffic control center using eye-tracking data and context data. *Advanced Engineering Informatics* 42, 100940.

Li, H., 2021. Sino-Russian center for space weather monitoring operational.

Li, S., Visich, J.K., Khumawala, B.M., Zhang, C., 2006. Radio frequency identification technology: applications, technical challenges and strategies. *Sensor Review* 26(3), 193-202.

Li, T., Wang, B., Shang, F., Tian, J., Cao, K., 2020. Dynamic temporal ADS-B data attack detection based on sHDP-HMM. *Computers & Security* 93, 101789.

Lieder, A., Briskorn, D., Stolletz, R., 2015. A dynamic programming approach for the aircraft landing problem with aircraft classes. *European Journal of Operational Research* 243(1), 61-69.

Lin, C.J., Lin, P.-H., Chen, H.-J., Hsieh, M.-C., Yu, H.-C., Wang, E.M.-Y., Ho, H.L., 2012. Effects of controller-pilot communication medium, flight phase and the role in the cockpit on pilots' workload and situation awareness. *Safety science* 50(9), 1722-1731.

Linty, N., Minetto, A., Dovis, F., Spogli, L., 2018. Effects of phase scintillation on the GNSS positioning error during the September 2017 storm at Svalbard. *Space Weather* 16(9), 1317-1329.

Liu, Y., Liu, Y., Hansen, M., Pozdnukhov, A., Zhang, D., 2019. Using machine learning to analyze air traffic management actions: Ground delay program case study. *Transportation Research Part E: Logistics and Transportation Review* 131, 80-95.

Lochard, J., Bartlett, D., Rühm, W., Yasuda, H., Bottollier-Depois, J., 2016. ICRP publication 132: radiological protection from cosmic radiation in aviation. *Annals of the ICRP* 45(1), 5-48.

Lopes, I.T., Ferraz, D.P., Rodrigues, A.M.G., 2016. The drivers of profitability in the top 30 major airlines worldwide. *Measuring Business Excellence*.

Loto'aniu, T., Singer, H., Rodriguez, J., Green, J., Denig, W., Biesecker, D., Angelopoulos, V., 2015. Space weather conditions during the Galaxy 15 spacecraft anomaly. *Space Weather* 13(8), 484-502.

Lu, N., Zhang, J., Zhong, L., 2019. Research on the Problem of Sorting Parallel Runway Aircraft in Terminal Area Based on Genetic Algorithm, *IOP Conference Series: Materials Science and Engineering*. IOP Publishing, p. 042040.

Luo, X., Gu, S., Lou, Y., Chen, B., Song, W., 2020. Better thresholds and weights to improve GNSS PPP under ionospheric scintillation activity at low latitudes. *GPS Solutions* 24, 1-12.

Luo, X., Xie, Z., Monico, J.F.G., Zhang, B., Pereira, V.A.S., Lou, Y., 2023. An ionospheric scintillation index derived from dual-frequency Doppler measurements released by geodetic GNSS receivers operating at 1 Hz. *Journal of Geodesy* 97(7), 70.

Ma, S., Kong, B., Liu, B., Liu, X., 2013. Biological effects of low-dose radiation from computed tomography scanning. *International Journal of Radiation Biology* 89(5), 326-333.

Mahmud, A.A.A., Jeberson, W., 2018. Aircraft landing scheduling using embedded flower pollination algorithm. *International Journal of Parallel Programming*, 1-15.

Manchester IV, W.B., Gombosi, T.I., Roussev, I., Ridley, A., De Zeeuw, D.L.,

Sokolov, I., Powell, K.G., Tóth, G., 2004. Modeling a space weather event from the Sun to the Earth: CME generation and interplanetary propagation. *Journal of Geophysical Research: Space Physics* 109(A2).

Marais, K., 2016. Environmental benefits of space-based ADS-B.

Marqué, C., Klein, K.-L., Monstein, C., Opgenoorth, H., Pulkkinen, A., Buchert, S., Krucker, S., Van Hoof, R., Thulesen, P., 2018. Solar radio emission as a disturbance of aeronautical radionavigation. *Journal of Space Weather and Space Climate* 8, A42.

Marqué, C., Posner, A., Klein, K.-L., 2006. Solar energetic particles and radio-silent fast coronal mass ejections. *The Astrophysical Journal* 642(2), 1222.

Marshall, R., Waters, C., Sciffer, M., 2010. Spectral analysis of pipe-to-soil potentials with variations of the Earth's magnetic field in the Australian region. *Space Weather* 8(5).

Matthiä, D., Heber, B., Reitz, G., Meier, M., Sihver, L., Berger, T., Herbst, K., 2009. Temporal and spatial evolution of the solar energetic particle event on 20 January 2005 and resulting radiation doses in aviation. *Journal of Geophysical Research: Space Physics* 114(A8).

Matthiä, D., Meier, M.M., Reitz, G., 2014. Numerical calculation of the radiation exposure from galactic cosmic rays at aviation altitudes with the PANDOCA core model. *Space Weather* 12(3), 161-171.

Matthiä, D., Schaefer, M., Meier, M.M., 2015. Economic impact and effectiveness of radiation protection measures in aviation during a ground level enhancement. *Journal of Space Weather and Space Climate* 5, A17.

Maxama, X.B., Markus, E.D., 2018. A survey on propagation challenges in wireless communication networks over irregular terrains, *2018 Open Innovations Conference (OI)*. IEEE, pp. 79-86.

Mazareanu, E., 2021. Air traffic - passenger growth rates forecast 2019-2040.

Mazzocchi, M., Hansstein, F., Ragona, M., 2010. The 2010 volcanic ash cloud and its financial impact on the European airline industry, *CESifo Forum*. München: ifo Institut für Wirtschaftsforschung an der Universität München, pp. 92-100.

McCrea, M.V., Sherali, H.D., Trani, A.A., 2008. A probabilistic framework for

weather-based rerouting and delay estimations within an airspace planning model. *Transportation Research Part C: Emerging Technologies* 16(4), 410-431.

Meehan, J., 2010. Understanding space weather customers in GPS-reliant industries. *Space Weather* 8(6).

Meier, M.M., Matthiä, D., 2014. A space weather index for the radiation field at aviation altitudes. *Journal of Space Weather and Space Climate* 4, A13.

Memarzadeh, Y., 2009. *Ionospheric modeling for precise GNSS applications*. Citeseer.

Mertens, C.J., Meier, M.M., Brown, S., Norman, R.B., Xu, X., 2013. NAIRAS aircraft radiation model development, dose climatology, and initial validation. *Space Weather* 11(10), 603-635.

Mishev, A., Adibpour, F., Usoskin, I., Felsberger, E., 2015. Computation of dose rate at flight altitudes during ground level enhancements no. 69, 70 and 71. *Advances in Space Research* 55(1), 354-362.

Moen, J., Oksavik, K., Alfonsi, L., Daabakk, Y., Romano, V., Spogli, L., 2013. Space weather challenges of the polar cap ionosphere. *Journal of Space Weather and Space Climate* 3, A02.

Moldwin, M., 2022. *An introduction to space weather*. Cambridge University Press.

Moreno, B., Radicella, S., De Lacy, M., Herraiz, M., Rodriguez-Caderot, G., 2011. On the effects of the ionospheric disturbances on precise point positioning at equatorial latitudes. *GPS solutions* 15(4), 381-390.

Morozova, A.L., Barlyaeva, T.V., Barata, T., 2020. Variations of TEC over Iberian Peninsula in 2015 due to geomagnetic storms and solar flares. *Space Weather* 18(11), e2020SW002516.

Muhm, J.M., Rock, P.B., McMullin, D.L., Jones, S.P., Lu, I., Eilers, K.D., Space, D.R., McMullen, A., 2007. Effect of aircraft-cabin altitude on passenger discomfort. *New England Journal of Medicine* 357(1), 18-27.

Mukherjee, A., Hansen, M., Grabbe, S., 2012. Ground delay program planning under uncertainty in airport capacity. *Transportation Planning and Technology* 35(6), 611-628.

Nagai, T., 1988. "Space weather forecast": Prediction of relativistic electron

intensity at synchronous orbit. *Geophysical research letters* 15(5), 425-428.

NASA, 2017. Space Radiation is Risky Business for the Human Body. *National Aeronautics and Space Administration*.

National Research Council, 2008. Severe space weather events: Understanding societal and economic impacts: A workshop report. *Washington, DC: The National Academies Press*.

NCRP, 2013. Preconception and Prenatal Radiation Exposure: Health Effects and Protective Guidance.

Neal, J.J., Rodger, C.J., Green, J.C., 2013. Empirical determination of solar proton access to the atmosphere: Impact on polar flight paths. *Space Weather* 11(7), 420-433.

Ng, K., Lee, C., 2016. Makespan minimization in aircraft landing problem under congested traffic situation using modified artificial bee colony algorithm, *2016 IEEE International Conference on Industrial Engineering and Engineering Management (IEEM)*. IEEE, pp. 750-754.

Ng, K., Lee, C., Chan, F., 2017. A robust optimisation approach to the aircraft sequencing and scheduling problem with runway configuration planning, *2017 IEEE International Conference on Industrial Engineering and Engineering Management (IEEM)*. IEEE, pp. 40-44.

Ng, K., Lee, C.K., Chan, F.T., Lv, Y., 2018. Review on meta-heuristics approaches for airside operation research. *Applied Soft Computing* 66, 104-133.

Ng, K.K., Lee, C., Zhang, S., Keung, K., 2020. The impact of heterogeneous arrival and departure rates of flights on runway configuration optimization. *Transportation Letters*, 1-12.

Nguyen, V.K., Rovira-Garcia, A., Juan, J.M., Sanz, J., González-Casado, G., La, T.V., Ta, T.H., 2019. Measuring phase scintillation at different frequencies with conventional GNSS receivers operating at 1 Hz. *Journal of Geodesy* 93, 1985-2001.

Nie, Z., Liu, F., Gao, Y., 2020. Real-time precise point positioning with a low-cost dual-frequency GNSS device. *Gps Solutions* 24, 1-11.

Nielsen, E., Wang, X.D., Gurnett, D., Kirchner, D., Huff, R., Orosei, R., Safaeinili, A., Plaut, J., Picardi, G., 2007. Vertical sheets of dense plasma in the

topside Martian ionosphere. *Journal of Geophysical Research: Planets* 112(E2).

NOAA, 2004. Intense Space Weather Storms October 19 - November 07, 2003.

Nuic, A., 2010. User manual for the Base of Aircraft Data (BADA) revision 3.10. *Atmosphere* 2010, 001.

O'Connell, J.F., Avellana, R.M., Warnock-Smith, D., Efthymiou, M., 2020. Evaluating drivers of profitability for airlines in Latin America: A case study of Copa Airlines. *Journal of Air Transport Management* 84, 101727.

Okoh, D., Seemala, G., Rabiu, A., Uwamahoro, J., Habarulema, J., Aggarwal, M., 2018. A Hybrid Regression-Neural Network (HR-NN) method for forecasting the solar activity. *Space Weather* 16(9), 1424-1436.

Opgenoorth, H., Pulkkinen, A., Buchert, S., Monstein, C., Klein, K.L., Marqué, C., Krucker, S., 2016. Solar activity during the space weather incident of Nov 4., 2015-Complex data and lessons learned, *EGU General Assembly Conference Abstracts*, pp. EPSC2016-12017.

Osunwusi, A.O., 2020. Aviation Safety Regulations versus CNS/ATM Systems and Functionalities. *International Journal of Aviation, Aeronautics, Aerospace* 7(1), 8.

Palm, M., 2002. The revised German radiation protection ordinance. *Kerntechnik* 67(1), 8-12.

Pamplona, D.A., de Barros, A.G., Alves, C.J., 2021. Performance-Based Navigation Flight Path Analysis Using Fast-Time Simulation. *Energies* 14(22), 7800.

Pankratius, V., Lind, F., Coster, A., Erickson, P., Semeter, J., 2014. Mobile crowd sensing in space weather monitoring: the mahali project. *IEEE communications magazine* 52(8), 22-28.

Panteli, M., Pickering, C., Wilkinson, S., Dawson, R., Mancarella, P., 2016. Power system resilience to extreme weather: Fragility modeling, probabilistic impact assessment, and adaptation measures. *IEEE Transactions on Power Systems* 32(5), 3747-3757.

Parker, E.N., 2006. Shielding space travelers. *Scientific American* 294(3), 40-47.

Pejovic, T., Noland, R.B., Williams, V., Toumi, R., 2009. A tentative analysis of

the impacts of an airport closure. *Journal of Air Transport Management* 15(5), 241-248.

Peng, Y., Scales, W.A., 2021. Ionospheric Remote Sensing with GNSS. *Encyclopedia* 1(4), 1246-1256.

Pesnell, W.D., 2012. Solar cycle predictions (invited review). *Solar Physics* 281(1), 507-532.

Phoomchusak, P., Leelaruji, N., Hemmakorn, N., 2013. The deterioration of GPS accuracy caused by ionospheric amplitude scintillation. Citeseer.

Pi, X., Iijima, B.A., Lu, W., 2017. Effects of ionospheric scintillation on GNSS-based positioning. *Navigation: Journal of The Institute of Navigation* 64(1), 3-22.

Pierpaoli, P., Rahmani, A., 2018. UAV collision avoidance exploitation for noncooperative trajectory modification. *Aerosp Sci Technol* 73, 173-183.

Pirjola, R., 2005. Effects of space weather on high-latitude ground systems. *Advances in Space Research* 36(12), 2231-2240.

Pirjola, R., Kauristie, K., Lappalainen, H., Viljanen, A., Pulkkinen, A., 2005. Space weather risk. *Space Weather* 3(2).

Plainaki, C., Belov, A., Eroshenko, E., Mavromichalaki, H., Yanke, V., 2007. Modeling ground level enhancements: Event of 20 January 2005. *Journal of Geophysical Research: Space Physics* 112(A4).

Poppe, B.B., Jorden, K.P., 2006. *Sentinels of the Sun: Forecasting space weather*. Big Earth Publishing.

Prakash, R., Piplani, R., Desai, J., 2018. An optimal data-splitting algorithm for aircraft scheduling on a single runway to maximize throughput. *Transportation Research Part C: Emerging Technologies* 95, 570-581.

Pulkkinen, A., Lindahl, S., Viljanen, A., Pirjola, R., 2005. Geomagnetic storm of 29–31 October 2003: Geomagnetically induced currents and their relation to problems in the Swedish high-voltage power transmission system. *Space Weather* 3(8).

Qing, C., ANG, H.J., Sameer, A., 2022. Collision risk assessment of reduced aircraft separation minima in procedural airspace using advanced communication and navigation. *Chinese Journal of Aeronautics*.

Quesnel, F., Desaulniers, G., Soumis, F., 2020. A branch-and-price heuristic for the crew pairing problem with language constraints. *European Journal of Operational Research* 283(3), 1040-1054.

Rathore, B.S., Kaushik, S.C., Firoz, K., Gupta, D., Shrivastava, A., Parashar, K.K., Bhaduriya, R.M., 2011. A correlative study of geomagnetic storms associated with solar wind and IMF features during solar cycle 23. *International Journal of applied physics and mathematics* 1(2), 149.

Reddybattula, K.D., Panda, S.K., Sharma, S.K., Singh, A.K., Kurnala, K., Haritha, C.S., Wuyyuru, S., 2020. Anomaly effects of 6–10 September 2017 solar flares on ionospheric total electron content over Saudi Arabian low latitudes. *Acta Astronautica* 177, 332-340.

Redmon, R., Seaton, D., Steenburgh, R., He, J., Rodriguez, J., 2018. September 2017's geoeffective space weather and impacts to Caribbean radio communications during hurricane response. *Space Weather* 16(9), 1190-1201.

Ricke, K., Drouet, L., Caldeira, K., Tavoni, M., 2018. Country-level social cost of carbon. *Nature Climate Change* 8(10), 895-900.

Ritter, S., Rotko, D., Halpin, S., Nawal, A., Farias, A., Patel, K., Diggewadi, A., Hill, H., 2020. International legal and ethical issues of a future carrington event: existing frameworks, shortcomings, and recommendations. *New Space* 8(1), 23-30.

Rockville, M., 2019. Customer Needs and Requirements for Space Weather Products and Services.

Rodrigues, F., Moraes, A., 2019. ScintPi: A low-cost, easy-to-build GPS ionospheric scintillation monitor for DASI studies of space weather, education, and citizen science initiatives. *Earth and Space Science* 6(8), 1547-1560.

Rodríguez-Díaz, A., Adenso-Díaz, B., González-Torre, P.L., 2017. Minimizing deviation from scheduled times in a single mixed-operation runway. *Computers & Operations Research* 78, 193-202.

Romano, V., Spogli, L., Aquino, M., Dodson, A., Hancock, C., Forte, B., 2013. GNSS station characterisation for ionospheric scintillation applications.

Advances in Space Research 52(7), 1237-1246.

Roy, B., Paul, A., 2013. Impact of space weather events on satellite‑based navigation. *Space Weather* 11(12), 680-686.

RTCA, 2009. Interoperability Requirements Document for Enhanced Air Traffic Services in Radar-Controlled Areas Using ADS-B Surveillance (ADS-BRAD).

Ruffner, J.W., Deaver, D.M., Henry, D.J., 2003. Requirements analysis for an Air Traffic Control Tower Surface Surveillance Enhanced Vision System. *Enhanced and Synthetic Vision 2003* 5081, 124-135.

Rutledge, R., Desbios, S., 2018. Space weather focus: Impacts of a severe space weather event on aviation operations. *World Meteorological Organization Commission for Aeronautical Meteorology (CAeM) Newsletter*(1).

Ryan, J.M., Lockwood, J.A., Debrunner, H., 2000. Solar energetic particles. *Space Science Reviews* 93(1), 35-53.

Saito, S., Wickramasinghe, N.K., Sato, T., Shiota, D., 2021. Estimate of economic impact of atmospheric radiation storm associated with solar energetic particle events on aircraft operations. *Earth, Planets and Space* 73(1), 1-10.

Salehipour, A., 2020. An algorithm for single-and multiple-runway aircraft landing problem. *Mathematics and Computers in Simulation* 175, 179-191.

Sanlorenzo, M., Wehner, M.R., Linos, E., Kornak, J., Kainz, W., Posch, C., Vujic, I., Johnston, K., Gho, D., Monico, G., 2015. The risk of melanoma in airline pilots and cabin crew: a meta-analysis. *JAMA dermatology* 151(1), 51-58.

Sato, T., 2020. Recent progress in space weather research for cosmic radiation dosimetry. *Annals of the ICRP* 49(1_suppl), 185-192.

Sato, T., Kataoka, R., Shiota, D., Kubo, Y., Ishii, M., Yasuda, H., Miyake, S., Miyoshi, Y., Ueno, H., Nagamatsu, A., 2019. Nowcast and forecast of galactic cosmic ray (GCR) and solar energetic particle (SEP) fluxes in magnetosphere and ionosphere–extension of WASAVIES to Earth orbit. *Journal of Space Weather and Space Climate* 9, A9.

Sato, T., Kataoka, R., Shiota, D., Kubo, Y., Ishii, M., Yasuda, H., Miyake, S., Park,

I.C., Miyoshi, Y., 2018. Real time and automatic analysis program for WASAVIES: Warning system for aviation exposure to solar energetic particles. *Space Weather* 16(7), 924-936.

Sato, T., Kataoka, R., Yasuda, H., Yashiro, S., Kuwabara, T., Shiota, D., Kubo, Y., 2014. Air shower simulation for WASAVIES: Warning system for aviation exposure to solar energetic particles. *Radiation protection dosimetry* 161(1-4), 274-278.

Sauer, H.H., Wilkinson, D.C., 2008. Global mapping of ionospheric HF/VHF radio wave absorption due to solar energetic protons. *Space Weather* 6(12).

Schatten, K., 2003. Solar activity and the solar cycle. *Advances in Space Research* 32(4), 451-460.

Schlickeiser, R., 2013. *Cosmic ray astrophysics*. Springer Science & Business Media.

Schrijver, C.J., Kauristie, K., Aylward, A.D., Denardini, C.M., Gibson, S.E., Glover, A., Gopalswamy, N., Grande, M., Hapgood, M., Heynderickx, D., 2015. Understanding space weather to shield society: A global road map for 2015–2025 commissioned by COSPAR and ILWS. *Advances in Space Research* 55(12), 2745-2807.

Schwenn, R., 2006. Space weather: The solar perspective. *Living reviews in solar physics* 3(1), 1-72.

SenthamilSelvan, R., Wahidabanu, R., Karthik, B., 2022. Intersection collision avoidance in dedicated short-range communication using vehicle ad hoc network. *Concurrency and Computation: Practice and Experience* 34(13), e5856.

Seo, J., Walter, T., Chiou, T.Y., Enge, P., 2009. Characteristics of deep GPS signal fading due to ionospheric scintillation for aviation receiver design. *Radio Science* 44(1).

Sharma, R., Hablani, H., 2014. High-accuracy GPS-based aircraft navigation for landing using pseudolites and double-difference carrier phase measurements. *IFAC Proceedings Volumes* 47(1), 200-204.

Shea, M., Smart, D., 2012. Space weather and the ground-level solar proton events of the 23rd solar cycle. *Space science reviews* 171(1), 161-188.

Shouop, C.J.G., Moyo, M.N., Mekongtso, E.J.N., Cho, K., Strivay, D., 2020. Radiological protection requirements with regard to cosmic ray exposure during air travel. *The European Physical Journal Plus* 135(5), 438.

Simonsen, L.C., Slaba, T.C., Guida, P., Rusek, A., 2020. NASA's first ground-based Galactic Cosmic Ray Simulator: Enabling a new era in space radiobiology research. *PLoS biology* 18(5), e3000669.

Singh, A., Siingh, D., Singh, R., 2010. Space weather: physics, effects and predictability. *Surveys in geophysics* 31, 581-638.

Skrypnik, O.N., 2019. *Radio Navigation Systems for Airports and Airways*. Springer.

Slaba, T.C., Whitman, K., 2020. The Badhwar-O'Neill 2020 GCR Model. *Space Weather* 18(6), e2020SW002456.

Smith, A.M., Mitchell, C.N., Watson, R.J., Meggs, R.W., Kintner, P.M., Kauristie, K., Honary, F., 2008. GPS scintillation in the high arctic associated with an auroral arc. *Space Weather* 6(3).

Smith, M., Moser, D., Strohmeier, M., Lenders, V., Martinovic, I., 2018. Undermining privacy in the aircraft communications addressing and reporting system (ACARS). *Proceedings on Privacy Enhancing Technologies* 2018(3), 105-122.

Sparks, L., Altshuler, E., Pandya, N., Blanch, J., Walter, T., 2022. WAAS and the Ionosphere–A Historical Perspective: Monitoring Storms. *NAVIGATION: Journal of the Institute of Navigation* 69(1).

Sreeja, V., 2016a. Impact and mitigation of space weather effects on GNSS receiver performance. *Geoscience letters* 3(1), 24.

Sreeja, V., 2016b. Impact and mitigation of space weather effects on GNSS receiver performance. *Geoscience letters* 3(1), 1-13.

Starita, S., Strauss, A.K., Fei, X., Jovanović, R., Ivanov, N., Pavlović, G., Fichert, F., 2020. Air Traffic Control Capacity Planning Under Demand and Capacity Provision Uncertainty. *Transportation Science*.

Strohmeier, M., Schäfer, M., Lenders, V., Martinovic, I., 2014. Realities and challenges of nextgen air traffic management: the case of ADS-B. *IEEE Communications Magazine* 52(5), 111-118.

Su, Y., Liu, Y., Zhou, Y., Yuan, J., Cao, H., Shi, J., 2019. Broadband LEO satellite communications: Architectures and key technologies. *IEEE Wireless Communications* 26(2), 55-61.

Su, Z.G., Deng, Q., Hao, J.T., 2020. A Study on the Collision Probability of Satellite-Based ADS-B Messages Based on Homogeneous Poisson Process. *Int J Aeronaut Space* 21(3), 845-857.

Sugiura, M., 1963. Hourly values of equatorial Dst for the IGY.

Sun, A.K., Chang, H., Pullen, S., Kil, H., Seo, J., Morton, Y.J., Lee, J., 2021a. Markov Chain-Based Stochastic Modeling of Deep Signal Fading: Availability Assessment of Dual-Frequency GNSS-Based Aviation Under Ionospheric Scintillation. *Space Weather* 19(9), e2020SW002655.

Sun, R., Hsu, L.-T., Xue, D., Zhang, G., Ochieng, W.Y., 2019. GPS signal reception classification using adaptive neuro-fuzzy inference system. *The Journal of Navigation* 72(3), 685-701.

Sun, R., Wang, G., Zhang, W., Hsu, L.-T., Ochieng, W.Y., 2020. A gradient boosting decision tree based GPS signal reception classification algorithm. *Applied Soft Computing* 86, 105942.

Sun, X., Wandelt, S., Zheng, C., Zhang, A., 2021b. COVID-19 pandemic and air transportation: Successfully navigating the paper hurricane. *Journal of Air Transport Management* 94, 102062.

Svestka, Z., 2012. Solar flares. *Springer Science & Business Media* 8.

Tao, C., Nishioka, M., Saito, S., Shiota, D., Watanabe, K., Nishizuka, N., Tsugawa, T., Ishii, M., 2020. Statistical analysis of short-wave fadeout for extreme space weather event estimation. *Earth, Planets and Space* 72(1), 1-16.

Taylor, C., Tien, S.-L., Vargo, E., Wanke, C., 2021. Strategic flight cancellation under ground delay program uncertainty. *Journal of Air Transportation* 29(1), 5-15.

Telloni, D., Carbone, F., Antonucci, E., Bruno, R., Grimani, C., Villante, U., Giordano, S., Mancuso, S., Zangrilli, L., 2020. Study of the Influence of the Solar Wind Energy on the Geomagnetic Activity for Space Weather Science. *The Astrophysical Journal* 896(2), 149.

Thierfeldt, S., Haider, C., Hans, P., Kaleve, M., Neuenfeldt, F., 2009. Evaluation

of the implementation of radiation protection measures for aircrew in EU member states. *Radiation protection dosimetry* 136(4), 324-328.

Thomsen, M., 2004. Why Kp is such a good measure of magnetospheric convection. *Space Weather* 2(11).

Tobiska, W.K., Atwell, W., Beck, P., Benton, E., Copeland, K., Dyer, C., Gersey, B., Getley, I., Hands, A., Holland, M., 2015. Advances in atmospheric radiation measurements and modeling needed to improve air safety. *Space Weather* 13(4), 202-210.

Tobisová, A., Mikula, B., Szabo, S., Blaško, D., Vajdová, I., Jenčová, E., Melníková, L., Němec, V., 2018. The Simulation of Fire and Rescue Services Operations by Airplane Accidents, *2018 XIII International Scientific Conference-New Trends in Aviation Development (NTAD)*. IEEE, pp. 144-149.

Toratani, D., 2019. Application of merging optimization to an arrival manager algorithm considering trajectory-based operations. *Transportation Research Part C: Emerging Technologies* 109, 40-59.

Tóth, G., Van der Holst, B., Sokolov, I.V., De Zeeuw, D.L., Gombosi, T.I., Fang, F., Manchester, W.B., Meng, X., Najib, D., Powell, K.G., 2012. Adaptive numerical algorithms in space weather modeling. *Journal of Computational Physics* 231(3), 870-903.

Tsagouri, I., Koutroumbas, K., Elias, P., 2018. A new short-term forecasting model for the total electron content storm time disturbances. *Journal of Space Weather and Space Climate* 8, A33.

Tsurutani, B., Mannucci, A., Iijima, B., Abdu, M.A., Sobral, J.H.A., Gonzalez, W., Guarnieri, F., Tsuda, T., Saito, A., Yumoto, K., 2004. Global dayside ionospheric uplift and enhancement associated with interplanetary electric fields. *Journal of Geophysical Research: Space Physics* 109(A8).

Tuo, F., Zhou, L., Xu, C., Yao, Y., Ren, T., Zhou, Q., 2012. Measurement of cosmic radiation dose to air crew connecting for a typical polar route flight. *Journal of Radioanalytical and Nuclear Chemistry* 293(3), 935-939.

Tuysuz, B., Urbina, J., Lind, F., 2013. Development of a passive VHF radar system using software-defined radio for equatorial plasma instability studies. *Radio science* 48(4), 416-426.

Vankadara, R.K., Panda, S.K., Amory-Mazaudier, C., Fleury, R., Devanaboyina, V.R., Pant, T.K., Jamjareegulgarn, P., Haq, M.A., Okoh, D., Seemala, G.K., 2022. Signatures of equatorial plasma bubbles and ionospheric scintillations from magnetometer and GNSS observations in the Indian longitudes during the space weather events of early September 2017. *Remote Sensing* 14(3), 652.

Vesnin, A., 2022. Real-Time Data Assimilation for Space Weather Effects Mitigation on GNSS/SBAS, *Space Weather Impact on GNSS Performance*. Springer, pp. 255-319.

Vial, G., 2019. Understanding digital transformation: A review and a research agenda. *The Journal of Strategic Information Systems* 28(2), 118-144.

Viereck, R., Kunches, J., Codrescu, M., Steenburgh, R., 2014. Customers and Requirements for Ionosphere Products and Services. *Modeling the Ionosphere–Thermosphere System*, 299-307.

Vilà-Valls, J., Linty, N., Closas, P., Dovis, F., Curran, J.T., 2020. Survey on signal processing for GNSS under ionospheric scintillation: Detection, monitoring, and mitigation. *NAVIGATION: Journal of the Institute of Navigation* 67(3), 511-535.

Viljanen, A., Pulkkinen, A., Pirjola, R., Pajunpää, K., Posio, P., Koistinen, A., 2006. Recordings of geomagnetically induced currents and a nowcasting service of the Finnish natural gas pipeline system. *Space Weather* 4(10).

Vincent, F.Y., Qiu, M., Pan, H., Chung, T.-P., Gupta, J.N., 2021. An Improved Immunoglobulin-Based Artificial Immune System for the Aircraft Scheduling Problem With Alternate Aircrafts. *IEEE Access* 9, 16532-16545.

Vismari, L.F., Junior, J.B.C., 2011. A safety assessment methodology applied to CNS/ATM-based air traffic control system. *Reliability Engineering & System Safety* 96(7), 727-738.

Vossen, T., Ball, M., 2006. Optimization and mediated bartering models for ground delay programs. *Naval research logistics (NRL)* 53(1), 75-90.

Walsh, J., Gill, E.W., Huang, W., Chen, S., 2015. On the development of a high-frequency radar cross section model for mixed path ionosphere–ocean propagation. *IEEE Transactions on Antennas and Propagation* 63(6),

2655-2664.

Walter, T., 2017. Satellite based augmentation systems, *Springer handbook of global navigation satellite systems*. Springer, pp. 339-361.

Wang, Q., Jin, S., Ye, X., 2022. A Novel Method to Estimate Multi-GNSS Differential Code Bias without Using Ionospheric Function Model and Global Ionosphere Map. *Remote Sensing* 14(9), 2002.

Wang, Y.-H., Lee, C.-H., Trappey, A.J., 2017. Modularized design-oriented systematic inventive thinking approach supporting collaborative service innovations. *Advanced Engineering Informatics* 33, 300-313.

Warnant, R., Lejeune, S., Bavier, M., 2007. Space weather influence on satellite-based navigation and precise positioning. *ASTROPHYSICS AND SPACE SCIENCE LIBRARY* 344, 129.

Watari, S., 2015. Estimation of geomagnetically induced currents based on the measurement data of a transformer in a Japanese power network and geoelectric field observations. *Earth, Planets and Space* 67(1), 1-12.

Webb, D.F., Howard, T.A., 2012. Coronal mass ejections: Observations. *Living Reviews in Solar Physics* 9(1), 1-83.

Wee, H.J., Lye, S.W., Pinheiro, J.-P., 2019. An integrated highly synchronous, high resolution, real time eye tracking system for dynamic flight movement. *Advanced Engineering Informatics* 41, 100919.

Wen, X., Chung, S.-H., Ji, P., Sheu, J.-B., 2022. Individual scheduling approach for multi-class airline cabin crew with manpower requirement heterogeneity. *Transportation Research Part E: Logistics and Transportation Review* 163, 102763.

Whalen, D.J., 2010. Communications satellites: making the global village possible. *NASA History Office Publications*.

Wingelaar-Jagt, Y.Q., Wingelaar, T.T., Riedel, W.J., Ramaekers, J.G., 2021. Fatigue in aviation: Safety risks, preventive strategies and pharmacological interventions. *Frontiers in physiology* 12.

World Health Organization, 2011. Guidelines for drinking-water quality fourth edition. *World Health Organization*.

Wu, L.-J., Zhan, Z.-H., Hu, X.-M., Guo, P., Zhang, Y., Zhang, J., 2019. Multi-runway Aircraft Arrival Scheduling: A Receding Horizon Control Based

Ant Colony System Approach, *2019 IEEE Congress on Evolutionary Computation (CEC)*. IEEE, pp. 538-545.

Xiong, C., Stolle, C., Lühr, H., 2016. The Swarm satellite loss of GPS signal and its relation to ionospheric plasma irregularities. *Space weather* 14(8), 563-577.

Xu, B., 2017. An efficient ant colony algorithm based on wake-vortex modeling method for aircraft scheduling problem. *Journal of Computational and Applied Mathematics* 317, 157-170.

Xu, R., Liu, Z., Chen, W., 2015. Improved FLL-assisted PLL with in-phase pre-filtering to mitigate amplitude scintillation effects. *GPS Solutions* 19(2), 263-276.

Xu, S., Bi, W., Zhang, A., Mao, Z., 2022. Optimization of flight test tasks allocation and sequencing using genetic algorithm. *Applied Soft Computing* 115, 108241.

Xue, D., Hsu, L.-T., Wu, C.-L., Lee, C.-H., Ng, K.K., 2021a. Cooperative surveillance systems and digital-technology enabler for a real-time standard terminal arrival schedule displacement. *Advanced Engineering Informatics* 50, 101402.

Xue, D., Liu, Z., Wang, B., Yang, J., 2021b. Impacts of COVID-19 on aircraft usage and fuel consumption: A case study on four Chinese international airports. *Journal of Air Transport Management* 95, 102106.

Xue, D., Ng, K.K., Hsu, L.-T., 2020a. Multi-Objective Flight Altitude Decision Considering Contrails, Fuel Consumption and Flight Time. *Sustainability* 12(15), 6253.

Xue, D., Yang, J., Liu, Z., 2020b. The Effect of Space Weather on ADS-B Data in Hong Kong Terminal Airspace, *AGU Fall Meeting 2020*. AGU.

Xue, D., Yang, J., Liu, Z., 2022a. Potential Impact of GNSS Positioning Errors on the Satellite-Navigation-Based Air Traffic Management. *Space Weather* 20(7), e2022SW003144.

Xue, D., Yang, J., Liu, Z., Wang, B., 2022b. An optimized solution to long-distance flight routes under extreme cosmic radiation. *Space Weather*, e2022SW003264.

Xue, D., Yang, J., Liu, Z., Wang, B., 2022c. An Optimized Solution to Long‑Distance Flight Routes Under Extreme Cosmic Radiation. *Space Weather* 20(12), e2022SW003264.

Xue, D., Yang, J., Liu, Z., Yu, S., 2023. Examining the economic costs of the 2003 Halloween storm effects on the North Hemisphere aviation using flight data in 2019. *Space Weather* 21(3), e2022SW003381.

Yamashiki, Y.A., Fujita, M., Sato, T., Maehara, H., Notsu, Y., Shibata, K., 2020. Cost estimation for alternative aviation plans against potential radiation exposure associated with solar proton events for the airline industry. *Evolutionary and Institutional Economics Review* 17(2), 487-499.

Yang, Z.-Y., Sheu, R.-J., 2020. An in-depth analysis of aviation route doses for the longest distance flight from Taiwan. *Radiation Physics and Chemistry* 168, 108548.

Yang, Z., Zhang, Q., Ding, X., Chen, W., 2020. Analysis of the quality of daily DEM generation with geosynchronous InSAR. *Engineering* 6(8), 913-918.

Yasyukevich, Y., Astafyeva, E., Padokhin, A., Ivanova, V., Syrovatskii, S., Podlesnyi, A., 2018. The 6 September 2017 X‑class solar flares and their impacts on the ionosphere, GNSS, and HF radio wave propagation. *Space Weather* 16(8), 1013-1027.

Yasyukevich, Y., Mylnikova, A., Vesnin, A., 2020. GNSS-based non-negative absolute ionosphere total electron content, its spatial gradients, time derivatives and differential code biases: bounded-variable least-squares and taylor series. *Sensors* 20(19), 5702.

Yiğit, E., Knížová, P.K., Georgieva, K., Ward, W., 2016. A review of vertical coupling in the Atmosphere–Ionosphere system: Effects of waves, sudden stratospheric warmings, space weather, and of solar activity. *Journal of Atmospheric and Solar-Terrestrial Physics* 141, 1-12.

Yu, S., Liu, Z., 2021a. Feasibility analysis of GNSS-based ionospheric observation on a fast-moving train platform (GIFT). *Satellite Navigation* 2(1), 1-18.

Yu, S., Liu, Z., 2021b. The ionospheric condition and GPS positioning performance during the 2013 tropical cyclone Usagi event in the Hong Kong region. *Earth, Planets and Space* 73(1), 1-16.

Zhang, S., Du, S., Li, W., Wang, G., 2019. Evaluation of the GPS precise orbit and clock corrections from MADOCA real-time products. *Sensors* 19(11), 2580.

Zhang, X., Mahadevan, S., 2017. Aircraft re-routing optimization and performance assessment under uncertainty. *Decision Support Systems* 96, 67-82.

Zhang, Z.Y., Zhang, J., Wang, P., Chen, L., 2018. Research on Operation of UAVs in Non-isolated Airspace. *Cmc-Comput Mater Con* 57(1), 151-166.

Zhao, D., Lei, Y., 2023. Effects of ionosphere dispersion on wideband GNSS signals. *Frontiers in Physics* 11, 95.

Zhao, D., Li, W., Li, C., Hancock, C.M., Roberts, G.W., Wang, Q., 2022. Analysis on the ionospheric scintillation monitoring performance of ROTI extracted from GNSS observations in high-latitude regions. *Advances in Space Research* 69(1), 142-158.

Zheng, P., Wang, Z., Chen, C.-H., Khoo, L.P., 2019. A survey of smart product-service systems: Key aspects, challenges and future perspectives. *Advanced Engineering Informatics* 42, 100973.

Ziv, S.Z., Yair, Y., Alpert, P., Uzan, L., Reuveni, Y., 2021. The diurnal variability of precipitable water vapor derived from GPS tropospheric path delays over the Eastern Mediterranean. *Atmospheric Research* 249, 105307.